Study of Stratospheric Composition using Airborne Submillimeter Radiometry and a Chemical Transport Model

Jayanarayanan Kuttippurath

Universität Bremen 2005

Study of Stratospheric Composition using Airborne Submillimeter Radiometry and a Chemical Transport Model

Vom Fachbereich für Physik und Elektrotechnik
der Universität Bremen
zur Erlangung des akademischen Grades eines
Doktor der Naturwissenschaften (Dr. rer. nat.)
genehmigte Dissertation

von
Jayanarayanan Kuttippurath

1. Gutachter   : Prof. Dr. Justus Notholt
2. Gutachter   : Prof. Dr. Klaus Künzi
1. Prüfer   : Prof. Dr. Joern Bleck-Neuhaus
2. Prüfer   : Prof. Dr. Cornelius Noack
1. Beisitzer   :   Dr. Holger Bremer
2. Beisitzer   :   Mathias Palm (M. Sc.)

Submitted on   : 09th March 2005
Defended (awarded) on : 18th April 2005

Contents

1 Abstract

The Airborne Submillimeter Radiometer (ASUR) was deployed aboard the Falcon research aircraft during the SCIAVALUE (SCIAMACHY - Scanning Imaging Absorption Spectrometer for Atmospheric ChartographY - Validation Utilization Experiment), the EUPLEX (European Polar and Lee wave Experiment), and the PAVE (Polar Aura Validation Experiment) campaigns. An impressive array of microwave measurements of O_3, N_2O, HCl, HNO_3 and ClO is amassed during the missions from the tropics to the Arctic in various seasons. The tropical and the mid-latitude profiles (south of $45°$N) are retrieved for the first time from the ASUR measurement spectra. The retrievals in comparison with independent measurements and model calculations show a good agreement. The mixing ratios retrieved with *'the Forward'* and the ARTS (Atmospheric Radiative Transfer System) models show negligible differences, which recommend the replacement of *'the Forward'* model with ARTS for the ASUR trace gas inversion.

The cross-validation shows that the deviation ASUR-SCIAMACHY OP is -4 to 6%, ASUR-SCIAMACHY UB is -12 to 15%, ASUR-MIPAS IPF is up to 5%, ASUR-MIPAS IMK is -3 to 6%, ASUR-OSIRIS is 3 to 15% and ASUR-SMR -4 to 15% at 20-40 km, depending on altitude. The HNO_3 and N_2O from MIPAS and N_2O from SMR also show a good agreement with the ASUR measurements. Hence, the satellite measurements can be used for various scientific analyses in consideration with the good intercomparison results.

The Bremen Chemical Transport Model (CTMB), a new model for the simulations of O_3, N_2O and NO_y, is introduced. Evaluation of the Linearized ozone chemistry shows that the ozone profiles simulated with the Linoz model are accurate enough to be used for stratospheric chemistry and transport studies though the simulations show a low bias of $\sim$9% in the middle stratosphere and a high bias of 10-30% in the lower and upper stratosphere, depending on altitude. The simulations for various years suggest that the N_2O and NO_y calculations depend greatly on the accuracy of the meteorological analyses used in the model. The simulations reveal that the N_2O VMRs calculated with the parameterized chemistry are slightly smaller in the lower stratosphere. The inaccuracies in the wind analyses, the model transport and uncertainties in the chemical reaction rates can be the reasons for the lower values. The N_2O-NO_y coupled chemistry is in good shape and the transport barriers are reasonably represented in the model. The comparison among the ASUR, the SLIMCAT and the CTMB profiles reveal the upper stratospheric ozone deficit in the SLIMCAT calculations. The comparisons also indicate that the transport process in the models is still to be improved.

Publications

Parts of this work have been used in the following journal articles.

Reviewed

1. Kuttippurath, J., A. Kleinböhl, H. Bremer, C. von Savigny, M. Sinnhuber, H. Küllmann, J. Notholt, K. Künzi, M. Milz, G. Stiller, S. Petelina, J. Urban, N. Lautié, D. Murtagh, J. de La Noë, P. Ricaud, and E. Le Flochmoën: Intercomparison of ASUR ozone measurements with data retrieved from the space-borne limb sensors SCIAMACHY, MIPAS, OSIRIS and SMR, *Submitted to **Atmos. Chem. Phys. Discuss.**, May 2005.*

2. Kuttippurath, J., H. Bremer, A. Kleinböhl, B.-M. Sinnhuber, H. Küllmann, J. Notholt, K. Künzi and S. Davis: Seasonal and latitudinal distribution of stratospheric trace gases: Observations and model calculations, *Submitted to **Atmos. Chem. Phys. Discuss.**, May 2005.*

3. Kuttippurath, J., J. Notholt, and B.-M. Sinnhuber: Evaluation of Linearised ozone chemistry with the Bremen CTM using ozonesondes and satellite measurements, *Submitted to **J. Geophys. Res.**, August 2005.*

4. Kleinböhl, A., **J. Kuttippurath**, M. Sinnhuber, B.-M. Sinnhuber, H. Küllmann, K. Künzi, and J. Notholt: Rapid meridional transport of tropical airmasses to the Arctic during the major stratospheric warming in January 2003, *Atmos. Chem. Phys., 5, 1291-1299, 2005.*

5. Fix, A., G. Ehret, H. Flentje, G. Poberaj, M. Gottwald, H. Finkenzeller, H. Bremer, M. Bruns, J. P. Burrows, A. Kleinböhl, H. Kllmann, **J. Kuttippurath**, A. Richter, P. Wang, K.-P. Heue, U. Platt, and T. Wagner: SCIAMACHY validation by aircraft remote measurements: Design, execution, and first results of the SCIA-VALUE mission, *Atmos. Chem. Phys., 5, 1273-1289, 2005.*

6. Kleinböhl, A., H. Bremer, H. Kllmann, **J. Kuttippurath**, E. Browell, T. Canty, R. Salawitch, G. Toon and J. Notholt: Denitrification in the Arctic mid-winter 2004/2005 observed by airborne submillimeter radiometry, ***Geophys. Res. Lett.**, in press, August 2005.*

7. Urban, J., N. Lautié, E. Le Flochmoën, P. Eriksson, J. de La Noë, E. Dupuy, L. El Amraoui, U. Frisk, F. Jégou, D. Murtagh, M. Olberg, P. Ricaud, C. Camy-Peyret, G. Dufour, S. Payan, N. Huret, M. Pirre, A. D. Robinson, N. R. P. Harris, H. Bremer, A. Kleinböhl, K. Küllmann, K. Künzi, **J. Kuttippurath**, M. Ejiri, H. Nakajima, Y. Sasano, T. Sugita, T. Yokota, C. Piccolo, P. Raspollini, M. Ridolfi: Odin/SMR limb observations of stratospheric gases: Validation of N_2O, ***J. Geophys. Res.**, 110, D09301, doi: 10.1029/2004JD005394, 2005.*

In preparation

8. Cortesi et al. (including **J. Kuttippurath**): MIPAS ozone validation by stratospheric balloon and aircraft measurements, *Atmos. Chem. Phys., 2005.*

9. Urban et al. (including **J. Kuttippurath**): Odin/SMR limb observations of stratospheric gases: Validation of HNO$_3$, *J. Geophys. Res., 2005.*

10. Kuttippurath, J., J. Notholt and B.-M. Sinnhuber: Impact of meteorological analyses on the simulations of stratospheric trace gases, *J. Geophys. Res., 2005.*

Conference Proceedings

11. Kuttippurath, J., H. Bremer, A. Kleinböhl, H. Küllmann, J. Notholt, and K. Künzi: Seasonal and latitudinal distribution of stratospheric ozone: Observations and model calculations, *Proceedings of Quadrennial Ozone Symposium, 107p, 2004.*

12. Kuttippurath, J., A. Kleinböhl, H. Bremer, H. Küllmann, and J. Notholt: Validation of SCIA-MACHY ozone limb profiles by ASUR, *Proceedings of the Second Workshop on the Atmospheric Chemistry Validation of* ENVISAT *(*ACVE*-2), 3-7 May, Frascati, Italy,* ESA SP*-562, 2004.*

13. Kuttippurath, J., A. Kleinböhl, H. Bremer, H. Küllmann, M. von König, and K. Künzi: Stratospheric trace gas measurements by the Airborne Submillimeter Radiometer ASUR during SCIA-VALUE 2002 (Validation and Utilization of ENVISAT and SCIAMACHY data products), *Proceedings of* IGARSS *03, Paper: a06-04.pdf, 2003.*

14. Küllmann, H., **J. Kuttippurath**, H. Bremer, A. Kleinböhl, C. von Savigny, J. Notholt, and K. Künzi: Submillimeter measurements of O$_3$ and N$_2$O and a first Comparison with SCIA-MACHY Ozone Profiles, *5th German* SCIAMACHY *Validation Team Meeting, 7-9 December, 2004.*

15. Kleinböhl, A., **J. Kuttippurath**, H. Bremer, M. Sinnhuber, H. Küllmann, K. Künzi: Retrieval of mesospheric ozone profiles from airborne submillimeter measurements, *Proceedings of μrad04, 24-27 February 2004.*

16. Kllmann, H., A. Kleinböhl, H. Bremer, **J. Kuttippurath**, M. Sinnhuber, J. Notholt, and K. Künzi: Radiometry of atmospheric chemical composition from SOFIA, *Proceedings* SOFIA *Upper Deck Science Opportunities Workshop,* NASA *Ames Research Center, Moffett Field,* CA, *June 22-23, 2004.*

17. Cortesi, U., C. E. Blom, C. Camy-Peyret, K. Chance, J. Davies, F. Goutail, **J. Kuttippurath**, C. T. McElroy, F. Mencaraglia, H. Ölhaf, A. Petritoli, M. Pirre, J. P. Pommereau, F. Ravegnani, J. B. Renard and K. Strong: MIPAS ozone validation by stratospheric balloon and aircraft measurements, *Proceedings of the Second Workshop on the* ACVE*-2, 3-7 May, Frascati, Italy,* ESA SP*-56, 2004.*

Conference Abstracts

18. Kuttippurath, J., et al., Cross validation of ozone profiles from MIPAS, SCIAMACHY, OSIRIS and SMR by comparison with microwave measurements, *13th European Physical Society conference, Bern, Switzerland, 9 - 15 July, 2005.*

19. Kuttippurath, J., A. Kleinböhl, H. Bremer, B.-M. Sinnhuber, H. Küllmann, J. Notholt, K. Künzi, S. Davis, and M. Chipperfield: Measurements and model calculations of stratospheric trace gases: Implications for chemistry in the models, *European Geoscience Union (EGU), 2nd General Assembly, Vienna, Austria, 24 - 29 April, 2005.*

20. Kuttippurath, J., A. Kleinböhl, H. Bremer, K. Küllmann, J. Notholt, and K. Künzi: Measurements and model calculations of Nitrous oxide: Implications for stratospheric transport, *3rd SPARC General Assembly, Victoria, Canada, 1-6 August, Abstract No:10097, 2004.*

21. Kuttippurath, J., Kleinböhl, A., Bremer, H., Küllmann, H., von Savigny, C., and K. Künzi: SCIAMACHY Ozone limb profiles: First validation by ASUR, EGU *1st General Assembly, Nice, France, 25-30 April, EGU04-A-04222, 2004.*

22. Kuttippurath, J., H. Bremer, A. Kleinböhl, H. Küllmann and K. Künzi: Airborne microwave observations of stratospheric trace gases during SCIAMACHY validation campaigns, *Deutschen Physikalischen Gesellschaft, Mnchen, 22 - 26 March, UP 17.7, 2004.*

23. Kleinböhl, A., **J. Kuttippurath**, M. von König, H. Küllmann, and K. Künzi: Results of stratospheric trace gas measurements by ASUR in Arctic winter and spring 2002/2003, SOLVE 2/VINTERSOL, *Joint Science Team meeting, 21-24 October, Orlando, USA, 2003.*

24. Kleinböhl, A., **J. Kuttippurath**, M. von König, H. Küllmann, and K. Künzi: Preliminary results of stratospheric trace gas measurements by ASUR in Arctic winter and spring 2002/2003, *Geophysical Research Abstracts, Vol. 5, 30-1-2003, 2003.*

25. Bremer, H., A. Kleinböhl, **J. Kuttippurath**, H. Küllmann, and K. Künzi: Measurements of HCN, NO, and Ozone during the LEONID MAC CAMPAIGN 2002, *35th COSPAR Scientific Assembly, Paris, France, 18 - 25 July, Abstract No: 02835, 2004.*

26. Bremer, H., Kleinböhl, A., **Kuttippurath, J.**, Sinnhuber, M., Küllmann, H., and K. Künzi: Denitrification and increase of middle stratospheric Ozone and N_3O in the Arctic Winter 02/03, *European Geophysical Abstracts, EGU04-A-03704, 2004.*

27. Küllmann, H. Bremer, A. Kleinböhl, **J. Kuttippurath**, A. Rozanov, and K. Künzi: Airborne microwave observations during SCIAMACHY validation campaigns: first results, *Geophysical Research Abstracts, Vol. 5, 1607-7962/gra/EAE03-A--11750, 30-1-2003, 2003.*

28. Bremer, H., et al (including **J. Kuttippurath**): SCIAMACHY Validation with the DLR Falcon, *Proceedings 16th ESA Symposium on European Rocket and Balloon Programmes and Related Research, St. Gallen, Switzerland, 2-5 June, ESA SP-530, 2003.*

29. Fix, A., Flentje, H., Ehret, G., Kllmann, H., Bremer, H., Kleinbï£¡l, A., **Jayanarayanan K**, Notholt, J., Knzi, K., Bruns, M., Wang, P., Richter, A., Gurlit, W., Gerilowski, K., Burrows, J.P., Heue, K., Platt, U., Pundt, I., Wagner, T.: SCIAMACHY *and* MIPAS *Validation with the* DLR *Falcon Aircraft. Envisat Validation Workshop,* ESRIN*, Frascati, Itali, 9-13 December, 2002.*

2 Acronym

Acronym	
ADEOS	Advanced Earth Observing Satellite
AMAXDOAS	Airborne Multiaxis Differential Optical Absorption Spectrometer
AMV	Altitude of Maximum Volume mixing ratio
ASUR	Airborne SUbmillimeter Radiometer
ASHOE	Airborne Southern Hemisphere Ozone Experiment
ATMOS	Atmospheric Trace Molecule Spectroscopy
CLAES	Cryogenic Limb Array Etalon Spectrometer
CPU	Central Processing Unit
CRISTA	CRyogenic Infrared Spectrometers and Telescopes for the Atmosphere
DAO	Data Assimilation Office
DASA	Daimler Chrysler Aerospace
DLR	Deutschen Zentrum fr Luft- und Raumfahrt
ECMWF	European Centre for Medium-Range Weather Forecasts
ENVISAT	ENVIronmental SATellite
ERS	European Remote sensing Satellite
EUPLEX	European Polar Stratospheric Cloud and Lee Wave Experiment
GCM	General Circulation Model
GISS	Goddard Institute for Space Studies
HALOE	Halogen Occultation Experiment
HYSPLIT	HYbrid Single-Particle Lagrangian Integrated Trajectory
ILAS	Improved Limb Atmospheric Spectrometer
IMK	Institut fr Meteorologie und Klimaforschung
IUP	Institut fr Umweltphysik
JPL	Jet Propulsion Laboratory
KIMRA	Kiruna Microwave Radiometer
KNMI	Koninklijk Nederlands Meteorologisch Instituut
LIDAR	LIght Detection And Ranging
MAESA	Measurements for Assessing the Effects of Stratospheric Aircraft
MIRA	Millimeter wave RAdiometry
MIPAS	Michelson Interferometer for Passive Atmospheric Sounding
MPV	Modified Potential Vorticity
MSIS	Mass Spectrometer Incoherent Scatter
NCEP	National Centers for Environmental Prediction
NDSC	Network for the Detection of Stratospheric Change
NOAA	National Oceanic and Atmospheric Administration
OLEX	Ozone Lidar Experiment
PAVE	Polar Aura Validation Experiment
OSIRIS	Optical Spectrograph and InfraRed Imager System
POAM	Polar Ozone and Aerosol Measurement
RAM	Radiometer for Atmospheric Measurements

continued

continued

Acronym

READY	Real-time Environmental Applications and Display sYstem
SAGE	Stratospheric Aerosol and Gas Experiment
SAMS	Stratospheric And Mesospheric Sounder
SCIAMACHY	Scanning Imaging Absorption Spectrometer for Atmospheric CHartographY
SCIAVALUE	SCIAMACHY VALidation and Utilization Experiment
SHADOZ	Southern Hemisphere Additional Ozonesondes
SMR	Submillimeter Radiometer (on Odin)
SOLVE	SAGE III Ozone Loss and Validation Experiment
THESEO	Third European Stratospheric Experiment on Ozone
UARS	Upper Atmospheric Research Satellite
UCI	University of California at Irvine
UK	United Kingdom
UKMO	UK Met Office
VINTERSOL	Validation of International Satellites and study of Ozone Loss
VMR	Volume Mixing Ratio
WMO	World Meteorological Organization

3 Acknowledgment

4 Preface

A freezing fear over an abrupt climate shift sometime in the distant future and the imposing challenges in predicting the 'upcoming' chilling event are the thriving quest and the heart and soul of research studies in the field of the atmosphere and the Earth sciences these days. The processes like atmospheric pollution, ozone depletion, and changes in the Brewer-Dobson circulation are some of the vital aspects of the entire climate process. The polar ozone depletion and related environmental issues are the examples of a regional scale phenomena which has a global impact. The regional and small scale scientific studies focused on different aspects of various components of the climate system are very important since the studies of all the components as a whole is impossible in a single turn. Thus, each and every component of the system being analyzed separately and then integrate to a single matrix. This integration is usually carried out with global climate models. Hence, in order to understand the climate processes, the current situation demands reliable observations and capable numerical models. This study address the issues in a stratospheric chemistry and dynamics perspective, which is apparently one of the critical components of the climate system, with observations from the airborne submillimeter wave measurements and with simulations using the Bremen chemical transport model.

How good is the linearized ozone chemistry/parameterized chemistry schemes to be integrated in the chemistry and climate models for long term trend analyses? What is the impact of meteorological analyses on the simulations of the stratospheric trace gases? Is there any bias in the stratospheric N_2O and NO_y mixing ratio distribution simulated with parameterized chemistry scheme? How the chemistry, transport and mixing barriers are represented in the current stratospheric chemical transport models? These are some of the specific questions that are answered with this study. In addition, this work also corroborate the capabilities of the airborne microwave measurements to be used for validating spaceborne sensors, diagnosing model simulations and to be employed for studying temporal and spatial variabilities in the trace gas distributions associated with chemistry and transport processes in the stratosphere.

Abundance of stratospheric ozone depends on many factors. The natural and anthropogenic influence on ozone is well understood now. However, the stratospheric ozone layer is to be monitored to study the evolution and future climate scenarios. Besides the polar ozone loss there is also a negative trend (4%) in the mid-latitude ozone, which is a major concern before the scientific community. A considerable number of groundbased, airborne, shipborne, and spaceborne sensors have been deployed to monitor ozone and other atmospheric constituents. These constituents are mostly related to the chemistry of atmospheric ozone ever since the groundbreaking discovery of the Antartic ozone hole (Farman et al., 1985). The Environmental Satellite (ENVISAT) and the Odin satellites are the new missions towards the continuous and better understanding of the Earth's atmosphere. However, data from these sensors have to be validated with accurate and proven instruments. SCIAVALUE (SCIAMACHY - Scanning Imaging Absorption Spectrometer for Atmospheric ChartographY - Validation Uti-

lization Experiment) was a part of the airborne campaign to validate the SCIAMACHY sensor aboard ENVISAT. Apart from its usage to examine the spaceborne sensors, the potential scientific applications to address specific issues in the stratospheric research is discussed within the framework of this thesis.

A large amount of data observed from a variety of platforms ranging from groundbased sensors to spaceborne systems are employed in this study. Data from the instruments OLEX (Ozone Lidar Experiment), MIRA-2 (Millimeter wave RAdiometer) and RAM (Radiometer for Atmospheric Measurements), a number of ozonesondes from NDSC (Network for the Detection of Stratospheric Change) and SHADOZ (Southern Hemisphere Additional Ozonesondes) clusters, ATMOS-3(Atmospheric Trace Molecule Spectroscopy), CRISTA-1(CRyogenic Infrared Spectrometers and Telescopes for the Atmosphere), and 2, HALOE (Halogen Occultation Experiment), POAM-3 (Polar Ozone and Aerosol Measurement), MIPAS (Michelson Interferometer for Passive Atmospheric Sounding), OSIRIS (Optical Spectrograph and InfraRed Imager System), SCIAMACHY and SMR (Submillimeter Radiometer) satellite sensors, ECMWF (European Center for Medium-Range Weather Forecasts), MSIS (Mass Spectrometer Incoherent Scatter model), NCEP (National Centers for Environmental Prediction) and UKMO (United Kingdom Met Office) meteorological analyses, UB (University of Bremen), HALOE v18, and KNMI (Koninklijk Nederlands Meteorologisch Instituut) ozone climatologies, and CLAES (Cryogenic Limb Array Etalon Spectrometer) N_2O climatology are exploited to cater various needs of this work. In addition, a suite of models comprising the CTMs (Chemical Transport Models) SLIMCAT, UCI (University of California at Irvine) and UCI GISS-II (UCI model with Goddard Institute for Space Studies winds), the forward models ARTS (Atmospheric Radiative Transfer System) and *'the Forward'*, the trajectory model HYSPLIT READY (HYbrid Single-Particle Lagrangian Integrated Trajectory - Real-time Environmental Applications and Display sYstem) have been used for various studies. Furthermore, the ASUR trace gas measurements from the EUPLEX (European Polar Stratospheric Cloud and Lee Wave Experiment), the SCIAVALUE, the SOLVE (Stratospheric Aerosol and Gas Experiment - Ozone Loss and Validation Experiment) and the latest PAVE (Polar Aura Validation Experiment) campaigns are taken as well. However, only references are cited for these datasets wherever applicable. For a detailed description of the campaigns, the measurements, the models, and the sensors, the reader is referred to the references noted in the relevant section.

A terse note on the stratospheric chemistry and dynamics is presented in *Chapter 5* to follow the rest of the thesis.

The airborne submillimeter radiometer is a unique instrument for atmospheric sounding. It inherits the legacy of an operational span of more than 14 years since 1991. The instrument paved the way to present many interesting scientific results in the arena of atmospheric science research and the contributions still continue to be unabated. A concise picture of the instrument, retrieval theory and inversion procedure applied to ASUR are introduced in *Chapter 6*.

Retrieval of the ASUR quasi-operational molecules ozone, ClO, HCl, HNO_3 and N_2O are presented in *Chapter 7*. As the sensor is operated on a campaign basis, SCIAVALUE, EUPLEX, and PAVE oriented trace gas retrievals are discussed in detail. Since the retrievals south of 45°N are for the first time from the ASUR measurement spectra, these retrievals have a special significance. In order to check the quality and consistency of the retrievals, intercomparison with other measurements and models calculations are also carried out. Moreover, intercomparison of the trace gas VMRs retrieved with two different radiative transfer models are discussed as

well. The error analysis related to the retrievals, the retrieval comparions and discrepancies are critically discussed in a following section.

Assessment of ozone profiles retrieved from MIPAS and SCIAMACHY on ENVISAT, OSIRIS and SMR on Odin satellite sensors with ASUR ozone and the cross-validation are presented in *Chapter 8*. The SCIAVALUE and the EUPLEX data are exploited for this study. The N_2O, HNO_3 and ClO measurement comparions with MIPAS and SMR data are performed in *Chapter 9*.

Studies of chemical morphology and transport processes in the atmosphere largely depend on global model calculations. Synthetic simulations of the state of the atmosphere with the models fill gaps between the limitations imposed by existing measurement systems, reach out all over the globe (within the span of the model grids) especially to the places where observations are infrequent, rare, or impossible and predicts tomorrow's atmosphere in a calculated perspective on the current state of knowledge. The model simulations are also extensively used to interpret observed features. Thus, the models that can imitate the measurements are powerful and inevitable tools in the arena of atmospheric research. *Chapter 10* introduces a new chemical transport model (CTM), the Bremen CTM (CTMB). A general introduction to the model, the chemistry schemes incorporated for the simulations of ozone, N_2O and NO_y, the limitations and advantages of the parameterized chemistry schemes are discussed in this section.

Simulated results are to be evaluated to understand the nature and accuracy of the calculations. The validation process helps to find out possible problems and biases in the simulated results. An assessment of the CTMB simulations are carried out in *Chapter 11* using an enormous amount of data gathered from various platforms ranging from groundbased to spaceborne sensors, climatologies and other model calculations.

As the trace gas distribution in the stratosphere is greatly influenced by the meridional circulation, most constituents show a prominent seasonal cycle. The mixing ratio distribution at a specific location will be in accord with a mixture of the chemistry and transport processes if the photochemical lifetime of the constituents is shorter than the transport time scale (eg: O_3). If the lifetime of a constituent is greater than that of the transport time scale, then its VMR distribution is solely determined by the transport processes (eg: N_2O). *Chapter 12* explores capabilities of the ASUR sensor to observe the minute details of the chemistry and transport processes in the stratosphere by canvassing the features of the latitudinal, longitudinal and seasonal variations of several constituents.

Comparisons of the measured features with simulated results are one of the best ways to diagnose model simulations and the real appreciation of measurements lies in its applicability of this sort too. The CTMB and the SLIMCAT calculations are used for the interpretation of the measured features. The discrepancies are discussed in terms of the chemistry and transport processes in the models.

The stratospheric transport process deduced from ASUR N_2O data are presented in *Chapter 13*. The tropical upwelling and its seasonal variations, the surf-zone, subtropical and polar barriers are delineated from the observations. The rapid meridional transport of the Arctic airmasses into northern mid-latitude in September 2002 and a similar airmass transport from subtropical to the Arctic in January 2003 are also discussed.

Chapter 14 summarises the main conclusions of this study.

5 Physics and chemistry of the stratosphere

A laconic description of the physical and chemical state of the middle atmosphere, the strato-sphere in particular will be drawn in this chapter. Only the processes which are relevant to follow the work will be covered.

5.1 The stratospheric physics

The vertical structure: The atmosphere is conveniently divided in the vertical into different layers in accordance with the temperature structure of each layer. The lowest layer is called the troposphere where the temperature decreases with altitude. The top of the troposphere, the tropopause, is not a sharp boundary as it varies from low to high latitudes. On average the height of the troposphere is 16 km in the tropics, 13 km in mid-latitudes, and 8 km in high latitudes. The lowest tropopause temperatures can be as low as 195 K and it is found at the tropical tropopause. All weather processes happen in this region of the atmosphere. Above the troposphere, the altitude from the tropopause to 48 km is called the stratosphere in which the temperature increases with height. This is the region where 90% of the atmospheric ozone resides. Since ozone has the capacity to absorb solar radiation, it heats up the atmosphere. So the stratospheric temperature increases with altitude. Above the stratopause, the region where the stratosphere ends (~ 50 km), the mesosphere starts. The temperature again decreases with altitude in the mesosphere. Polar mesospheric clouds, auroral activities, solar proton events and meteoritic showers are observed in this region. Gravity waves in the mesosphere impart a great momentum for the mesospheric circulations. The rest of the section of the atmosphere, shown in Figure 5.1, is not relevant to this work and will not be covered.

The trace gases: The gases in the atmosphere in small amounts are called trace gases. Though the amounts of these gases are very small, they play a vital role in the physics and chemistry of the atmosphere. The gases are generally scaled in their number density or volume mixing ratios (VMRs). Number density is the number of molecules per volume and volume mixing ratio is the ratio of the number of molecules to the total number of molecules in a given volume. The number density can be calculated from the volume mixing ratio. That is,

$$\mu = \frac{\eta k_B T}{p} \tag{5.1}$$

where, μ is the volume mixing ratio, η is the number density of the molecule, T is the temperature, p is the pressure, and $k_B = 1.38 \times 10^{-23}$ JK^{-1} is the Boltzmann constant.

Since VMR does not depend on air parcel as it is a ratio to total air density, it is conserved in all atmospheric motions. Thus, VMR is employed in most analyses of transport studies. The constant VMR surfaces are called isopleths. The vertical integral of the number density is called the column of the trace gas. The ozone column is expressed in Dobson Unit (DU) (after Gordon Miller Bourne Dobson, $1\text{DU} = 2.69 \times 10^{16}$ molecules cm^{-2}).
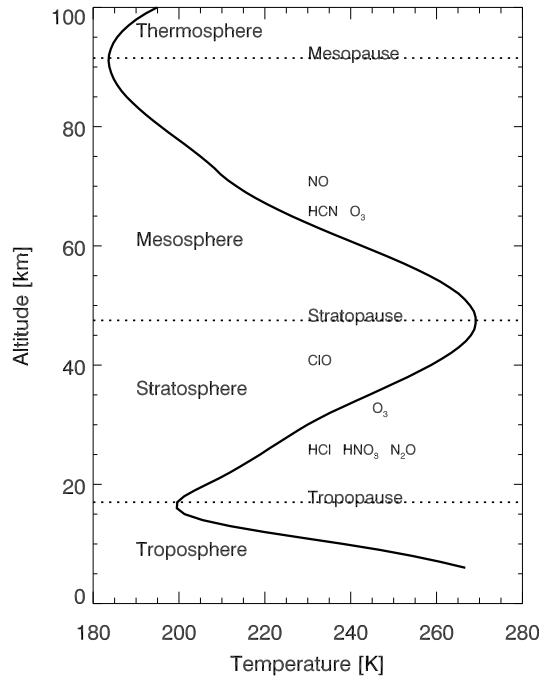
Figure 5.1: The vertical structure of the atmosphere derived from a tropical Mass Spectrometer Incoherent Scatter (MSIS) (Hedin, 1991) model profile for 25 September 2002. It has been divided in to different layers according to the temperature in each layer. The quasi-operationally molecules that ASUR can measure in the stratosphere and some of the molecule that can measure in the mesosphere are also noted.

Transport processes: Movements in the atmosphere are collectively called atmospheric transport. Different kinds of motions are present in the atmosphere and are related to the transport of air parcels. An air parcel is an entity which always posses the same number of molecules. Following is a short introduction of the co-ordinates for the transport processes in the stratosphere.

Atmospheric pressure decreases exponentially with altitude. Most of the atmospheric motions are solely related to the pressure gradient forces described by the hydrostatic equilibrium between the pressure gradient force and gravity. Thats is,

$$\frac{\partial p}{\partial z} = -\rho g \tag{5.2}$$

where p is the pressure, z is the altitude, ρ is the density of air, and g is the gravitational constant (g=9.8 ms^{-2}). Atmospheric transport studies, which are related to mass conservations use pressure as the vertical co-ordinate.

Thermodynamic processes which take place without heat exchange are called adiabatic processes. Interestingly, most stratospheric processes are *adiabatic* in the order of a few days. The potential temperature (Θ) is the temperature an air parcel would have if brought adiabatically to standard pressure surface (1000 hPa). Isentropes are the surfaces of constant potential temperature, Theta (Θ) can be defined as (Holton, 1992),

$$\Theta = T\left(\frac{P_0}{P}\right)^k \tag{5.3}$$

where P is the local pressure, T is the local temperature, P_0 is the standard pressure (1000 hPa), and $k = \frac{R}{C_p} = \frac{2}{7}$, where R is the universal gas constant and C_p is the specific heat capac-

ity at constant pressure. Potential temperature is conserved in adiabatic processes. Chemical transport models often use isentropes as a vertical coordinate since the vertical transport is purely diabatic.

In a similar fashion the potential vorticity (PV) is used as a co-ordinate in the horizontal direction when dealing with the polar vortex processes. After Holton (1992) the potential vorticity P can be defined as,

$$P = (\xi_p + f) g \frac{\delta\theta}{\delta p} \tag{5.4}$$

where, ξ_p is the angular velocity and f is the coriolis parameter. The vertical component of the relative vorticity evaluated on an isentropic surface θ is constant.
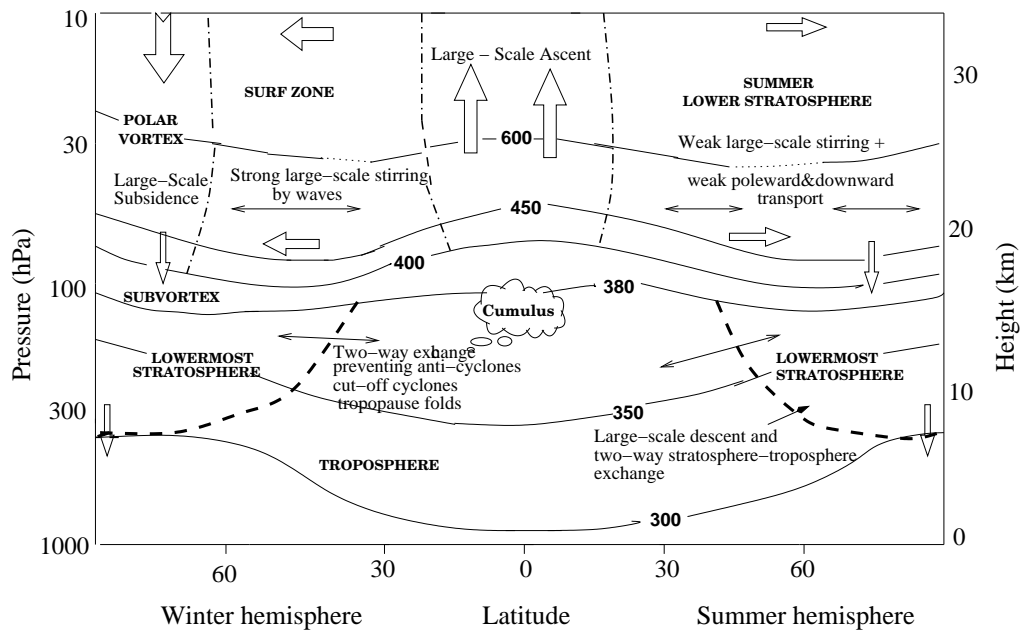
Figure 5.2: A schematic representation of the stratospheric circulation in the summer and winter hemispheres. The important dynamical features in the stratosphere are marked in the relevant sections. The size of the arrow indicates the relative strength of the transport as well. The work is modified from Haynes and Shuckburgh (2000a) and from Holton (1995).

Meridional circulation: The meridional circulation in the stratosphere comprises a two cell-structure in the lower stratosphere, with upwelling in the tropics and subsidence in the middle and high latitudes and a single cell from the tropics to the winter hemisphere at higher altitudes (Plumb, 2002). The circulation depends on the differential heating of the atmosphere and on the planetary-scale Rossby waves. The difference in solar heating from the equator to the pole, together with infrared cooling to the atmosphere results in a pressure gradient on cyclostrophic balance producing the zonal flow. When the amplitude of a planetary wave in the winter hemisphere gets large enough, it breaks at the tropical tropopause and induces a momentum to stir and drive the air masses away from the region. This results into an ascending motion of the airmasses in the tropics, drifting through the midlatitude surf-zone to the high latitudes and descending as cold airmasses at the poles. This over turning circulation is known as the Brewer-Dobson circulation. A schematic description of the processes is depicted in Figure 5.2

The polar vortex: The polar vortex is a strong area of high pressure at the surface of the tropopause and a cutoff low above the surface in a cold polar stratosphere. Due to the radiative cooling and the absence of solar heating in the winter polar regions a strong temperature gradient is formed. The temperature gradient together with the coriolis force drive a quasi-zonal cyclonic circulation over the pole with an area of relatively still air in its center. The zonal flow with the high band of winds is called the polar jet. The polar jet makes a dynamical barrier between the mid-latitudes and the polar regions with high wind velocities, which prevents horizontal exchange of airmasses across the barrier. Thus, the air inside the vortex is effectively isolated from the air outside. As a result, chemical states of stratospheric constituents might be different inside and outside the vortex region.

5.2 The stratospheric chemistry

Ozone chemistry: Ozone is produced in the stratosphere primarily through the photolysis of molecular oxygen. The wavelength region restricts the altitude of the formation of this molecule mainly due to ozone and oxygen absorption. The relevant reactions are shown below.

$$O_2 + h\nu \rightarrow O + O \qquad\qquad \lambda \leq 242 \ nm \tag{5.5}$$

$$O + O_2 + M \rightarrow O_3 \tag{5.6}$$
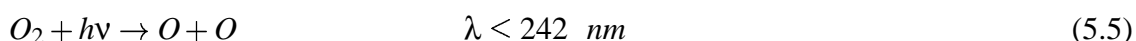
where M is an air molecule needed for the conservation of momentum. At higher wavelengths it is destroyed through the following photolytic processes.

$$O_3 + h\nu \rightarrow O_2 + O(^3P) \qquad\qquad \lambda \leq 1100 \ nm \tag{5.7}$$

$$O_3 + h\nu \rightarrow O_2 + O(^1D) \qquad\qquad \lambda \leq 310 \ nm \tag{5.8}$$
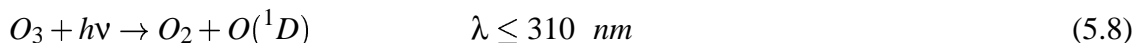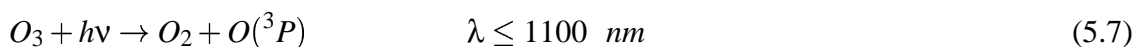
The excited state $O(^1D)$ can relax to the ground state $O(^3P)$ by collision as follows,

$$O + O_3 \rightarrow O_2 + O_2 \tag{5.9}$$

$$O + O + M \rightarrow O_2. \tag{5.10}$$

The above cycle of reactions are called the Chapman cycles. However the Chapman's pure oxygen chemistry was not enough to explain the observed ozone profile, which had significantly lower ozone values. Later it was discovered that the cycle includes a number of catalytic reactions to destroy ozone,

$$X + O_3 \rightarrow XO + O_2 \tag{5.11}$$

$$XO + O \rightarrow X + O_2 \tag{5.12}$$

$$net : O + O_3 \rightarrow O_2 + O_2. \tag{5.13}$$

Here the X can be H, OH, NO, Cl or Br. Since the formation of ozone is controlled by the wavelength dependent photolysis reactions, the process is confined to certain heights in the atmosphere. As the UV is the highest in the tropics, the tropical middle stratosphere has the maximum ozone mixing ratios (around 33 km). Since the number density depends on the density of the air, number density of the molecule is maximum at the lower altitudes, around 25 km. The lifetime of the molecule is about 6 months in the lower, weeks in the middle and days in the upper stratosphere. However, in the polar vortex conditions the lifetime of the molecule is in the order of a year (Proffitt et al., 1989).

N$_2$O chemistry: N$_2$O is mainly produced by complex nitrification and denitrification process in the tropical soils. Ocean emissions and biomass burning are the other major processes that produce N$_2$O. The molecule is inert and well-mixed in the troposphere. The major sink is the photodissociation in the stratosphere and the reaction with $O(^1D)$ in the tropical middle and upper stratosphere. The reaction follows,

$$N_2O + h\nu \rightarrow N_2 + O(^1D). \qquad\qquad \lambda \leq 230 \;\; nm \qquad\qquad (5.14)$$
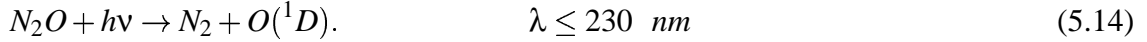
This reaction accounts for 90% of the total sink. The reaction with excited atomic oxygen accounts for the rest 10%,

$$N_2O + O(^1D) \rightarrow 2NO \qquad\qquad (58\%) \qquad\qquad (5.15)$$

$$N_2O + O(^1D) \rightarrow N_2 + O_2. \qquad\qquad (42\%) \qquad\qquad (5.16)$$
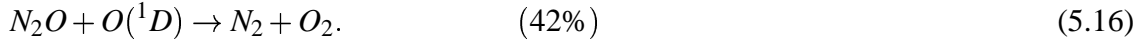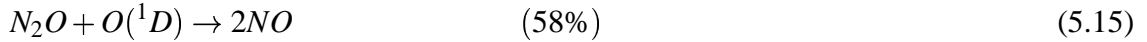
Oxidation of nitrous oxide by $O(^1D)$ yields Nitric oxide (NO). This is the major reaction that injects NO to the stratosphere. Thus, it acts as a major source of NO$_x$ in the stratosphere. The NO$_x$ cycle plays an important role in the catalytic destruction of ozone in the stratosphere. Because of its green-house effect, it also serves as a climate relevant gas. N$_2$O VMR is maximum in the tropical lower stratosphere and gradually decreases with altitude as the photolysis takes place in the upper stratosphere. The lifetime of the molecule in the troposphere is estimated to be 120 years (WMO, 2002).

HNO$_3$ chemistry: HNO$_3$ is a molecule of great interest in the stratosphere since it catalytically controls the ozone abundance (22-40 km) and is a reservoir of the odd nitrogen (Brasseur et al., 1999). Nitric acid (HNO$_3$) in the stratosphere is formed primarily by a homogeneous three-body reaction. That is,

$$NO_2 + OH + M \rightarrow HNO_3 + M \qquad\qquad (5.17)$$

and is destroyed by photolysis

$$HNO_3 + h\nu \rightarrow OH + NO_2 \qquad\qquad (5.18)$$

and reaction with OH

$$HNO_3 + OH \rightarrow NO_3 + H_2O. \qquad\qquad (5.19)$$

The HNO$_3$ photolysis takes place in the wavelength region between 200 and 320 nm. The molecule has its maximum VMR in the high-latitude winter lower stratosphere. Since the tropical stratosphere is very conducive for its photolytic destruction, the lowest mixing ratios are found in the low latitudes. The photochemical lifetime of HNO$_3$ is in the order of weeks in the lower stratosphere and days in the upper stratosphere.

5.3 Summary

This chapter gives a brief introduction to the basics of the stratospheric physics and chemistry. The vertical structure of the atmosphere, the meridional circulation, and polar vortex are only mentioned. Since the thesis is dealing with stratospheric ozone, nitrous oxide and nitric acid chemistry, those subjects with relevant importance are also been presented. Though this work includes chemical transport modeling, introduction to that subject is leaving in the reference mentioned here. For a detailed description on the stratospheric chemistry, physics, and chemical transport modeling the reader is referred to Brasseur and Solomon (1984), Wayne (1991), Holton (1992), and Andrews (2000).

6 The ASUR sensor: Characteristics, retrieval and inversion theory

Since the study mostly deals with the measurements from ASUR, this chapter gives a brief introduction to the instrument, its measurement features, and the inversion theory applied to the sensor.

6.1 Measurement principle

Heterodyne theory: ASUR is a passive heterodyne receiver operating at frequencies between 604.3 and 662.3 GHz, which corresponds to wavelengths of about 0.5 mm. The sensor makes use of the heterodyne principle to detect radiation. Reginald Aubrey Fessenden (1866-1932), a Canadian engineer is the inventer of the heterodyne principle. A heterodyne system is, being employed to generate new frequencies by mixing two or more signals in a nonlinear device such as a vacuum tube, transistor, or diode mixer. In this process, the received radio frequency (RF) signal is down converted into lower frequencies (intermediate frequency-IF) without loosing information such as spectral shape or spectral intensity. Thus, it makes it possible to amplify, filter and analyse the spectral band using electronic devices. This principle can be formulated as

$$\nu_{IF} = \nu_{LO} - \nu_{RF,LSB} \quad and \quad \nu_{IF} = \nu_{RF,USB} - \nu_{LO}. \tag{6.1}$$

Where, ν_{IF} is the intermediate frequency, ν_{LO} is the LO signal, ν_{RF} is the signal frequency, LSB is the lower sideband, and USB is the upper sideband.

The output frequencies contain information from both upper and lower sidebands of the receiver. If both sidebands be converted with comparable intensity the receiver works in double sideband mode (DSB). If one of the sidebands is suppressed the receiver works in single sideband mode (SSB). One of the two Martin Pupplet Interferometers (MPIs) in ASUR acts as the SSB filter and suppresses the unwanted frequency. These optical systems are generally designed to work with Gaussian beams at millimeter and submillimeter wavelengths. Separation of the beams is done by a grid that splits the beam into two perpendicular polarized beams. The beams are reflected by mirrors that turn the polarization such that they interfere after passing through the grid again. The distance between the mirrors and the grid are chosen in a way that, in one sideband a constructive interference and in the other sideband a destructive interference is to take place. The constructive sideband is termed as the signal band and the destructive sideband is called the image band.
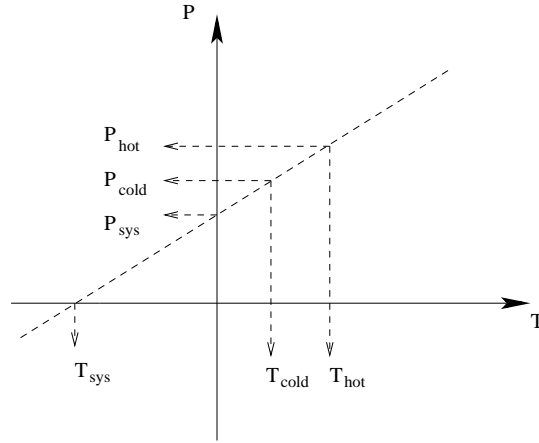
Figure 6.1: The definition of the system noise temperature of a total power receiver.

6.2 Calibration

The detected signal (power, P) is the sum of the atmospheric signal (antenna power, P_{ant}) collected by the antenna and the radiometric noise (system power, P_{sys}) caused by the receiver components. That is,

$$P = P_{ant} + P_{sys}. \tag{6.2}$$

Applying the Nyquist theory and assuming the validity of the Rayleigh-Jeans approximation, which holds at submillimeter frequencies around 650 GHz (Urban, 1998), result in a relationship between the radiated power P and the temperature of a blackbody T. That is,

$$P = k_B T \Delta(\nu) \tag{6.3}$$

where, k_B is the Boltzmann Constant and $\Delta(\nu)$ is the bandwidth. The equation states the relation between noise power and noise temperature,

$$T = T_{ant} + T_{sys}. \tag{6.4}$$

Since it is impossible to distinguish between the two noise terms P_{ant} and P_{sys}, a calibration procedure is needed to separate the atmospheric signal from the receiver noise. A schematic representation of the calibration procedure is illustrated in Figure 6.1. The ASUR receiver is a *Total Power receiver* and the calibration is done by observing the radiation from hot (P_{hot}, ambient temperature) and cold loads (P_{cold}, 77 K-liquid nitrogen temperature). Then the atmospheric temperature T_{atm} is

$$T_{atm} = T_{cold} + (P - P_{cold}) \frac{T_{hot} - T_{cold}}{P_{hot} - P_{cold}}. \tag{6.5}$$

The Y factor method can be used to find the T_{sys}. If $P_{hot.sys}$ and $P_{cold.sys}$ are the power at hot and cold temperatures respectively then,

$$Y = \frac{P_{hot.sys}}{P_{cold.sys}}. \tag{6.6}$$

The calibration allows to determine the noise of the system. This can be stated as,

$$T_{sys} = \frac{T_{hot.ant} - Y T_{cold.ant}}{Y - 1}. \tag{6.7}$$
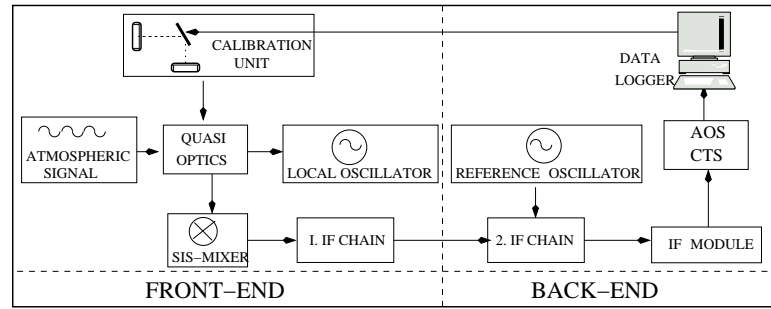
Figure 6.2: The general setup and prime components of the ASUR sensor.

$T_{hot.ant}$ and $T_{cold.ant}$ are the physical radiative temperatures of the hot and cold loads. The sensitivity of the radiometer can be found using the *radiometer formula*,

$$\Delta T_{sig} = \frac{K T_{sys}}{\sqrt{\Delta \nu \tau}} \tag{6.8}$$

where, ΔT_{sig} is the minimum detectable signal, K is a constant determined by the receiver type. For a total power receiver like ASUR, $K = 1$ and τ is the integration time.

6.3 Radiometer components

The main parts of the radiometer are divided into two sections called the front-end and the back-end. The calibration unit, quasi-optical bench, the SIS mixer, 1st LO, and 1st IF chain are in the front-end. The back-end consists of the 2nd LO, 2nd IF chain, the spectrometers and the data logger system. A schematic representation of this set-up can be found in Figure 6.2.
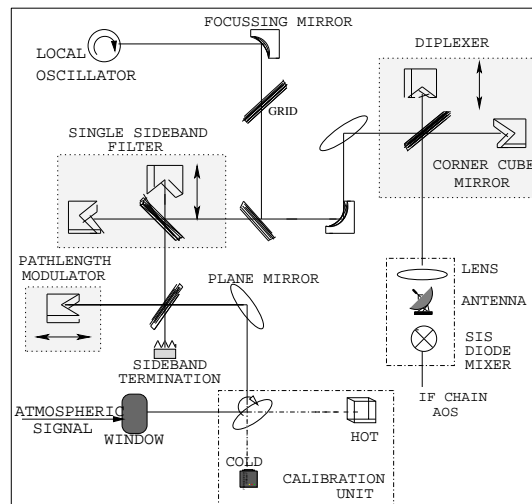
Figure 6.3: The key players in the quasi-optical bunch of the ASUR sensor.

Front-end: A special window made from the high density polyethelene (HDPE) is designed to fit the aircraft body to transit the atmospheric radiations. The transmissivity of this material is $0.9(\pm 0.01)$ at frequencies around 650 GHz. Since the observations have to be performed at a constant elevation angle, a mirror-control is employed in the quasi-optical bench. The mirror-control adjusts the deviation in the roll angle due to roll of the aircraft. The roll-angle

is also monitored by the navigation system of the aircraft and is recorded by the on-board system. The calibration of the signal needs hot and cold loads. The *dewar* contains liquid nitrogen which is lined with **Ecosorb** is the cold load. This AN-72 type ecosorb material has a reflectivity in the order of -26 dB around 650 GHz. The hot load is a plastic cube at ambient temperature. The PT-1000 type resistors are used to measure the temperature of the calibration loads. A pathlength modulator is applied to reduce standing waves. One of the MPIs serves as the diplexer and the other MPI acts as the SSB filter. A schematic representation of the quasi-optical components are shown in Figure 6.3 and the working principle of the IF chain is presented in Figure 6.4. The detector is a superconductor-insulator-superconductor (SIS) junction (as shown in Figure 6.5), cooled to the liquid helium temperature (4 K). Mixers of this kind provide very low system noise temperature as compared to other techniques like Schottky diodes.
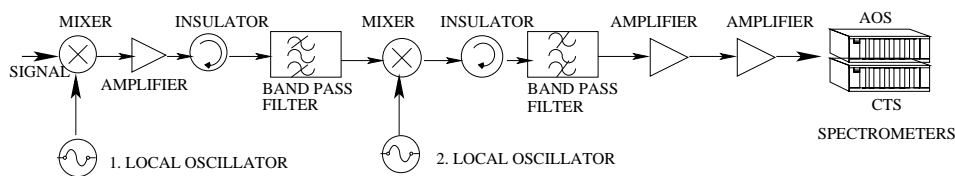
Figure 6.4: A schematic representation of the working principle of the ASUR IF chain.

Back-end: There are two spectrometers the acousto-optical spectrometer (AOS), and the chirp-transform spectrometer (CTS) in the ASUR back-end. Table 1 summarises the important specifications of these spectrometers.

The **AOS** was developed by the Observatoire de Paris-Meudon in 1994. The total bandwidth of the instrument is 1.5 GHz and the resolution is 1.26 MHz. It has 1758 channels with 0.89 MHz spacing between them. The spectrometer is equipped with a comb generator that generates $\delta - shaped$ signals of 100 MHz spacing which are used for frequency calibration. Frequent calibrations are done during measurement flights to account for temperature drifts of the optical components. Stratospheric measurements with the AOS are analyzed for this study.

The **CTS** was developed by Deutsche Aerospace (DASA, now: EADS Astrium) in 1994. It has a bandwidth of 178 MHz in 640 channels with a spacing of 278 kHz. The center frequency of the CTS can also be adjusted to the frequencies other than the center frequency of the AOS using a frequency synthesizer. By connecting a frequency synthesizer to the CTS input, δ signals of 30 MHz are generated, which are used for the frequency calibration of the CTS. Only one calibration per flight is performed because of the high frequency stability of the spectrometer.

6.4 Working procedure

The radiation enters the quasi-optical system through the HDPE aircraft window. The rotatable mirror switches between the atmospheric and calibration signals sequentially as *hot* ⤳ *atmosphere* ⤳ *cold* ⤳ *atmosphere* ⤳ *hot* ⤳ *...* At each position the radiation is integrated for two seconds. The radiation passes through a pathlength modulator, which is designed to reduce standing wave formation, to the first of the two MPIs. The MPI serves itself as the SSB filter. By adjusting the phase shift in the interferometers, the desired frequencies are suppressed in the order of 20-30 dB. The second MPI is the diplexer which injects the signal from
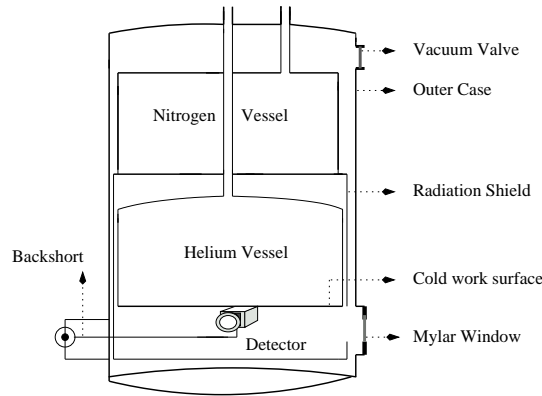
Figure 6.5: The cryogen container of the ASUR sensor and the important parts.

the first LO into the signal path. The heterodyned signal enters the SIS detector. In order to achieve a very low system noise temperature the first amplifier is also cooled down to the liquid helium temperature. After the first mixing and amplification processes, the signals of frequency 11.08+2.77 GHz and 11.08-2.12 GHz are obtained. These signals are subsequently amplified and heterodyned with a second oscillator at 14.78 GHz resulting in the front-end output signal with a frequency of 3.7($\pm$1.0) GHz. Further mixing processes take place in the back-end, where an LO at 6 GHz down converts the received signal into the input frequency of the AOS at 2.3 GHz. The tunable LO around 5.05 GHz heterodynes the input signal for the CTS at 1.35 GHz. The spectrometers detect the signal and the spectra are displayed and stored in the data logger system.

Feature	AOS	CTS
No. of channels	1754	640
Usable channels	1728	638
Center frequency	2.3 GHz	1.35 GHz
Bandwidth	1.26 GHz	178 MHz
Channel width	0.89 MHz	278 kHz
Resolution	~1.3MHz	278 kHz
Frequency linearity	$\pm$ 1 MHz	$\pm$ 200 kHz
	(cubic fit)	(linear fit)
Input level	-30 to 0 dBm	-25 to -10 dBm
Dynamic range	30 dB	15 dB

Table 6.1: The Specifications the ASUR spectrometers.

6.5 Retrieval theory

The radiative processes absorption, emission and scattering are the path ways through which the energy exchange happens. Bodies having a temperature above absolute zero emit radiation. Passive instruments like ASUR detect this emission, which contains information of the parameters concerned. The knowledge about the radiative transfer (RT) process is necessary to perform retrievals from remote sounding sensors. This section explores the theoretical aspects of the RT applied in the ASUR trace gas retrievals.
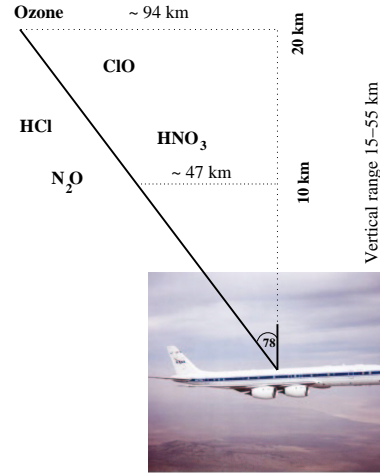
Figure 6.6: A schematic representation of the ASUR trace gas observation from an aircraft platform.

6.5.1 Radiative transfer

Although the RT in the atmosphere is governed by absorption, emission and scattering, the ASUR retrievals assume a non-scattering atmosphere for the RT calculations. In the submillimeter frequencies the Rayleigh scattering due to air particles is negligible. Since the measurements are carried out above the tropopause, the effects of clouds can be neglected as well. Nevertheless, as some of the observations are performed well below the tropical tropopause, the scattering on cirrus clouds may have a very small effect on the RT calculations. Since the particle sizes are very small, the scattering on cirrus clouds will be very small. A schematic representation of the ASUR trace gas observation from an aircraft is shown in Figure 6.6. Hence, taking only the absorption and emission into account the RT equation can be derived as,

$$\frac{dI\nu}{ds} \quad = \quad -\alpha_\nu I_\nu + S_\nu. \tag{6.9}$$

Here I_ν is the intensity of the radiation at the frequency ν, α is the absorption coefficient, and S_ν is sources of radiation. In the case of thermodynamic equilibrium, the radiation can be expressed in terms of the Kirchoff's and the Planck's law. As far as the ASUR frequencies are concerned, a thermal equilibrium can be assumed in the stratosphere. Hence, the term can be written in terms of frequency (ν) and temperature (T). Taking the Planck's function B and the speed of light c, the equation can be written as,

$$S_\nu \quad = \quad \alpha_\nu B_\nu \quad = \quad \frac{2h\nu^3}{c^2} \frac{1}{e^{\frac{h\nu}{k_B T}} - 1} \; \alpha_\nu. \tag{6.10}$$

The intensity of the radiation received by the sensor from the cosmic background I_0 at altitude h in the zenith direction can be stated as,

$$I_\nu \quad = \quad I_0 . e^{-\tau(h,\alpha)} + \int_h^\infty \alpha_\upsilon B(\nu,s) \; e^{-\tau(h,s)} \mathrm{ds}. \tag{6.11}$$

Here τ is the optical thickness between the altitudes h and s,

$$\tau(h,s) \quad = \quad \int_h^s \alpha_\nu(s\prime) ds\prime. \tag{6.12}$$

The unit of the measured intensity is the brightness temperature, which is adapted from the millimeter wave spectroscopy where the Planck's equation can be replaced by the Rayleigh-Jeans approximation.

Absorption coefficients: Absorption coefficient has to be calculated in order to solve the RT equation. The absorption coefficient is a comprehensive representation of the medium (air) and the electromagnetic field. The summation of the contribution from individual lines (line by line calculations) is the main part of the calculation. In addition, nonresonant absorption of water vapor, nitrogen and oxygen are also to be considered. However, both calculations are treated differently. Absorption coefficient of a molecule is defined by its line strength(S), the line shape describing the distribution in frequency $f(\nu, \nu_0)$, and its position given by the central frequency ν_0. Thus, the molecular absorption is given by the summation over the contribution from all transitions between the energy levels,

$$\alpha_\nu = n \sum_i^j f(\nu, \nu_0) \tag{6.13}$$

where n is the number of molecules and i and j are the indices of the upper and lower levels of the energy transition states. However, sometimes it will be more convenient to calculate the absorption cross-sections at each altitude levels. The ASUR retrievals use a scheme developed by von König (2001) to calculate the absorption cross-sections,

$$\alpha_h = \frac{\alpha_\nu}{n}, \tag{6.14}$$

where, α_h is the absorption crosssection at altitude h and n is the number of molecules to be considered in the calculations.

   Line strength: Line strength is the rate at which the transition from one state to another takes place. It depends on the nature of the molecule, population of the molecules in the transition levels and temperature of the system. At submillimeter frequencies, the thermodynamic equilibrium and hence a Boltzmann distribution can be assumed. Then the strength of the line is,

$$S_{ij} = \frac{8\pi^3 \nu_0 g_i g_j |\mu_{ij}|^2}{3hcQ(T)} E_t, \tag{6.15}$$

where

$$E_t = \left(e^{-\frac{E_i}{k_B T}} - e^{-\frac{E_j}{k_B T}} \right), \tag{6.16}$$

where g_i and g_j are the degeneracies, E_i, and E_j are energies of the states i and j, $|\mu|$ is the magnetic dipole of the molecule, and Q(T) is the partition function. The partition function can be expressed as,

$$Q = Q_{ele} Q_{rot} Q_{vib}. \tag{6.17}$$

The Q describe the internal energies of the molecule between the rotational Q_{rot}, vibrational Q_{vib} and electronic Q_{ele} states. These energy states are well separated as expressed in the above equation in which the nuclear spin has been included in the Q_{rot}. The Q_{ele} and Q_{vib} can be approximated as unity for the temperatures found in the atmosphere (the bending mode of N_2O is an exception to this since the degeneracy of the molecule is 2, instead of unity for Q_{vib}). The importance of the partition function lies on its control over the temperature dependence of the lineshape. The temperature dependence for the rotational partition function is

$$Q_{rot}(T) = Q_{rot}(T_0) \left(\frac{T}{T_0}\right)^n \tag{6.18}$$
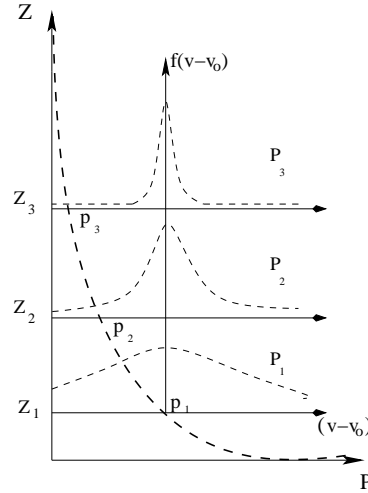
Figure 6.7: The pressure broadening with the altitude and its effect on the line shape are schematically represented.

where $n = 1$ for linear molecules (includes all diatomic molecules and some other molecules like CO_2 and N_2O). However, $n = 3/2$ for asymmetric molecules such as O_3, H_2O and NH_3.

Line shape: The shape of a spectral line is determined by natural, Doppler and pressure broadening mechanisms. The natural broadening is the result of the Heisenberg's uncertainty principle: The limited lifetime (τ) of an exited state leads to an uncertainty in the transition energy (ΔE) so that

$$\tau \Delta E = \frac{h}{2\pi}. \tag{6.19}$$

The natural line width need not be considered in the submillimeter spectroscopy in the atmosphere as it deals with rotational states.

Doppler broadening arises from the motions of the molecules themselves. This can happen even without pressure and natural broadening. It corresponds to thermal movement of the molecules in the atmosphere (thermal broadening) as well. The Doppler shift is the shift in the frequency (/wavelength) due to the relative motion of the molecule. This shift in the frequency produce the Doppler broadening. The associated velocity distribution is usually a Maxwell distribution, which results into a Gaussian line shape (GS),

$$f_D(\nu - \nu_0) = \frac{1}{\gamma_D \sqrt{\pi}} \, e^{\left(\frac{\nu - \nu_0}{\gamma_D}\right)^2} \tag{6.20}$$

where the Doppler width γ_D in terms of the molecular mass (m) is defined by

$$\gamma_D = \frac{\nu_0}{c} \sqrt{\frac{2k_B T}{m}}. \tag{6.21}$$

Pressure broadening is the result of frequent molecular collisions in the atmosphere. Since the collisions are frequent in the stratosphere, local thermo-dynamic equilibrium (LTE) can be assumed and the energy state can be approximated to follow a Boltzmann distribution. The simple illustration of this collision broadening is the Lorentz shape. The Lorentz function is expressed as,

$$f_L(\nu, \nu_0) = \frac{\gamma_L}{\pi} \frac{1}{\gamma_L^2 + (\nu - \nu_0)^2} \tag{6.22}$$

with the Lorentz width,

$$\gamma_L = \frac{1}{2\pi\tau}. \tag{6.23}$$

It is the measure of the distance of the half power point of the line and is called the Lorentz width (LW). The LW has a strong pressure dependence and is expressed as

$$\gamma_L \propto \frac{p}{T^2} \tag{6.24}$$

where p is the pressure (and T is the temperature) and hence the LW varies proportional to the pressure. The relationship is schematically shown in Figure 6.7.

In order to calculate line shapes with contributions from the stratosphere and the mesosphere a formulation is necessary, which contains both the Lorentian (pressure broadening) and the Gaussian (Doppler broadening) shape. The Voigt function is the convolution of these two line shape functions. Hence, the formulation is given by,

$$f_{voigt} = \int f_L(\nu,\nu')f_D(\nu',\nu_0)d\nu'. \tag{6.25}$$

The retrievals performed in this study use this line function calculated with an inhouse radiative transfer model using Drayson (1976).

Continuum: Between the observed and the calculated line spectra an offset exists based on the differences caused by the non-resonant absorption. This phenomenon is called the continuum absorption. There are two types of continua, the water vapor continuum and the dry air continuum by N_2, O_2 and CO_2. Only water vapor continuum and N_2 continuum are significant in the ASUR frequency range. The water vapor continuum can be explained by the perturbations of the molecular wave function by collision, absorption from the far wings of strong water vapor lines in the infrared region, and the contribution of water vapor dimers. The water vapor continuum depends quadratically on its partial pressure. Though the N_2 molecule does not have an electric or magnetic dipole moment to give rise to a rotational spectrum, it can have an electric quadruple moment. Thus, collisions with molecules can produce a temporary dipole and hence the absorption. So the continuum depends on the total pressure and temperature. In order to account for the continuum absorption in the ASUR trace gas retrievals, the semi-empirical models Liebe et al. (1993) for the water vapor continuum and Rosenkranz (1998) for dry air continuum are used. A detailed discussion on the continua and appropriate continuum models for the millimeter and submillimeter region can be found in Kuhn (2003).

6.6 Inversion procedure

The information about the desired atmosphere is contained indirectly in the measured thermal emission spectra. The parameter concerned such as the vertical distribution of a certain molecule has to be retrieved from the measurements. The measured intensity at a given frequency can thus be expressed as,

$$y = f(x,b) + \varepsilon. \tag{6.26}$$

Here, y is the measurement vector, x is the vector of the considered constituent profiles, b is the model parameters. Since the measured quantities with a finite accuracy are not free from

noisy disturbances, the error contribution ε is also to be considered here. In addition, although the measurement vector y is known and finite, the quantity to be retrieved is a continuous function. So a method is need to discretize the state vector y. This is done with the forward model f. The forward model function f describes the physics of the measurement, the RT and the instrumental features. Thus, in the atmospheric remote sensing the measurements are retrieved by inverting the RT equation, hence the name inversion. Generally, inversion assumes ε is Gaussian with zero mean and a symmetric and positive definite covariance matrix.

6.6.1 The optimal estimation method

A numerical method is needed to solve the RT equation since the equation cannot be inverted analytically in general. The optimal estimation method (OEM), the Bayesian approach (Rodgers, 1976, 1990) is applied to invert the ASUR measurements. In this method, the difference between the measured and the simulated values is termed as a cost function χ, which is minimized through a χ^2 test. The cost function is given by,

$$\chi^2 = (y - f(x,b))^T s_\varepsilon^{-1} (y - f(x,b)).$$ (6.27)

The parameter s_ε describes the measurement noise covariance and its correlation to other measured parameters. However, it is possible to have many states of x that could satisfy y. So the ill-posed problem makes a simple χ^2 test unable to solve the equation. Thus, the situation demands an iteration scheme that suits to get a minimum (/convergence) and a stable cost value. This is achieved through an additional χ^2 test with a suitable iteration scheme,

$$\chi_a^2 = (x - x_a)^T S_a^{-1} (x - x_a).$$ (6.28)

The vector x_a is the *a priori* information about the state of the atmosphere (before the measurement) and S_a is the variance of x_a and its expected correlation (between one altitude and another in the case of a profile). The *a priori* and *a priori* covariance values are taken from climatology. However, for some molecules the climatological data are still not available (e.g., ClO, HNO_3, N_2O). In such situations the *a priori* and *a priori* covariance values are taken from model results or from other independent measurements.

Hence, the cost function is the sum $\chi^2 + \chi_a^2$. For weakly non linear cases a simple Newtonian iteration scheme is sufficient to get a minium cost value (Press et al., 1992). If the situation is more non-linear the Levenberg-Marquardt iteration scheme can be applied (Press et al., 1992). The ASUR retrievals employ the Newtonian iteration scheme, though the retrieval of some of the molecules cannot be regarded as weakly-non linear. Convergence and thus a stable retrieval are achieved after a specified number of Newtonian iteration in these cases.

Calculation of Jacobians: In order to test the information content in the measurements the most convenient way is to consider the inversion as a linear problem. It is usually done through linearising the forward model about a reference state say, x_0 such that $f(x)$ is linear within the error bounds of the retrieval. Hence,

$$y - f(x_0) = \frac{\delta f(x)}{\delta x}(x - x_0) + \varepsilon$$ (6.29)

where,

$$\frac{\delta f(x)}{\delta x} = K.$$ (6.30)

Here K is a *Jacobian matrix* and is called the *weighting function*. Not necessarily be square, the matrix contains the partial derivative of the forward model element with respect to the state vector element,

$$K_{i,j} = \frac{\delta F_i(x)}{\delta x_j}. \tag{6.31}$$

Since the calculations of the Jacobians are time consuming, analytical methods are exploited, for which the ASUR retrievals make use of a scheme developed by von König (2001).

Resolution: Resolution of the retrieved profiles is given in terms of the averaging kernel matrix (AKM). The AKM is expressed as

$$A = GK; \qquad where, G = S_a K^T (K S_a K^T + S_\varepsilon)^{-1}. \tag{6.32}$$

The AKM has an approximate Gaussian shape with a peak at the altitude of the retrieved VMR (in the optimal case). The retrieved VMR at any altitude is the weighted mean of the mixing ratio at a certain altitude layer and the contribution from the *a priori* information. The width of the AKM shows the resolution of the retrieval for which, the narrower the width the better the resolution. If the sum of the row elements of the AKM is near to unity then the retrieval is very good in which the contributions from the *a priori* information is very small. Should the sum is nearer to zero then the *a priori* knowledge dominates over the measured information.

Errors: The errors in the estimated profiles can originate from various sources. The important ones are the measurement errors in the spectrum, errors in the forward model parameters and errors from the coarse altitude resolution. These can be stated as,

$$(x - x_a) = G_y \Delta f(x, b, b') \qquad \textit{forward model errors} \tag{6.33}$$

$$+ G_y (K_b(b - b')) \qquad \textit{model parameter errors} \tag{6.34}$$
$$+ G_y \varepsilon_y \qquad\qquad \textit{measurement errors} \tag{6.35}$$
$$+ (A - I)(x - x_a). \qquad \textit{smoothing errors} \tag{6.36}$$

The parameter G is also called the contribution function. The reader is referred to Rodgers (1976, 1990) for a detailed discussion on the characterization.

Convolution: The convolution of a profile is performed by using the formula,

$$x_s = x_a + A(x - x_a). \tag{6.37}$$

The convolved profile is represented by the notation x_s, the *a priori* profile is x_a, the original profile that is to be smoothed is x, and A is the AKM. The equation has widely been applied in this thesis for convolving the high resolution profiles (from independent measurements and model calculations) to make them comparable with the lower resolution ASUR trace gas profiles, when comparing with the ASUR profiles.

6.7 Summary

The ASUR instrument is a passive heterodyne sensor operates in a tuning frequency range of 604.3-662.3 GHz. The total power method is employed for the sensor calibrations. The SIS mixer helps the system noise temperature to be reduced considerably. The AOS in ASUR

is mainly used for stratospheric measurements, whereas the high resolution CTS is used for probing mesospheric constituents. Apart from ozone, ASUR measures a range of stratospheric molecules like ClO, HCl, HNO$_3$, N$_2$O. The instrument is operated onboard a high flying research aircraft to avoid the signal absorption due to the tropospheric water vapor. Mounted on the right side of the aircraft, ASUR looks upward at a constant stabilized zenith angle of 78°. An in-house RT model is employed for the inversion for a non-scattering atmosphere. Since the sensor measures thermal emissions from the rotational lines of the observed molecules, the shape of the pressure broadened lines contain information about the altitude of emitting species. Using the OEM mixing ratio profiles of various molecules are retrieved. An *a priori* information is used to stabilize the inversion problem. The information content of the measurements is derived from sum of the averaging kernel functions.

7 Retrieval of stratospheric trace gases from ASUR measurements

Retrieval of stratospheric trace gases from the ASUR *measurement spectra, which were observed during* SCIAVALUE *(Fix et al., 2004),* EUPLEX *(Kleinböhl et al., 2004b) and* PAVE *(conducted in January/February 2005 aboard the* NASA DC-8 *research aircraft for the validation of the* NASA AURA *satellite) are described in this chapter. Comparison of the* VMR*s retrieved with two different* RTM*s, error analyses for the retrieved profiles and comparisons of the profiles with other independent measurements and model calculations are also discussed.*

7.1 Retrieval of quasi-operational molecules

Retrieval of selected species are performed in a quasi-operational basis. The molecules include ozone, ClO, HCl, N_2O, and HNO_3. In order to get a sufficient signal to noise ratio the spectra are averaged over a certain period of time. The AOS data are binned to 4 MHz channel spacing to assure that the individual channels are uncorrelated. Using an in-house forward model, the retrievals for the individual molecules are performed for an equidistant altitude grid of 2 km spacing. Ozone lines are a common feature at the spectral windows considered for the other molecules. However, all these lines are not analyzed for the ASUR ozone retrievals. The ozone line in the HCl spectrum is used so that a simultaneous retrieval for both HCl and O_3 is possible. When retrieving the other molecules ozone is also retrieved though it is not used for any scientific analysis. The standard ozone retrieval from the HCl line wing is used as the *a priori* information for these retrievals.

7.1.1 Ozone and HCl

A spectral line at 625.371 GHz is used for the retrieval of ozone in a setting for which the AOS center frequency is at 625.918 GHz, which corresponds to a HCl line. Since the line center of ozone and HCl are close enough, a joint retrieval is possible. The spectra are averaged over 80 to 100 seconds (15 single spectra) to get a reasonable signal to noise ratio. Climatological profiles of ozone and HCl are used for the *a priori* information. Only a single *a priori* profile is used for the whole latitude band from the tropics to the Arctic for both molecules. Sensitivity tests show that the ozone and HCl retrievals are robust and are insensitive to the changes in *a priori* values used in the retrievals (the results of the sensitivity analysis are presented in the discussion section). The square root of the *a priori* values are given as its covariance spectrum. Since the individual channels in the AOS spectrum are uncorrelated, a diagonal covariance matrix is employed in the inversion, which is applicable to the inversion of all molecules too. The retrieved profiles have a horizontal resolution of 20 km (due to the same

Figure 7.1: (a) The typical AOS spectra at low (3.00°N, 14.6°E - red), mid (37.2°N, 3.50°E - green), and high (77.5°N, 14.8°E - blue) latitudes, (b) the *a priori* profiles of ozone and HCl and square root of the *a priori* covariance used for the ozone and HCl retrievals. The figures (c) and (e) are the averaging kernel functions, and (d) and (f) are the vertical resolution derived from Full width at Half Maximum (FWHM) of the averaging kernel functions of ozone and HCl respectively.

integration time) and a vertical resolution of 6 km in the lower stratosphere, increasing to 18 km in the upper stratosphere. An overview of the relevant information about the inversion is given in Table 7.1.4. The ozone/HCl spectra, *a priori* profiles, averaging kernels and resolution matrices are shown in Figure 7.1.

7.1.2 N_2O

A line at 652.833 GHz is analyzed for the N_2O retrieval. An integration time of up to 150 seconds (20-25 single spectra) is used for averaging of the spectra. Three different *a priori* profiles that represent the tropics, mid-latitude and the Arctic are used in the retrieval. The vortex averaged N_2O profile from the SLIMCAT model (Chipperfield, 1999) for December 2000 is used as the Arctic *a priori* (Bremer et al., 2002). The same *a priori* has been shifted

Figure 7.2: The typical AOS spectra at low (0.20°N, 29.2°E - red), mid (41.2°N, 10.3°E - green), and high (73.3°N, 19.1°E - blue) latitudes. (b) the *a priori* profiles and the square root of the covariance spectrum used for the retrievals, (c) the averaging kernels of N_2O retrievals and (d) the vertical resolution derived from the FWHM of the averaging kernels.

by $+6$ and $+12$ km to be used at the mid and the tropical latitudes to account for the elevated tropopause heights at the respective latitude sections. Sensitivity tests showed more reasonable and consistent results with these *a priori* profiles than the climatological profiles used in the tests. However, a constant covariance matrix, the square root of the Arctic *a priori* values, is used for all latitudes. The other information regarding the retrievals are listed in Table 7.1.4. Figure 7.2 shows the features of the ASUR N_2O retrievals.

7.1.3 HNO$_3$

The HNO$_3$ retrieval makes use of a set of lines around 606.71 GHz. The individual spectra are averaged over a time span of 80 to 100 seconds (15 single spectra). The retrieval employs a zero *a priori* information at all latitudes. Considering very low values of HNO$_3$ at the tropical and mid-latitude regions and a denitrified winter stratosphere in the Arctic, the zero *a priori* profile is a reasonable estimate and it gives reliable and stable results irrespective of latitude sections. Covariances of 2.50, 5.00 and 1.00 ppb are used at low, mid and high latitudes respectively. The information content in the HNO$_3$ retrieval is up to 35 km. The photochemistry and thermal decomposition of HNO$_3$ in the stratosphere produces only a little amount above 30 km. So the altitude range of ASUR HNO$_3$ measurements is sufficient to carry out scientific studies in the stratosphere (von König et al., 2002; Kleinböhl et al., 2003). The other details about the retrieval are given in Table 7.1.4 and in Figure 7.3.
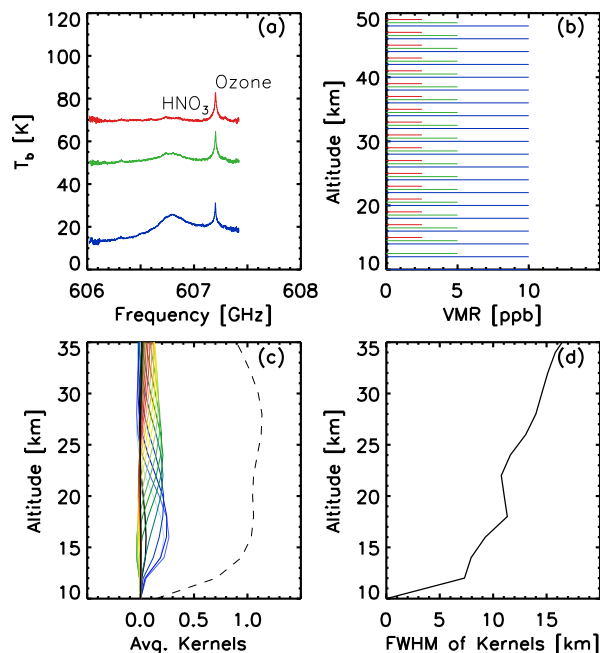
Figure 7.3: (a) The typical AOS spectra at low (0.70°N, 24.6°E - red), mid (30.9°N, 08.0°E - green), and high (78.8°N, 12.0°E - blue) latitudes, (b) the zero *a priori* profile and the square root of the covariance spectrum used for the retrievals, (c) the averaging kernels of HNO_3 retrievals and (d) the vertical resolution derived from the FWHM of the averaging kernels.

7.1.4 ClO

A spectral region centered around 649.448 GHz is used for the retrieval of ASUR ClO measurements. Because of weak lines and rather noisy spectra, a long integration time in the order of 200 seconds (40 single spectra) is used to get a sufficient signal to noise ratio. Climatological data are used for the *a priori* information and its variance is given as the covariance spectrum. The high latitude *a priori* used by von König (2001) is applied at all latitudes after a sensitivity analysis. Figure 7.4 shows the retrieval features of ASUR ClO measurements.

Molecule	Altitude range (km)	Vertical resolution (km)	Horizontal resolution (km)	Estimated accuracy
O_3	15 - 50	6-20	18	$\leq$ 15%
N_2O	15 - 50	8-16	30	$\leq$ 15%
HCl	15 - 50	7-18	18	$\leq$ 20%
ClO	15 - 43	7-18	60	$\leq$ 10%
HNO_3	15 - 35	4-14	18	$\leq$ 15%

Table 7.1: The retrieval features of ASUR quasi-operational molecules.

7.2 Comparison of VMRs retrieved with two different RTMs

Radiative transfer modeling is an important and essential process in the analyses of remotely gathered data. The remote sensors need accurate and fast forward models to simulate the mea-
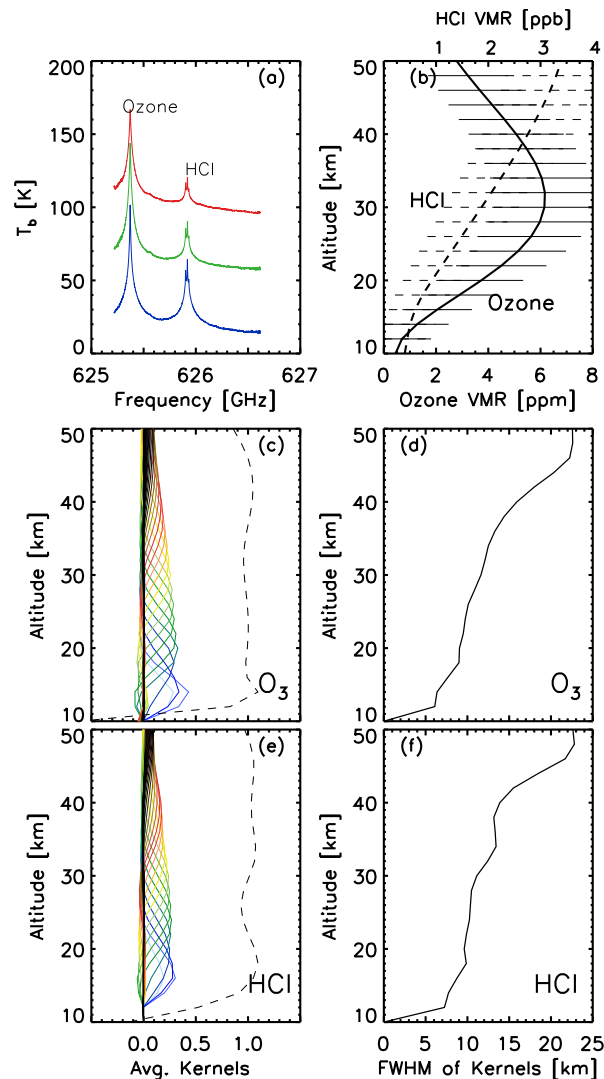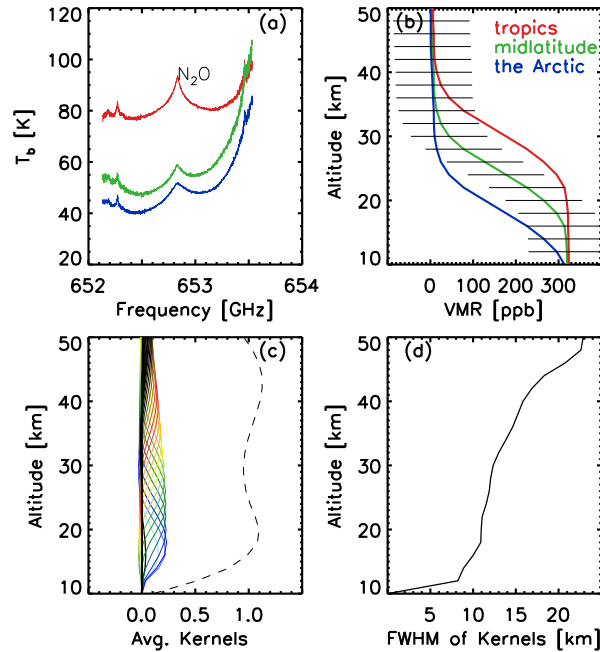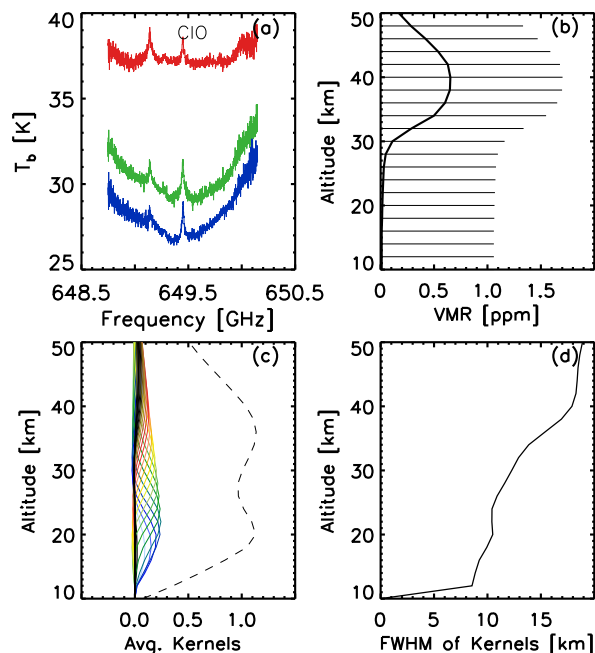
Figure 7.4: (a) The typical AOS spectra at low (0.40°S, 40.2°E - red), mid (52.0°N, 08.0°E - green), and high (77.4°N, 15.0°E - blue) latitudes, (b) the *a priori* profiles and the square root of the covariance spectrum used for the retrievals, (c) the averaging kernels of ClO retrievals and (d) the vertical resolution derived from the FWHM of the averaging kernels.

surements for a given state. Since the ASUR retrieval in the previous studies (Greenblatt et al., 2002; von König et al., 2002; Bremer et al., 2002; Kleinböhl et al., 2003) were based on *the Forward* model (Bühler and Eriksson, 2000), and now being switched to the much faster and up-to-date Atmospheric Radiative Transfer Simulator (ARTS) (Bühler et al., 2004), it is necessary to check the consistency of the retrieved VMRs using both radiative transfer models (RTMs). ARTS is an improved version of *the Forward* model with essentially the same line catalogues as well as the continuum codes. Therefore, only small differences are expected between the simulated results. Radiative transfer models are usually compared by analysing the difference between the brightness temperatures (BTs) simulated with the models for different scenarios (Melsheimer et al., 2004). Since most scientific analyses deal with VMR rather than the BT, the comparison of mixing ratios retrieved using the models *the Forward* and ARTS for the ASUR quasi-operational products are discussed.

7.2.1 Data analyses

The data gathered during the SOLVE (Newman et al., 2002), the SCIAVALUE and the EUPLEX campaign are analyzed. The retrievals with *the Forward* for the SOLVE dataset are taken from Bremer et al. (2002) for ozone, HCl and N_2O, von König et al. (2002) for ClO and Kleinböhl et al. (2003) for HNO_3. These data are again retrieved with the ARTS model for the analyses presented. The SCIAVALUE and the EUPLEX data are retrieved with both models. The profiles are selected in such a way that they are observed above a flight altitude of 10 km and fulfill the standard signal to noise ratio criterion (sufficient integration time) for each molecule. The profiles are compared individually and then binned into latitude regimes as the tropics (07°N-
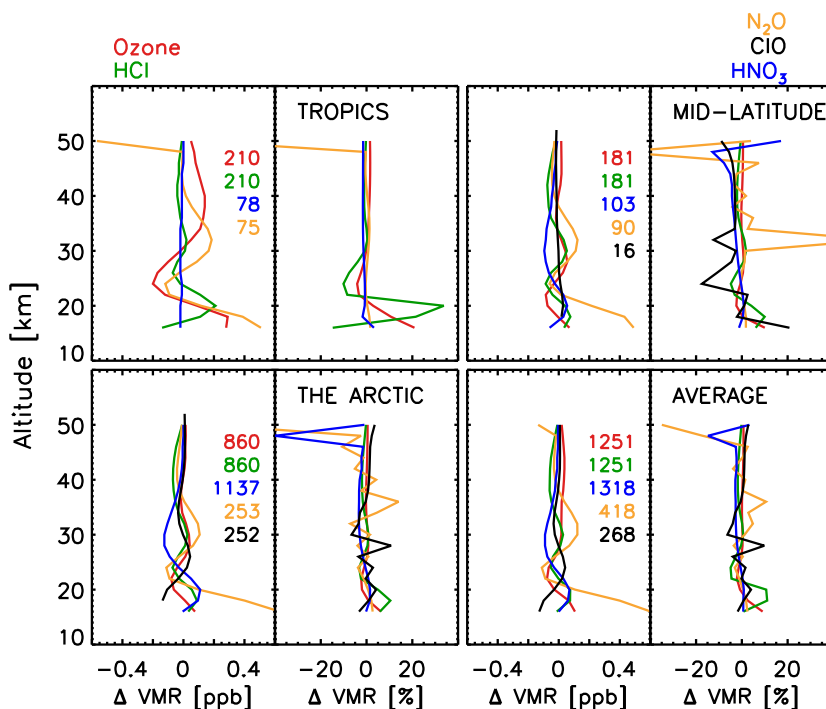
Figure 7.5: The difference in the retrieved mixing ratios with the RTMs *the Forward* and ARTS for the ASUR quasi-operational molecules at different latitude sections. The ozone VMRs are divided by 10^3 and the N_2O VMRs are divided by 10 here. The average of all the latitudes from tropics to the Arctic is also plotted. The numbers on the plots represent the number of Δ profiles averaged over each case in respective color codes.

$30°N$), mid-latitude ($30°N$-$60°N$) and the Arctic ($60°N$-$90°N$) and averaged over the entire region.

7.2.2 Results

Figure 7.5 gives an overall statistical analysis of the *the Forward* - ARTS Δ profiles for the ASUR quasi-operational molecules. In the tropics, the difference is within 0.2 ppb (5-50 ppb for ozone) or 2% above 20 km for ozone, HCl and HNO_3. The N_2O Δ profiles show a deviation of about $\pm$ 15 ppb or $\pm$ 1%. The HCl profiles in the lower stratosphere have slightly higher values. In the mid-latitude, the difference of ozone, HCl and HNO_3 profiles are within 0.1 ppb (5-20 ppb for ozone) or 1% above 20 km. The deviation of Δ N_2O is -2 to 12 ppb or 1% in the same altitude range, except at 32 km. Around 32 km a deviation of about 30% is found. The ClO Δ profiles show a deviation of about $\pm$ 0.01 ppb or 10% from the limited (16) instances, depending on altitude. In the Arctic the difference is within 0.1 ppb (5-20 ppb for ozone) or 2% for ozone, HCl and ClO. The deviation of N_2O profiles is about 7 ppb or 10% above 20 km. The common features of the analysis are, (a) the Δ profiles are consistent with latitudinal analyses, (b) the deviations are the least in the tropics, (c) the difference below 20 km is relatively high, and (d) among the molecules ozone and HCl show the least deviation.

Sensors	Lat.	Lon.	Mol.
Ozonesondes			
De Bilt	52.10°N	5.18°E	O_3
Hohenpeissenberg	47.80°N	11.02°E	O_3
Keflavik	63.97°N	22.60°W	O_3
Nairobi	1.27°S	36.80°E	O_3
NyÅlesund	78.92°N	11.93°E	O_3
Payerne	46.82°N	6.95°E	O_3
Uccle	50.80°N	4.35°E	O_3
Radiometers			
MIRA	67.84°N	20.41°E	O_3
RAM	78.55°N	11.55°E	O_3
OLEX lidar	All latitudes		O_3
Models	All latitudes		
CTMB			N_2O
SLIMCAT			HCl, HNO_3, and ClO

Table 7.2: The ozonesonde stations, radiometers, lidar, and the model data used for comparisons with the ASUR trace gas retrievals The location of the sonde stations with latitudes (Lat.), longitude (Lon.) and the molecule (Mol.) compared are also listed.

7.3 Comparison with independent measurements and model calculations

The goal of this section is twofold. Firstly, to test the consistency of the retrieval performance. This is especially important in the tropical and mid-latitude regions as the ASUR tropical/subtropical data are retrieved for the first time. Secondly, there are a large number of independent measurements and model calculations from two different CTMs to assess the quality of ASUR trace gas retrievals.

7.3.1 Data analyses

The intercomparison of ozone makes use of a number of ozonesonde measurements across the latitudes from Nairobi (1.27°S) to NyÅlesund (78.1°N). Apart from ozonesondes, the OLEX (Wirth and Renger, 1996) and the microwave instruments MIRA (Kopp et al., 2003) and RAM (Sinnhuber et al., 1998) are also used. In addition, two stratospheric CTMs, the SLIMCAT and the CTMB (Sinnhuber et al., 2003) calculations are exploited as well. The N_2O measurements are compared with simulations from SLIMCAT and CTMB and ClO, HNO_3 and HCl measurements make use of the SLIMCAT calculations for the comparisons. The simulated profiles are interpolated to the the ASUR measurement points and convolved using the ASUR trace gas averaging kernels and *a priori* profiles. The MIRA and RAM ozone measurements have comparable vertical resolution with ASUR ozone ($\sim$10 km) and hence, these profiles are compared without convolution. The list of the instruments and sonde stations are noted in Table 7.2.
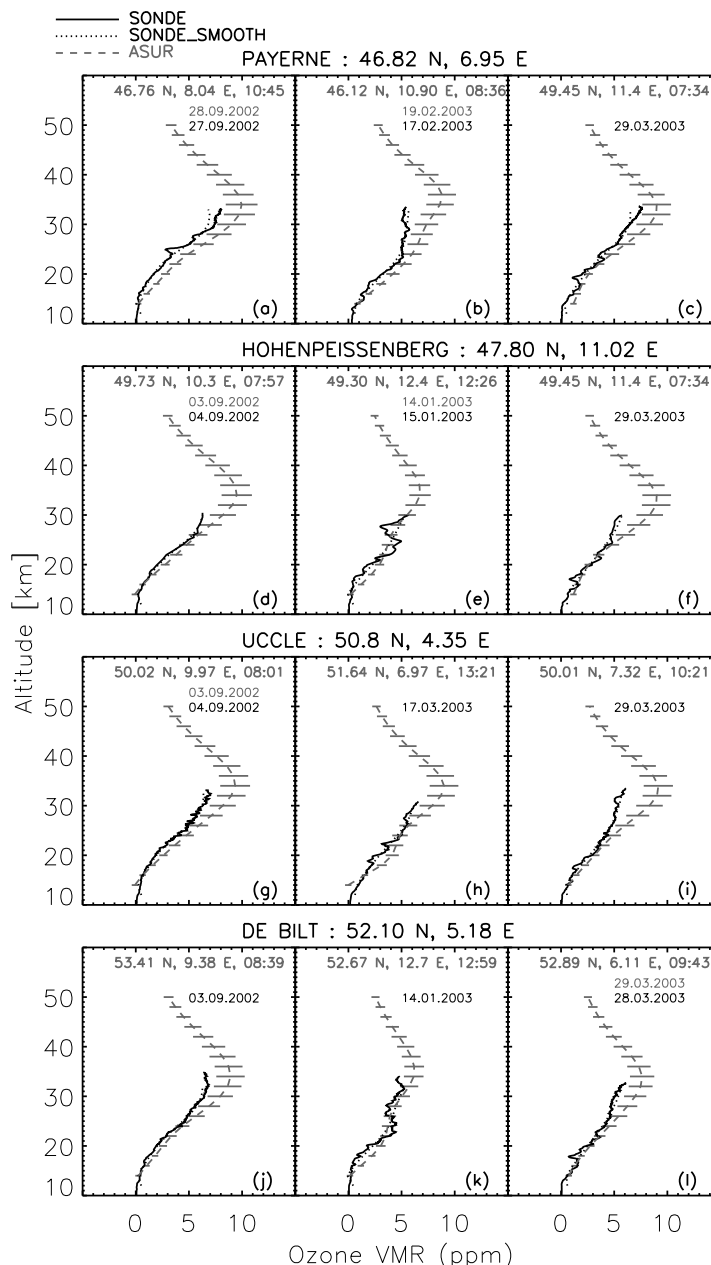
Figure 7.6: The ozone profiles from ASUR measurements are compared with various ozonesonde measurements. The co-ordinates of the sonde stations, date and time of the measurements are also noted.

7.3.2 Results

Ozone: Figure 7.6 compares the ASUR ozone with sonde measurements at Payerne, Hohenpeissenberg, Uccle and De Bilt. The sonde profiles are in good agreement with the ASUR profiles at all stations. The ASUR profiles are also successful even in capturing the features like double peak structure in ozone profiles. However, above 25 km the ASUR ozone show slightly higher values.

Figure 7.7 (upper panel) illustrates the comparisons for Keflavik, NyÅlesund and Nairobi sonde measurements. A very good agreement between the ASUR and the sonde ozone is found up to 30 km in all comparions. Since Nairobi is a tropical station, the good agreement between
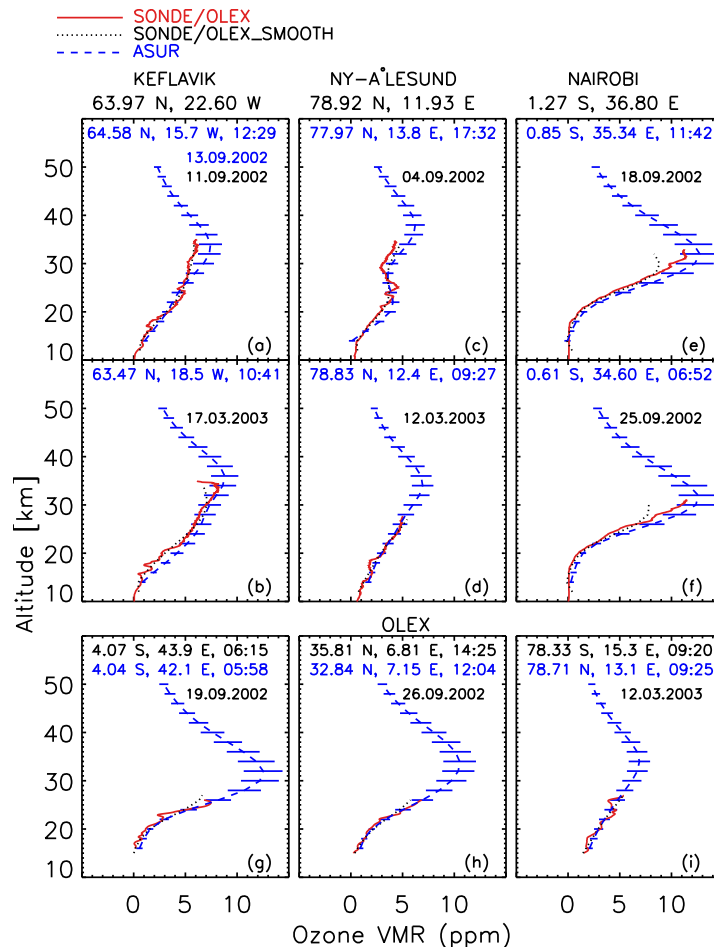
Figure 7.7: Same as Figure 7.6, but for other ozonesonde stations and for the OLEX measurements.

the measurements shows the stability of the ASUR ozone retrievals in the tropics. The double peak structure in winter/spring NyÅlesund ozone profile is a common feature. The ASUR profile is in good agreement with the sonde measurement with the double peak structure as well.

Figure 7.7 (lower panel) shows the comparison between the OLEX and the ASUR measurements at different latitudes. The closest ASUR measurement profiles are taken for the comparisons. The comparion restricted to lower stratosphere due to OLEX's limited vertical range. The ASUR and the OLEX profiles are in very good agreement throughout the latitudes.

Figure 7.8 depicts the comparison among the microwave radiometers: ASUR, MIRA at Kiruna and RAM at Spitzbergen. All the observations are carried out in winter 2003 and the RAM measurements are taken between 5 and 12 a.m of a single day. The nearest ASUR measurement is compared with all three RAM ozone profiles. A very good agreement is found in the lower and upper stratosphere. However, a slight offset is found in the middle stratosphere in some profiles like Figure 7.8(e) and Figure 7.8(g), where the ASUR ozone shows slightly higher (about 0.3 ppm) values.

Comparisons with model calculations: As the simulations are not as good as measurements to make a comparison statistics because of relatively large uncertainties in the simulations, a general retrieval performance with respect to the simulations will only be discussed. Also, the aim is mainly to analyse the consistency of the ASUR retrievals with the new retrieval setup: the nature of the vertical distribution, the altitude of maximum VMR, the distribution of
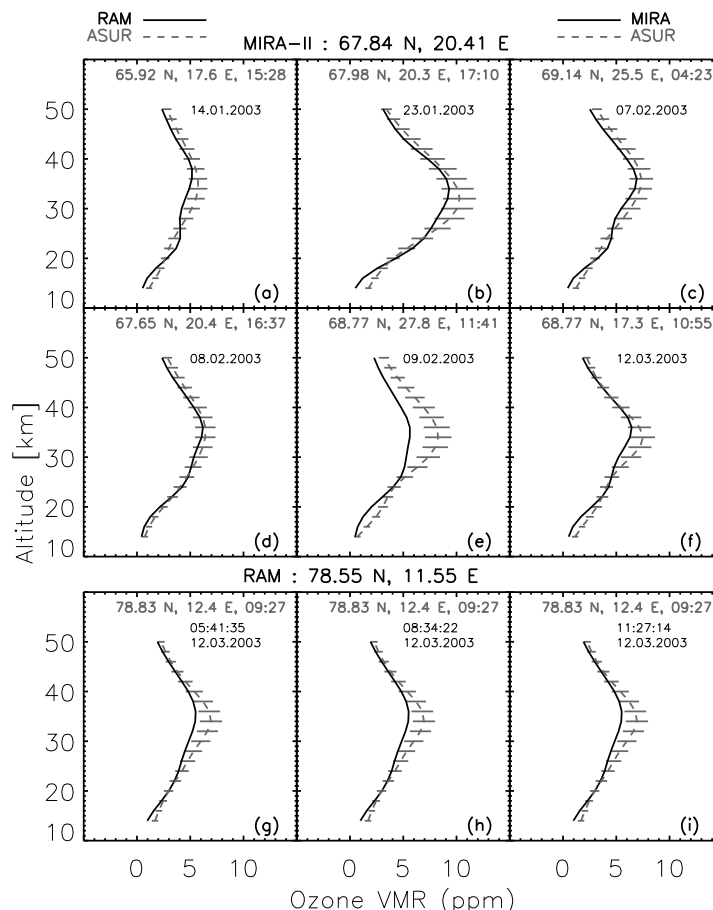
Figure 7.8: Same as Figure 7.6, but for microwave measurements.

the latitudinal gradients, and the interannual variability in the mixing ratio distributions of the molecules.

HCl and N$_2$O: Figure 7.9 compares the asur HCl and N$_2$O retrievals with slimcat simulations at different latitudes. The lower stratospheric mixing ratios are in agreement with the slimcat calculations. However, the upper and middle stratospheric retrievals overestimate the calculations. The asur HCl has a high bias (of about 15%) in this region as shown by von König (2001). Hence, the retrieved results are consistent with previous studies. The vertical distribution and latitudinal variations in N$_2$O are in very good agreement with the model calculations qualitatively and quantitatively. However, the tropical lower stratospheric retrievals show relatively higher values.

Figure 7.10 illustrates the comparability of asur N$_2$O measurements during the solve and the euplex campaign period with the ctmb simulations. The goal of this re-retrieval was to examine the mid and the high latitude asur N$_2$O. The retrieval setup for the molecule was the same that applied for sciavalue. Hence, this inversion differs slightly from the retrieval of Bremer et al. (2002). The selection of the *a priori* profiles at mid and high latitudes is done the same way as for the sciavalue data. The observations in the high latitudes from solve, sciavalue and euplex show the interannual variability in the mixing ratio distributions. These variations are mostly attributed by the different dynamical situations in the Arctic winter stratosphere. The good agreement between the simulations and the observations shows that the asur N$_2$O retrieval is very consistent. Though the values below 20 km are slightly higher, the deviations are still within the estimated accuracy of asur N$_2$O measurements.
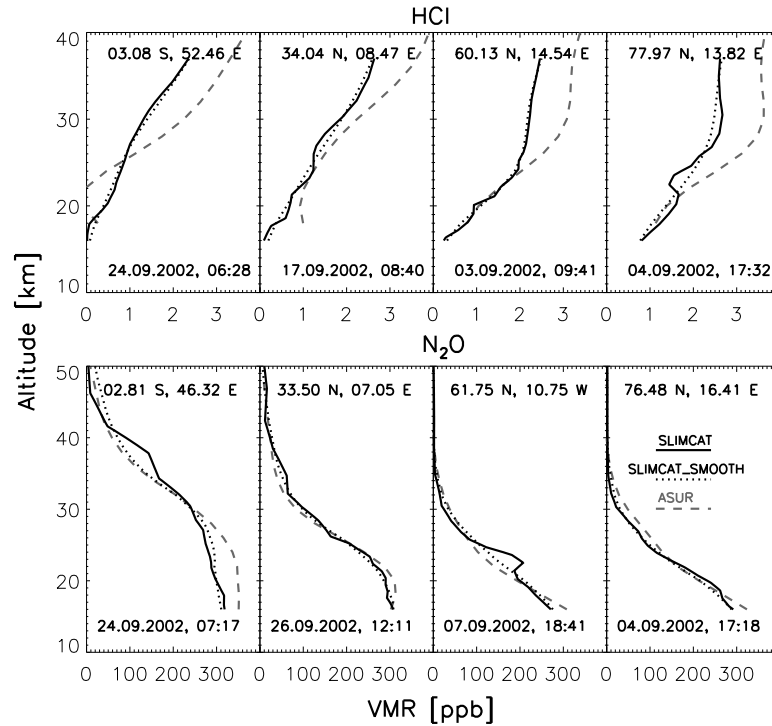
Figure 7.9: The ASUR HCl (upper) and N$_2$O profiles are compared with the SLIMCAT profiles at different latitude regions. The measurement co-ordinates, day and time of the measurements are also noted on the plots.
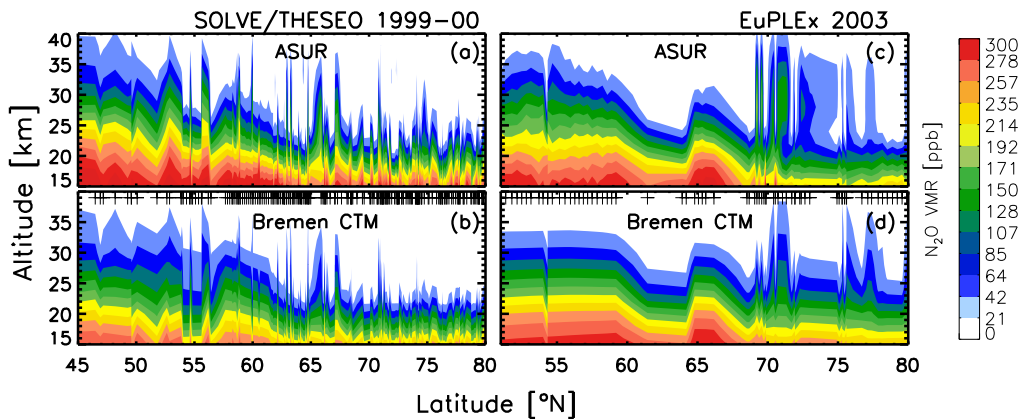
Figure 7.10: The ASUR N$_2$O retrievals are compared with the CTMB calculations for the SOLVE and the EUPLEX data. The black plus signs on the bottom of the figures represent measurement locations of the molecule.

HNO$_3$ and ClO: Figure 7.11 (top) shows the individual profile comparison between the ASUR measurements and the SLIMCAT simulations. The ASUR profiles are in good agreement with the simulated profiles. However, The ASUR HNO$_3$ shows slightly higher values in the lower stratosphere. There is a small difference between the measured and the calculated ClO profiles in the tropics (leftmost plot) as well.
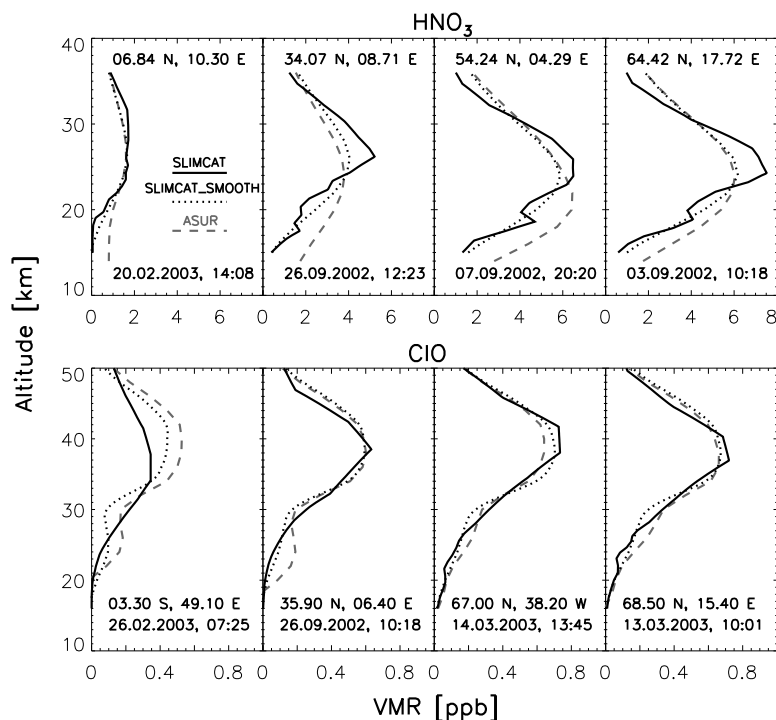
Figure 7.11: The ASUR HNO_3 (upper) and ClO profiles are compared with the SLIMCAT profiles at different latitude regions. The measurement co-ordinates, day and time of the measurements are also noted on the plots.

7.4 Discussion

7.4.1 Retrieval errors

The probability of error sources: A detailed error analyses and characterization of the ASUR quasi-operational products were performed by von König (2001). Since the low latitude retrievals are performed for the first time from the ASUR measurement spectra, a sensitivity analysis is performed to check the consistency of the retrieved results. The tests are mainly carried out with the *a priori* profiles used in the retrievals, which were the main difference (in the RTM input) between this retrieval and the previous one by von König (2001).

Error analyses: ASUR ozone retrieval is very robust. The sensitivity tests show that the ozone profiles can be retrieved even with a zero *a priori* profile without considerable changes from the one retrieved with present retrieval setup. The altitude shifts in the *a priori* profiles do not change the retrieved VMRs as well. Below 18 km, a change of ~10% is found in the retrieved VMRs with different *a priori* values for N$_2$O. However, above 18 km the retrievals are insensitive to changes in the *a priori* values. Moreover, the accuracy of 15% estimated previously by Bremer et al. (2002) holds at all latitude sections. Though there are slight changes in the VMRs retrieved with a zero and a non-zero *a priori* information for HNO$_3$, to keep the denitrification into account and to be consistent with the previous retrievals, the same procedure that used by Kleinböhl et al. (2003) is also applied in this study.

The sensitivity tests with the old and new water vapor profiles [created from the HALOE climatology by Lautié (2003)] in the retrievals produced no change in the retrieved mixing ratio profiles for all the quasi-operational molecules irrespective of latitude regions. However, for a given uncertainty of the water vapor profiles, the retrieved VMR changes slightly around

the tropopause altitudes, which is the highest in the tropical latitudes (decreasing with latitude in accord with the water vapor abundance in the region). However, a 100% change in the *a priori* values are needed even for these changes. The difference is inversely proportional, decreasing with altitude and maximum at the tropopause. The maximum difference is found for HNO_3 in the tropics (0.1 ppb) and the minimum is noted for ozone. Change in the N_2O and ClO VMRs are in between those for the other two molecules. Furthermore, the ozone and HCl retrievals show hardly any change in the retrieved VMRs even with $\pm$ 100% uncertainty in the H_2O *a priori* values above 20 km.

Newtonian iteration is sufficient for ASUR trace gas retrievals since convergence is easily reached after a few iterations. The number of iterations were increased for SCIAVALUE retrievals, especially for the tropical retrievals for all molecules. The changes in the number of iterations for individual molecules were ozone/HCl 4 to 6, N_2O 8 to 10, HNO_3 5 to 6, and ClO 8 to 9. However, no change is found in the retrieved mixing ratios.

7.4.2 The *Forward* and ARTS comparison

The likelyhood of the differences: The difference in the ozone VMR retrieved with *the Forward* and ARTS is around 50 ppb and the highest deviation is found below 20 km. The difference in HCl VMR is 0.05 ppb and the Δ profile has a peculiar ($'s'$) shape. Thus, the difference also depends on the altitude. Both ozone and HCl mixing ratios show insignificant differences in using the different radiative transfer models for the retrievals. The relative difference in the N_2O VMRs is negligibly small above 20 km. Below 20 km the deviation is 1-5 ppb or 2-3%. The altitude range from 10 to 20 km is a difficult region to make a perfect retrieval. The sensitivity tests show that the N_2O retrieval in this region is influenced by (a) water vapor *a priori* profile, (b) input N_2O *a priori* profile, (c) ozone retrieval from the same spectra and (d) the N_2O covariance spectrum applied in the retrieval. Though the contributions of the aforementioned parameters are relatively small, they could alter the absolute VMRs in the order of 2-3 ppb. Considering the deviation of 3 ppb in comparison with the current tropospheric value of 320 ppb, the difference *the Forward*-ARTS mixing ratio is negligibly small. The absolute difference in the HNO_3 mixing ratios is very small and is within 0.1 ppb. In addition, the deviation at the altitudes of maximum VMR is around zero. Thus, the difference does not seem to cause any problems in the scientific analyses of the data. The change in the ClO mixing ratios retrieved with the models is negligible. The altitude of the maximum mixing ratio values in the Arctic upper stratosphere records a difference of 0.01 ppb. The deviation 0.01-0.04 ppb is beyond the detection limit of ASUR ClO. So the ClO differences can also be neglected.

The reasons for the deviations: Since the radiative transfer codes are basically the same, the retrieved results are showing insignificant differences. Nevertheless, the negligible offsets can be due to (a) the additional *a priori* profiles used in the ARTS and (b) the difference in line catalogues used in the ARTS and in *the Forward* retrievals. The *Forward* model retrievals were making use of a combined catalogue of HITRAN (Rothman et al., 1992) and the JPL (Sander, 2000). Since the line intensity and line positions for the microwave region are more precise in JPL, the JPL values were adopted. ARTS retrievals were also using a combined catalogue from the JPL (Sander, 2000) and HITRAN for specific reasons. However, the catalogue is different from the one used for *the Forward* retrievals. The main differences are the following. The catalogue compiled for ARTS includes the latest pressure broadening coefficients for ozone

and ClO. The HCl and HNO_3 retrievals use the new pressure shift values calculated from ASUR measurements by von König (2001). In addition, the combined catalogue incorporates pressure broadening and self broadening coefficients from HITRAN 96 and line frequency, intensity and energy from JPL 2000. Furthermore, the ARTS HNO_3 retrievals with HITRAN 96 and HITRAN 2K give huge differences in *the Forward*-ARTS profiles. The JPL catalogues perform better and JPL 2001 gives the best among them. So the combined catalogue has a greater significance in the ARTS oriented ASUR retrievals. (c) The additional continuum models to account for various continua is another difference in the model input. Liebe et al. (1993) or Rosenkranz (1998) was used in *the Forward* to represent the continua. However, in ARTS, Liebe et al. (1993) for water vapor and Rosenkranz (1998) for dry air continuum are used.

7.4.3 Comparison with independent measurements

The deviations: The agreement in the lower and the upper stratosphere between the profiles (ASUR, ozonesondes, MIRA, or RAM) is very good. The middle stratospheric values in the ASUR ozone are slightly higher in these cases. It has to be noted that the high bias cases are mostly do not match in time. In addition, above 25 km the sonde measurements cannot be realistic as the drop in the atmospheric density affects the accuracy of the measurements. The high bias in the order of 0.3 ppm to MIRA and RAM are well inside the ASUR ozone error bars as well. The comparisons with the Nairobi and the OLEX ozone in the tropics are particularly important that the retrievals from ASUR measurements in the tropics are for the first time. The very good agreement shown by these comparisons underpin the consistency of the ASUR ozone retrievals.

   The reasons for the deviations: The middle stratospheric ASUR ozone is slightly higher than those of other independent measurements as shown by Bremer (2001). The work showed the mid ($\geq 45°N$) and high-latitude ozone retrieved from ASUR measurements are on the higher side by 10-15%, depending on altitude. The MIRA and the RAM ozone profile comparison also showed a similar feature. Nonetheless, the differences in these cases are very small, in the order of 0.3 ppm. (a) The reason for the ASUR high bias is the uncertainties in the pressure broadening coefficient, in the cold load reflectivity and in the window transmission. (b) Validation shows that the RAM ozone generally underestimates other independent measurements by 10%. Moreover, it slightly overpredicts other measurements below 20 km too (Langer, 1999). Considering the deviation of about 0.3 ppm with respect to the RAM ozone validation results, the differences are reasonably explained. (c) The accuracy of MIRA ozone is about 10%. The deviation among the microwave sensors is well inside the accuracy range of the measurements. (d) Atmospheric variability during the measurements can be another reason for the deviations.

7.4.4 Comparison with model calculations

The observed vertical distributions of the mixing ratios, the altitude of maximum VMRs, the latitudinal gradients, the position of the steep latitudinal gradients (for eg: N_2O), and the seasonal variations are in good agreement with the calculations. The possible reasons for the differences between the measurements and the model simulations are the uncertainties in the

forcing windfield in the models, issues related to the model resolution, uncertainties in the chemical reaction rate constants and inaccuracies in the model transport.

7.5 Conclusions

This chapter explains the features of the inversion techniques employed to retrieve mixing ratio profiles of the ASUR quasi-operational molecules O_3, N_2O, HCl, HNO_3 and ClO. The main conclusions of this study are the following. (a) The tropical and mid-latitude profiles (south of 45 °N) are retrieved for the first time from the ASUR measurement spectra. The retrieved (O_3, N_2O, HCl, HNO_3 and ClO) profiles are in good agreement with the independent measurements and model calculations. (b) The comparison between the mixing ratios retrieved with *the Forward* and ARTS models show negligible differences. Because of the insignificant differences, this study recommend the replacement of *the Forward* model with ARTS for the ASUR trace gas inversions. (c) The ozone retrievals in comparison with the independent measurements show that ASUR ozone is in very good shape, the lower stratospheric ozone in particular. The comparisons reveal that there is a high bias in the ASUR ozone in the middle stratosphere, which can be due to the uncertainties in the pressure broadening coefficient, in the cold load reflectivity and in the window transmission. (d) The retrieved and simulated VMRs of N_2O, HCl, HNO_3 and ClO are in good agreement in producing the right vertical distributions, the altitudes of the maximum VMRs, the latitudinal gradients and seasonal signatures.

8 Cross-validation of MIPAS, OSIRIS, SCIAMACHY and SMR by comparison with the ASUR ozone.

Satellite sensors play a vital role in monitoring the Earth's environment. They can measure over any region on the Earth and provide global maps of various constituents in very short time intervals. New sensors are necessary to supplement the existing space-borne systems and execute novel measurement techniques applied for a better understanding of the current atmospheric composition and climate scenarios. Decommissioned spaceborne systems are also to be replaced with new sensors for a continuous monitoring and thus to keep watching the atmosphere. The ENVISAT and the Odin satellite are new experiment platforms to observe the atmosphere from space. It is necessary to validate newly installed satellite sensors with well-tested and proven instruments to assess the quality of the data provided by the sensor, vertically resolved data products in particular. The validation helps the sensor to perform better through the improved calibration, refined algorithms and de-bugging.

Measurements from aircraft platforms have a high level of flexibility to gather data for intercomparison with satellite observations in order to assess quality of the sensor retrievals. Aircraft observations can be performed over any terrain (or any region of the scientific interest) and wide range of latitudes can be covered with such measurements. Flexibility of these airborne measurements are the idea behind the planning of the SCIAVALUE and EUPLEX missions. Unlike SCIAVALUE, the EUPLEX mission was not planned exclusively for validating satellite sensors. The ASUR has been used for validating ILAS on ADEOS (Sugita et al., 2002; Kanzawa et al., 2003) previously. Since validation of space borne sensors are usually carried out with correlative data including high resolution sondes and lidar measurements, this cross-validation study does not serve as the validation of the sensors. Validation papers of the respective satellite sensors discussed here are also under preparation. However, intercomparison with measurements from different sensors is the primary stage of a validation process, which is the significance of this comparison study as it compares the ASUR measurements with various satellite sensor observations. Additionally, the study gives an opportunity to make a cross-comparison of ozone profiles among the satellite sensors to diagnose the quality of the sensor measurements. This chapter aims at the cross-comparisons of SCIAMACHY (Bovensmann et al., 1999), MIPAS (von Clarmann, 2003), OSIRIS (Llewellyn et al., 2004) and SMR (Frisk et al., 2004) ozone limb profiles with the ASUR data collected during the SCIAVALUE and the EUPLEX campaigns.

8.1 Collocation criteria

ASUR measurements that are performed within a ± 1000 km radius and ± 6 hours of the satellite measurements are considered for the comparison. The difference is calculated from the individual profile comparisons (Δ ozone = ASUR ozone - the satellite sensor ozone). The indi-
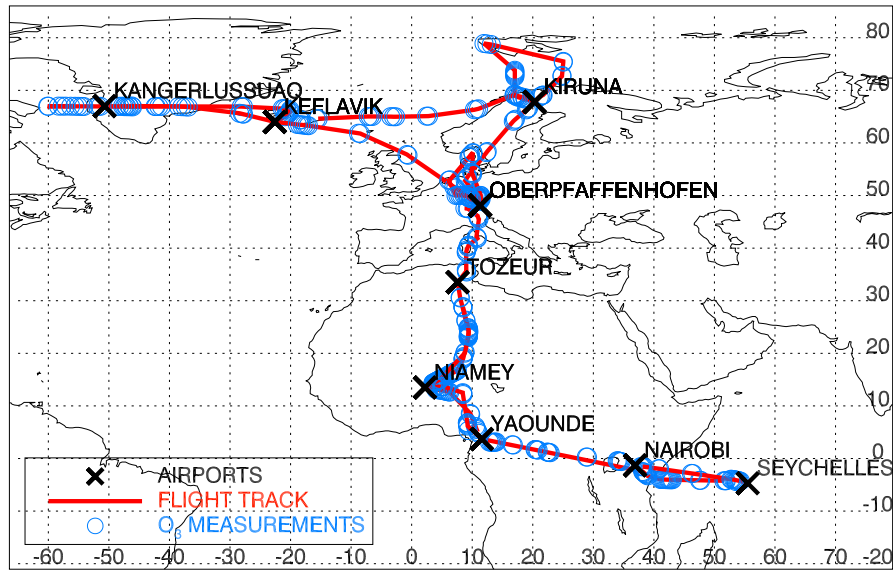
Figure 8.1: The flight route and the ASUR ozone measurements during the SCIAVALUE 2003 in February-March 2003. A similar flight track was chosen for the SCIAVALUE September 2002 deployment as well.

vidual Δ profiles are then averaged over the climatic regions tropics (5°S-30°N), mid-latitudes (30°N-60°N) and the Arctic (60°N-90°N). The results are presented in terms of the climatic regions and the average of all the Δ profiles from tropics to the Arctic. A sensitivity test was carried out with two other selection criteria for the ASUR measurements: (a) $\pm$ 500 km in $\pm$ 3 hours and (b) $\pm$ 2° latitude $\times$ 10° longitude in 2 hours. However, the resulted Δ profiles did not differ significantly. So in order to have more coincident measurements and thus to make better statistical analysis from the comparison, the criterion of 1000 km and 6 hours was adopted for the data analyses.

8.2 ASUR-SCIAMACHY comparisons

8.2.1 Data analyses

ASUR ozone measurements from the SCIAVALUE campaign are used for the comparison. The flight route of the Falcon research aircraft and the ASUR ozone measurement during the campaign are shown in Figure 8.1. Two SCIAMACHY datasets are analyzed: The official European Space Agency (ESA) operational product version 1.0 (hereafter OP 1.0) and the in-house scientific product version 1.6 (hereafter UB 1.6) (von Savigny et al., 2004). The ESA OP data were available only for a few dates (for 9 ASUR measurement flights) in September 2002 and most of them belong to the tropics. The vertical resolution of the ozone profiles for both datasets is about 3-4 km and vertical range of the OP 1.0 profiles is 16 to 50 km. However, the vertical coverage of UB 1.6 is 15 to 40 km only. Because of the limited vertical resolution of the ASUR ozone, the SCIAMACHY ozone profiles are convolved with the ASUR ozone averaging kernels for the comparisons.

The UB 1.6 ozone retrievals for 5 ASUR measurement flights in September 2002, 3 flights in February 2003 and 3 flights in March 2003 are analyzed. The UB 1.6 ozone concentration
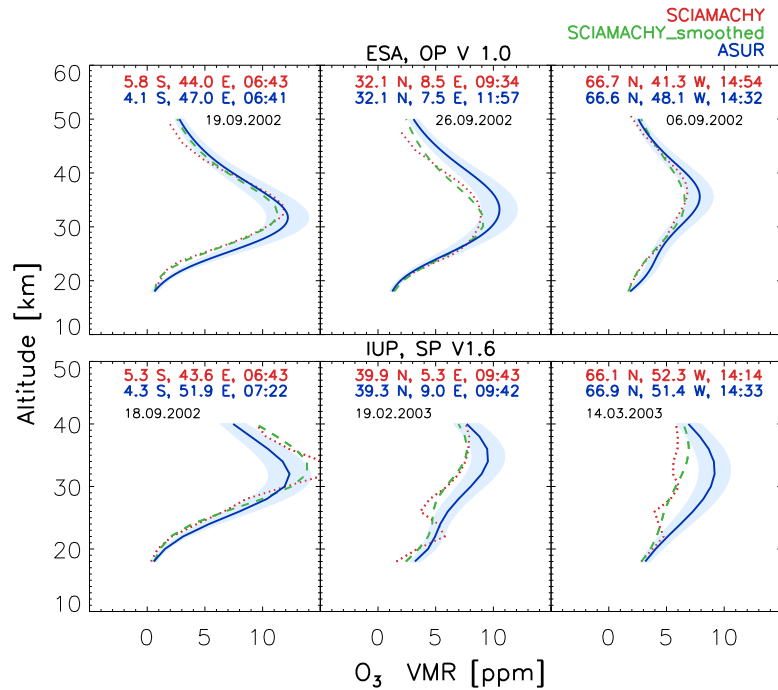
Figure 8.2: Typical examples of the individual SCIAMACHY-ASUR coincident profiles in the tropical, mid-latitude and the Arctic regions for the operational and scientific products. The co-ordinates and date of the measurements are noted in the plots. The pale blue shade on ASUR ozone profile shows its estimated accuracy. The OP 1.0 and UB 1.6 profiles represent different days because of unavailability of typical profiles for the same latitudes on the same day.

profiles are converted into volume mixing ratio profiles using synoptic pressure and temperature profiles from the National Center for Environmental Prediction (NCEP), which were used for retrieving the ASUR ozone profiles. The resulted mixing ratio profiles are smoothed by ASUR ozone averaging kernels. Typical examples of individual profile comparisons for the coincident measurements in the tropics, mid-latitudes and the Arctic are shown in Figure 8.2.

The SCIAMACHY limb data from the beginning of the mission to December 2003 are affected by errors in the tangent height information. Tangent height errors of up to 3 km (and more in a few extreme cases) have been detected with various methods (Kaiser et al., 2004). The tangent height errors could be traced back to inaccurate knowledge of the spacecraft attitude and/or position. The limb pointing was found to be very accurate after the updates of the orbit propagator model on ENVISAT, that occur twice a day. Between these updates, the pointing slowly deviates from nominal pointing. For the UB 1.6 ozone profile retrievals used here a pointing retrieval employing the TRUE (Tangent Height Retrieval by UV-B Exploitation) method (Kaiser et al., 2004) was performed for every limb measurement and the retrieved tangent height offset was corrected prior to the retrieval of the ozone profiles.

8.2.2 Results

Figure 8.3 (left panel) shows the statistics derived from the comparison between ASUR and OP 1.0 ozone profiles at different climatic regions. There are 12 coincidences in the Arctic, 58 in the mid-latitude and 65 in the tropics. The ASUR-OP 1.0 deviation is up to 2 ppm or 15-20% in the Arctic, 1.5 ppm or up to 15% at mid-latitudes and up to 2 ppm or 15% in the

ASUR - SCIAMACHY, OP V1.0   ASUR - SCIAMACHY, IUP V1.6
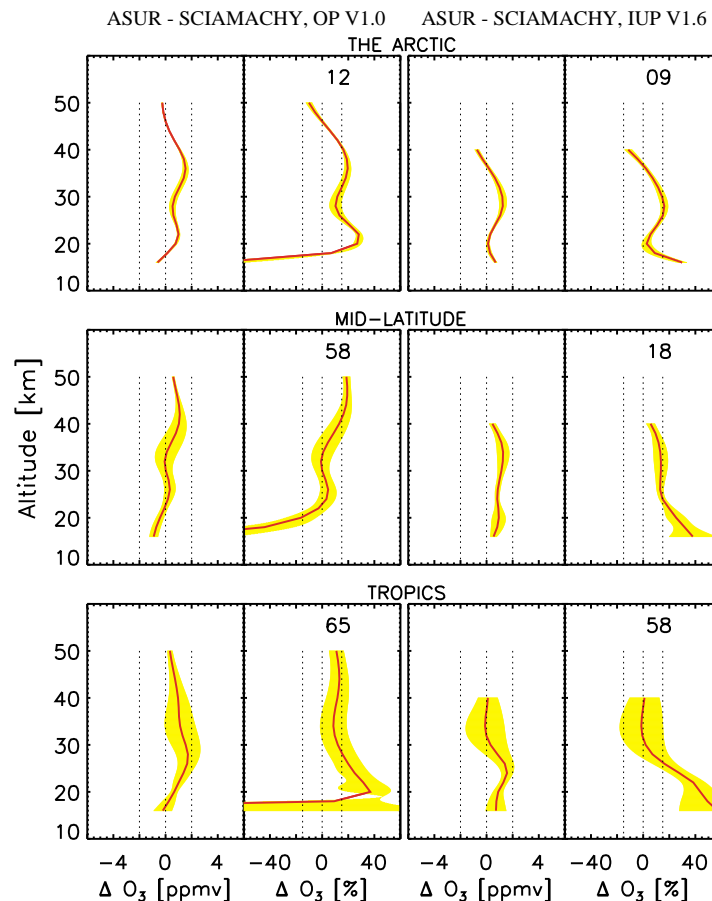
Figure 8.3: The absolute (Δ = ASUR-SCIAMACHY VMR in ppm) and percentage (Δ VMR in %) difference between the ASUR and SCIAMACHY ozone profiles, the Arctic (top), mid-latitude (middle) and at tropical regions. The left panel stands for ASUR-OP 1.0 and the right panel stands for ASUR-UB V1.6 for each latitude sections as noted in the figure. The thick red line indicate the mean Δ profile at each section and the yellow shaded area represents the standard deviation from the mean Δ profile.

tropics between 20 and 40 km. The difference is higher in the lower stratosphere especially in the tropics and the Arctic regions. It should be noted that the lower stratospheric values are very sensitive and if one of the profiles deviates from the other with even for a small fraction of *ppm* (parts per million), that can lead to a huge change in the percentage scale. This is very evident in the tropical region, where the absolute difference is small but the difference in the percentage is very large.

Figure 8.3 (right panel) depicts the comparison between ASUR and UB 1.6. From the 9 coincident measurements, the difference in the Arctic is found to be about -0.5 to 1.7 ppm or -14 to 16% at 20-40 km. The deviation deduced from 18 mid-latitude coincident measurements is between 1 and 1.5 ppm or 5-17% in the same altitude range. The difference in the tropics is up to 2 ppm or -1 to 30% at 20-40 km for the 58 instances. The peculiar (*s − shape*) shape due to the altitude mismatch is pronounced in the Arctic profiles. The pointing problem related to SCIAMACHY retrievals can be the reason for the altitude mismatch in the profiles.
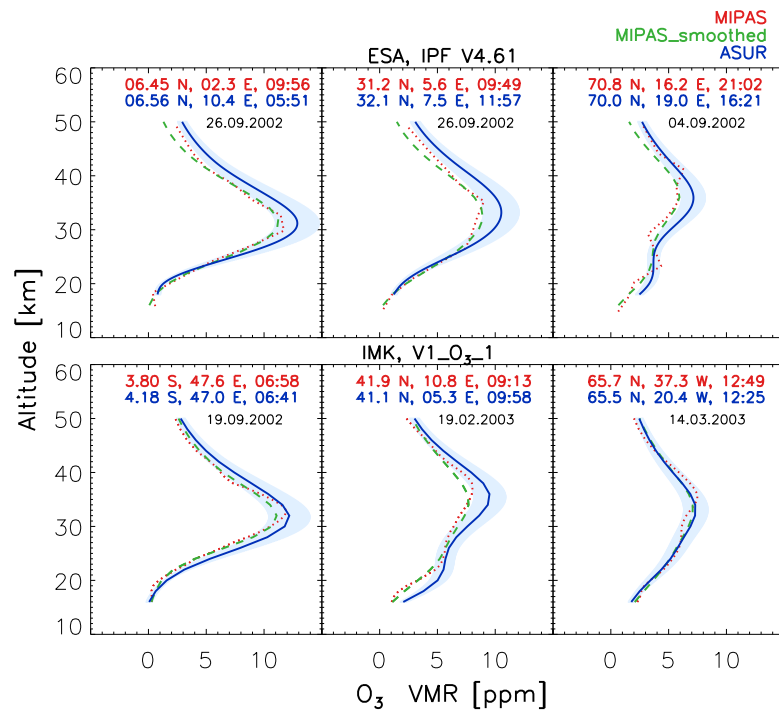
Figure 8.4: Same as Figure 8.2, but for MIPAS.

8.3 ASUR-MIPAS comparisons

8.3.1 Data analyses

The ESA operational product IPF (Instrument Processing Facility) V4.61 (hereafter IPF 4.61) and the IMK (Institut für Meteorologie und Klimaforschung, Karlsruhe) scientific product V1-O3-1 (hereafter IMK 1.0) are considered. The IPF 4.61 data are analyzed for September while the IMK 1.0 data are analyzed for September 2002, February and March 2003. The MIPAS ozone profiles have a vertical resolution of about 3 km and a vertical range of 10 to 50 km. The VMR profiles are convolved with ASUR ozone averaging kernels for the comparisons. Typical coincident measurements at different latitude regions are depicted in Figure 8.4.

8.3.2 Results

Figure 8.5 (left panel) shows the comparison statistics derived from the ASUR and the IPF 4.61. There are 415 coincident measurements in the Arctic, 95 in the mid-latitude and 207 in the tropics. The deviation in the tropics is 0.5 to 2.5 ppm or 14-30%, whereas in the mid-latitudes the difference is within 2 ppm or 15% between 20 and 40 km. The ASUR-IPF 4.61 is within 1.5 ppm or 15% in the Arctic at 20-40 km. Compared to the tropics, the agreement of the mid and high latitude profiles is rather good, 20 to 40 km in particular.

Figure 8.5 (right panel) illustrates the statistics derived from the comparison between ASUR and the IMK 1.0 scientific product. A deviation up to 2 ppm or 16% is found in the Arctic from 125 coincident measurements. The deviation in the mid-latitude is within 2 ppm or 17% at 20-40 km for the 45 instances. There are 68 coincident measurements in the tropics, the largest among the latitudinal sections, where the difference is up to 2.5 ppm or 22% at 20-40 km. The difference is relatively small in the mid and high latitudes.
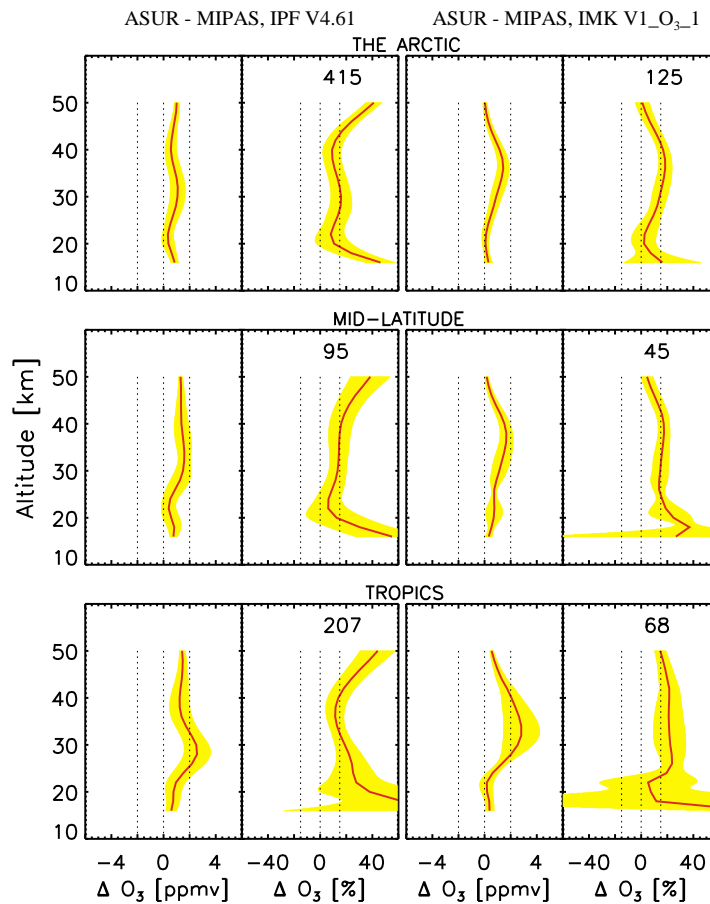
Figure 8.5: Same as Figure 8.3, but for MIPAS.

8.4 ASUR-OSIRIS comparisons

8.4.1 Data analyses

The stratospheric ozone profiles are retrieved, in number density, from the OSIRIS limb radiance data in the Chappuis absorption band. Profiles are calculated between 10 km and 50 km on a 2 km vertical grid using the paired radiance method developed by Flittner et al. (2000) and McPeters (2000) for the Shuttle Ozone Limb Sounding Experiment. This method was adopted to OSIRIS retrievals by von Savigny et al. (2003). OSIRIS-ASUR coincident ozone profiles are analyzed for the months of September 2002 and January-March 2003. The latest version 012 of the OSIRIS retrievals is used in the present comparison study. The OSIRIS ozone are taken from 16 to 40 km only because of sensitivity issues outside this altitude range (Petelina et al., 2004). It must be noted that as the time difference between the ENVISAT and Odin measurements over the same geographic area is about 8 hours, the coincidence criteria adopted for this study had to be increased to 8 hours or less in time. To facilitate the comparisons, OSIRIS ozone number density profiles are converted into the volume mixing ratio profiles using the synoptic meteorological data collected from NCEP and then convolved with the ASUR ozone averaging kernels. Typical examples of the individual OSIRIS-ASUR coincident profiles in the tropical, mid-latitude and the Arctic regions are shown in Figure 8.6.
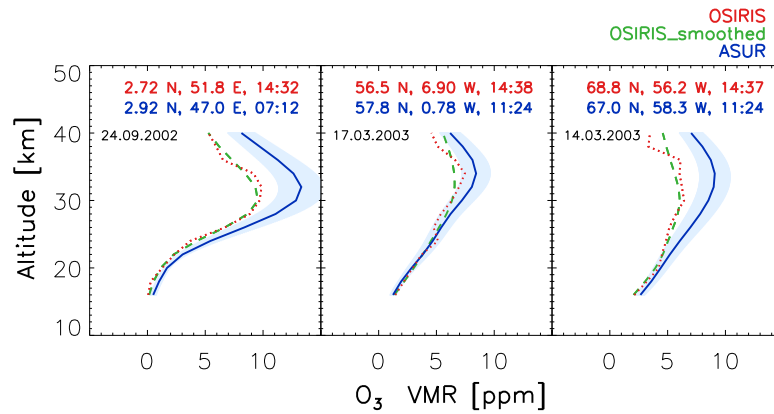
Figure 8.6: Examples of individual profile comparisons between ASUR and OSIRIS. The pale blue shaded area represents the estimated accuracy of ASUR ozone profiles.

8.4.2 Results

The statistical results for the OSIRIS-ASUR ozone comparisons in the tropics, mid-latitudes and the Arctic, as well as for all of these regions combined, are shown in Figure 8.7. The total number of coincidences is 177 with the majority, 117 instances, in the Arctic, 27 instances in the mid-latitudes, and 33 instances in the tropics. Apparently, the mean profile difference in the tropics is more than 30% below 20 km, about 25% between 20 km and 30 km and nearly 30% above 35 km. At mid-latitudes, the mean profile difference is around 20% between 16 km and 30 km and about 25% above 30 km. In the Arctic, the difference is within 10% below 22 km, from 10% to 20% between 22 km and 30 km, and 30% or more above 30 km.
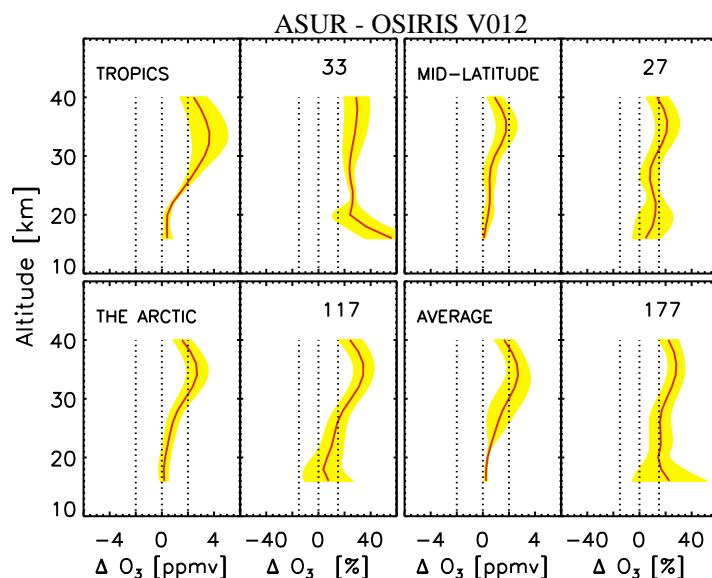
Figure 8.7: Same as Figure 8.3, but for OSIRIS.

8.5 ASUR-SMR comparisons

8.5.1 Data analyses

Stratospheric mode measurements of a small ozone line centered at 501.5 GHz are used in this study, based on version CTSO-222 retrievals of the Chaîne de Traitement Scientifique Odin (CTSO) (Urban et al., 2004; Urban, 2005). The ASUR data from 11 flights during the SCIAVALUE are used for this assessment. Since the SMR profiles are rather noisy, averaging of the profiles was necessary to get a reasonable low-noise profile. The SMR profiles were therefore averaged to the location of the nearest ASUR measurements over $7.5°$ latitude$\times 7.5°$ longitude area. However, the number of profiles averaged are not the same for all cases as it vary from 3 to 11. This is because of the unavailability of sufficient number of SMR profiles for a given ASUR measurement co-ordinate. The co-ordinates were also averaged along with the profiles to obtain the measurement co-ordinates of the new resultant profile. The averaged profiles are convolved with ASUR ozone averaging kernels to make them comparable with lower vertical resolution of ASUR ozone. The altitude range of the SMR ozone profiles is ~ 20 to 47 km and the vertical resolution is about 2.5 km with a single-scan precision in the order of 25% (Urban et al., 2004; Urban, 2005). The estimated systematic error of 501.5 GHz ozone measurements is less than 0.4 ppm at 25-50 km and less than 0.7 ppm below 25 km (Urban, 2005). Examples of the individual profile comparisons in the tropics, mid-latitudes and the Arctic are shown in Figure 8.8.
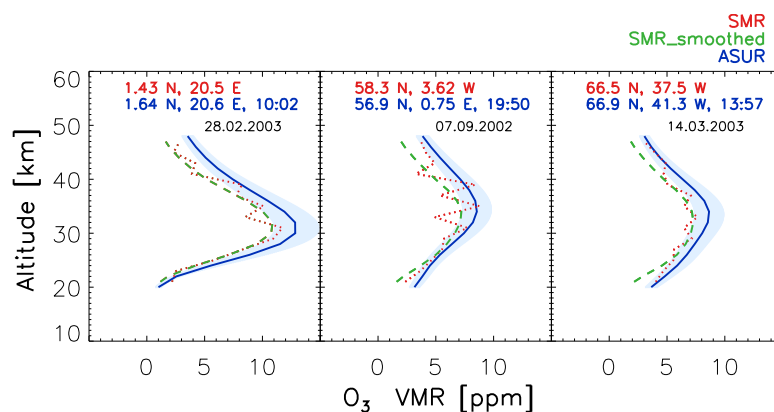
Figure 8.8: Same as Figure 8.2, but for ASUR and SMR.

8.5.2 Results

Figure 8.9 compares the SMR ozone with 25 tropical, 29 mid-latitude and 59 high latitude ASUR coincident measurements. In the tropics a constant deviation of 2 ppm is found from 25 km ownwards (to 47 km). At mid and high latitudes, the deviation in the lower stratosphere is up to 2 ppm, where the lowest deviation is found around 25 km and the highest around 18 km. Above 30 km the deviation is about 2 ppm or 10-30%, which is consistent with the tropical average. The deviation ASUR-SMR has the maximum in the upper stratosphere and the minimum around 25 km.
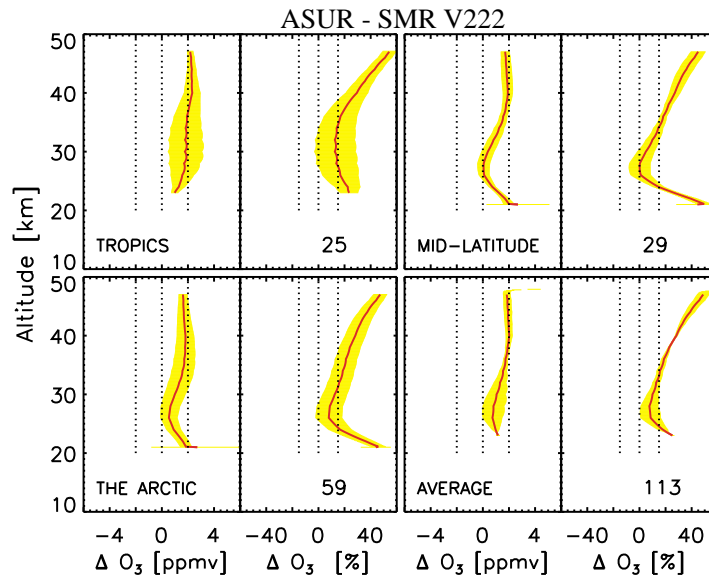
Figure 8.9: Same as Figure 8.3, but for ASUR and SMR.

8.6 Discussion

8.6.1 General features

Figure 8.10 shows that the deviation ASUR-SCIAMACHY is about 10-17% in 20 to 40 km at all latitude sections. In the lower stratosphere, though the absolute difference is reasonable, the difference in percentage is high. This can be due to the relatively higher mixing ratios in the ASUR against the near-zero values in the SCIAMACHY profiles. There are some systematic differences between the operational and the scientific products. The ASUR-UB 1.6 difference is getting smaller with altitude and even reversing the sign of the deviation in the upper altitudes. Also the lower stratospheric deviation in this dataset is larger than that of the OP 1.0 dataset. Comparing the scientific (IMK 1.0) and operational (IPF 4.61) products, the difference ASUR-MIPAS is within 2 ppm or 10-19% between 20 and 40 km. However, the difference in the tropics is relatively larger and shoots up to 2.5 ppm or 25%. Also, the deviation ASUR-IMK 1.0 is systematic and the maximum deviation is found at the peak ozone mixing ratio altitudes at all latitudes. The difference ASUR-IMK 1.0 is within 19% except in the tropical lower stratosphere. In general, the difference between ASUR and MIPAS is 15-25%. The relative difference between ASUR and OSIRIS is up to 4 ppm or 30%. The highest difference is found in the tropical upper stratosphere. The maximum difference always coincides with the altitudes of the maximum mixing ratios of ozone irrespective of the latitude regions. The deviation in the lower stratosphere is comparatively smaller. On average the ASUR-SMR difference is 2 ppm or 10-30% between 20 and 40 km.

Figure 8.10 illustrates the latitudinal average of the Δ profiles from all the analyses. There are a few common features in the deviation between the ASUR and the satellite ozone profiles. (a) The agreement at mid and high latitudes is comparable, (b) the deviation at the tropics is relatively larger and contributes significantly to the total deviation, (c) the lower and upper stratospheric differences are relatively high. However, the deviation in the upper stratosphere has no common trend. Considering an altitude range between 20 and 40 km, the difference is always in one direction. (d) It shows that the ASUR measurements overestimate the satellite
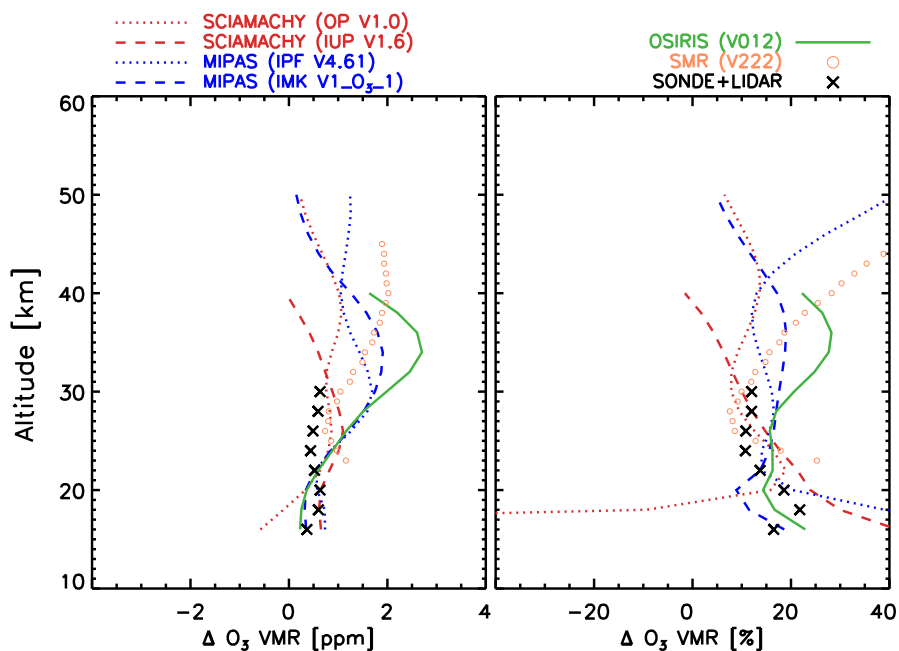
Figure 8.10: The average difference between ASUR and different sensors for all latitude bands. The resulted lines are representing the difference Δ = ASUR-satellite sensor in absolute and percentage scales. The SONDE+LIDAR measurements are adapted from Bremer (2001)

measurements by a certain factor. Except the case of OSIRIS the deviation is within within 2 ppm or 19%.

8.6.2 Reasons for the deviations

The ASUR ozone high bias: Bremer (2001) compared ASUR ozone measurements with numerous measurements from ozonesondes and Lidar (Light Detection And Ranging) instruments during the SOLVE (SAGE-III-Stratospheric Aerosol and Gas Experiment- Ozone Loss and Validation Experiment) mission (Newman et al., 2002), which was carried out in the winter of 1999/2000. This comparison is very reliable and robust and the analysis was produced from a large dataset. The independent measurement comparisons from SCIAVALUE or EUPLEX had no such detailed comparison and statistical analysis. So this study uses Bremer (2001) as a reference for the validation of ASUR ozone and the the following section briefly presents the data.

The selected ozonesonde measurements were from NyÅlesund (78.92°N, 11.93°E), Sodankyla (67.37°N, 26.65°E) and Orland (63.42°N, 09.50°E) and the Lidar instruments were the airborne Differential Absorption Lidar (DIAL) (Browell et al., 1983) and Airborne Raman Ozone, Temperature, and Aerosol Lidar (AROTEL) (McGee et al., 1995). The DIAL and ARO-TEL instruments were onboard the National Aeronautics and Space Administration (NASA) research aircraft DC-8 together with ASUR during the SOLVE campaign. So the measurements match temporally and spatially within a small horizontal offset of the ASUR observations, which comes from the high zenith angle of the ASUR measurements compared to the zenith geometry of the Lidar. The horizontal displacement ASUR-Lidar is 45 km at 20 km and 90 km at 30 km. The measurements from the Lidar sensors have been averaged over ±2.5 minutes around the mean time of the ASUR ozone measurements. The ozonesonde observations are

selected from the closest overpass measurements of the sonde station within a short interval of time. There were 787 coincident measurements with DIAL, 662 with AROTEL and 19 with the sondes together.

Figure 8.10 with the legend 'SONDE+LIDAR' shows the results from Bremer (2001). Since the deviation is unidirectional, it is obvious that the ASUR ozone has a high bias. As the SONDE+LIDAR also shows a positive deviation of 10-15%, it points out that ASUR ozone has a high bias of 12% in general. The bias could come from the uncertainties in the window transmission, uncertainties in the cold reflectivity (Kleinböhl et al., 2003) or from the uncertainty in the pressure broadening coefficient (von König, 2001). The pressure broadening coefficient used in the retrievals of ozone is taken from Rothman et al. (1992). Sensitivity studies show that for a given uncertainty of $\pm$ 10% for the pressure broadening coefficient, a change in the retrieved VMR up to $\pm$20% is expected for ASUR ozone (von König, 2001). The deviation is $\pm$ 8-12% between 20 and 40 km, $\pm$ 12-16% between 40 and 50 km, and the maximum difference is found around 19 km. The change is very systematic and can be in positive or negative direction. So this might be the main reason for the systematic high bias in the ASUR ozone. (a) As the ASUR ozone high bias contributes to the deviation significantly, which explains the systematic difference between the ASUR ozone and the SCIAMACHY, MIPAS, OSIRIS and SMR ozone. (b) With regard to the accuracy of the ASUR ozone measurements of 15%, the agreement between the profiles is reasonable as well.

Reasons for the statistical offset: Another reason for the deviation between the ASUR and the satellite ozone comes from the satellite ozone retrieval method. (c) The OSIRIS and UB V1.6 apply similar techniques to retrieve the ozone density profiles. With this technique the retrieved information content below 15 km (though it is not applicable to this study) and above 35 km is limited. It is because the optical depth becomes large below 15 km and thus limb retrievals cannot see the atmosphere any deeper. Above 38 km the absorption in the Chappius band becomes very weak, so the information content is low. (d) Moreover, the retrievals use only two orders of scattering terms as it neglects the higher orders because of smaller contribution from the higher orders. This negation of the scattering terms give rise to a few percent errors in the retrieved quantities. However, this effect is generally small and is about 1-2%, except below the altitudes of ozone maximum, where the gradient is relatively large (von Savigny et al., 2004). (e) The UB 1.6 and OP 1.0 initial validation shows that products agree within 10-15% compared to HALOE (Halogen Occultation Experiment) and SAGE-III (Bracher et al., 2004a). These results reasonably agree to our findings as well, barring the high bias in the ASUR ozone. (f) A previous study by Petelina et al. (2004) showed that the agreement between the OSIRIS and the POAM-III (Polar Ozone and Aerosol Measurements) ozone profiles is about 5 to 10% at 15-32 km and 15% above 32 km. It has also been noticed that the OSIRIS profiles have a low bias as compared to the POAM profiles above 30 km. Thus, the bias in the mixing ratio values of the sensor contributes to the deviation between the profiles. (g) In addition, the OSIRIS profiles have a downward altitude shift of about 1.0 km in April-July 2002 and March-June 2003 periods due to the incorrect altitude registration of the Odin satellite. The OSIRIS ozone comparisons with other instruments produced poor agreement during this period. The deviations were found up to 30% in this particular case (Petelina et al., 2004). This information is very important here as the ASUR-OSIRIS comparison include the data from March 2003 and the deviation is also in the same order of 30% at peak mixing ratio altitudes. So the inaccurate pointing registration of the satellite is also one of reasons for the offset between ASUR and the satellite (UB 1.6, OP 1.0, IPF 4.61, IMK 1.0, OSIRIS) ozone

profiles. (h) The IMK ozone in comparisons with HALOE and SAGE-III also show an agreement within 10-15% (Bracher et al., 2004b), in which the ASUR-IMK differences are found as well. (i) Other possible reasons for the deviation can be spatial and temporal differences in the measurements between the ASUR and the satellite sensors. The limb pixels of the satellite sensors on the ground can considerably deviate from the boundary limits of the ASUR observation. (j) The temporal difference can also contribute to the deviations due to the uncertainty in atmospheric variations.
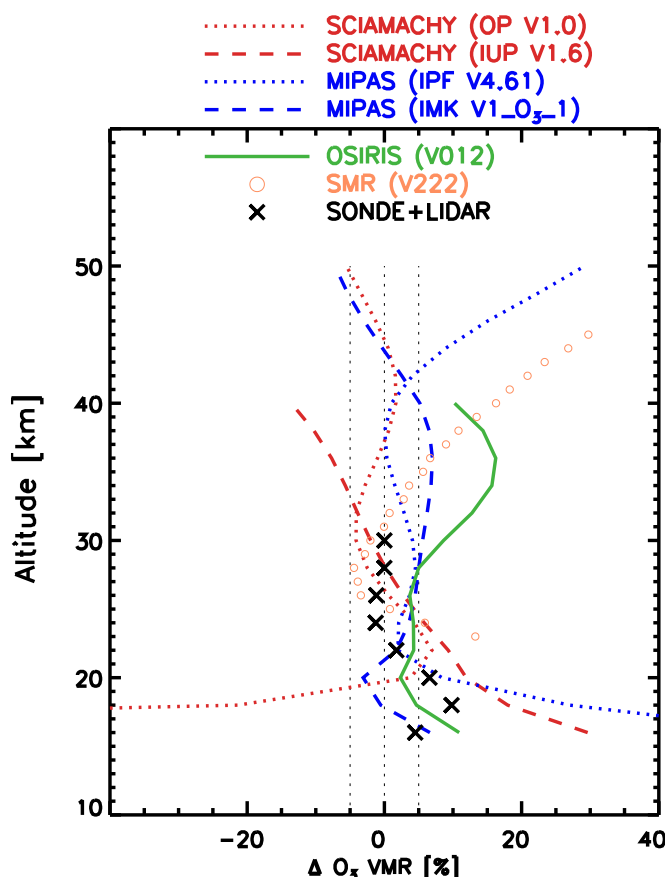
Figure 8.11: Same as Figure 8.10, but after subtracting the high bias of 12% in ASUR ozone. The dotted lines represent 5%.

Since there is an obvious bias in the ASUR ozone, a statistical analysis is made after subtracting the high bias of 12% (which is the difference in the middle stratosphere). These results are shown in the Figure 8.11. The individual deviations ASUR-OP V1.0 is -4 to 6%, ASUR-UB V1.6 is -12 to 15%, ASUR-IPF V4.61 is up to 5%, ASUR-IMK V1-O_3-1 is -3 to 6%, ASUR-OSIRIS is 3 to 15% and ASUR-SMR is -4 to 15% at 20-40 km, which show a very good agreement between the ASUR and the satellite ozone.

8.7 Conclusions

The SCIAMACHY, MIPAS, OSIRIS, and SMR ozone profiles are compared with ASUR ozone data which are gathered during the SCIAVALUE and the EUPLEX campaigns. The comparison criterion, measurements within $\pm$ 1000 km and $\pm$ 6 hrs, was common to all datasets except

for the OSIRIS coincidence, where the measurements were selected within $\pm$ 8 hours instead of $\pm$ 6 hours. The comparison analyses were performed for the tropical, mid-latitude and the Arctic sections separately. The analyses reveal that irrespective of the latitude sections the difference between the ASUR and respective sensor profiles is within 2 ppm or 19% at 20-40 km. Since the upper and lower stratospheric ozone mixing ratios are rather low, small absolute deviations result in large differences in percentage. The causes of the deviations are discussed in terms of ASUR and satellite sensors point of view. The analyses show that the deviation ASUR-SCIAMACHY (OP 1.0) is -4 to 6%, ASUR-SCIAMACHY (UB 1.6) is -12 to 15%, ASUR-MIPAS (IPF 4.61) is up to 5%, ASUR-MIPAS (IMK 1-O_3-1) is -3 to 6%, ASUR-OSIRIS (012) is 3 to 15% and ASUR-SMR is (222) -4 to 15% at 20-40 km, depending on altitude. The numbers are deduced after subtracting the ASUR high bias of 12%. Because of the good agreement between the profiles, the satellite sensor ozone profiles can be used for scientific studies in consideration with the results obtained from this study.

9 Validation of MIPAS and SMR: Intercomparisons with ASUR N_2O, HNO_3 and ClO measurements

This chapter deals with the comparison of MIPAS N_2O, HNO_3 and ClO and SMR N_2O measurements with the ASUR data. There are only a few instruments that can measure the aforementioned stratospheric constituent profiles, low latitudes in particular. So the comparisons with the ASUR measurements across the latitudes have a considerable significance in the accuracy estimation of the profiles. The ASUR observations of the trace gases during both the SCIAVALUE and the EUPLEX campaigns are used for these comparisons.

9.1 Nitrous oxide

9.1.1 MIPAS

Data analyses: The available IMK 1.0 data for the measurement days are analyzed. Most of the data belong to the tropics and mid-latitudes (within $35°N$) for the measurement days in September 2002. The ASUR measurements are selected within a ± 1000 km in ± 6 hours of the MIPAS measurements. The same criterion is applied for the comparison of N_2O, HNO_3 and ClO as well.
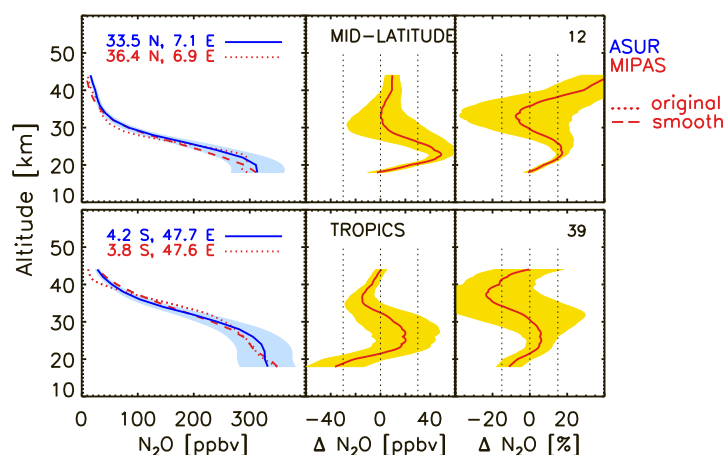
Figure 9.1: The absolute (Δ = ASUR-MIPAS VMR in ppb) and percentage (Δ VMR in %) difference between the ASUR and MIPAS N_2O profiles for tropics (bottom) and mid-latitudes (top). The first plot on the figure shows an example profiles for comparison at specific locations as noted in the figure. The yellow shade on the ASUR profile represents its estimated accuracy and the shade on the Δ profiles represent the standard deviation from the mean Δ profile.

Results: The comparison between ASUR and MIPAS N_2O profiles is shown in Figure 9.1. The left most plots illustrates the examples of the coincident measurements. The upper panel

stands for the mid-latitude and the bottom panel stands for the tropical analysis. The statistics derived from the 12 mid-latitude profiles are shown in the middle and right plots (upper panel), where the Δ VMR (ASUR-MIPAS) is up to 30 ppb or - 5 to 40%. The deviation in the tropics (lower panel) is within $\pm$30 ppb or - 20 to 10% as deduced from the 39 coincidence measurements.

9.1.2 SMR

Data analyses: The SMR data (CTSO V222) from September 2002, February and March 2003 are analyzed for the N₂O comparison. The data are averaged for the nearest ASUR measurement over 7.5°latitude × 7.5°longitude area within $\pm$6 hours. The number of profiles averaged vary from 4 to 11. The altitude range of the SMR profiles considered is 17-40 km due to the sensitivity issues outside this altitude limits. One tropical, two mid-latitude and one high latitude SMR profile remained as coincident measurements after the averaging.

   Results: The collocated N₂O measurements of SMR and ASUR are shown in Figure 9.2. Examples of the individual profile comparison are shown on the left, the Δ VMRs (ASUR-SMR) are shown in the middle, and the deviations in percentage are marked on the right plot respectively. The difference in the tropics and in the Arctic is up to 30 ppb or 15%, whereas the difference in the mid-latitude is within $\pm$10 ppb or -5 to 10%, except at 40 km.
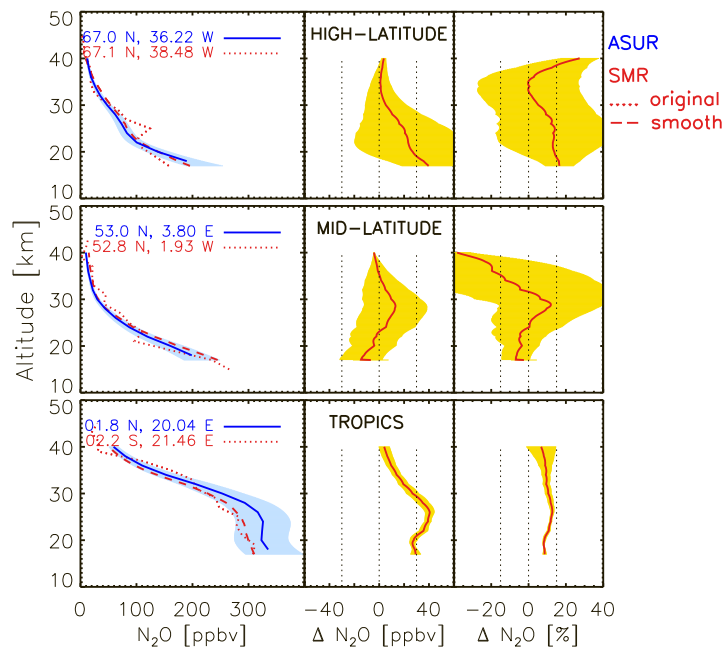
Figure 9.2: Same as Figure 9.1, but for SMR/Odin.
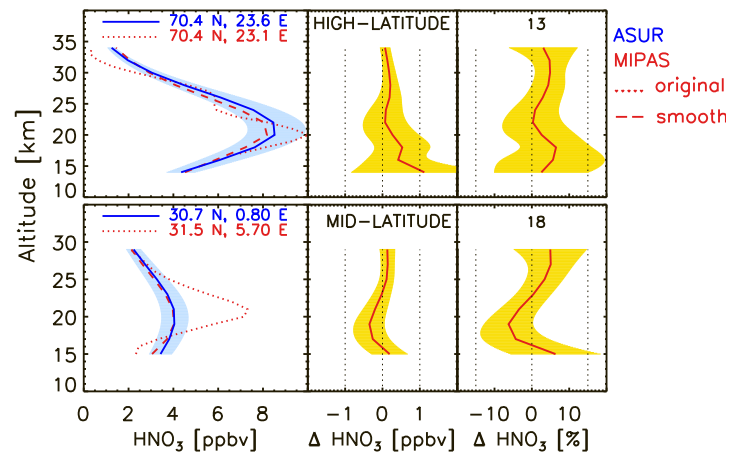
Figure 9.3: Same as Figure 9.2, but for MIPAS HNO$_3$.

9.2 Nitric acid

9.2.1 MIPAS

Results: Figure 9.3 shows the results from ASUR-MIPAS HNO$_3$ comparisons in the mid and high latitudes ($\geq 30°$N). There are 13 coincident measurements in the Arctic and 18 in the mid-latitudes. The procedure of data analysis is the same as done for the MIPAS N$_2$O. A very good agreement is found between the ASUR and MIPAS profiles at all latitudes. The difference in the mid-latitude is -0.3 ppb to 2 ppb or within 5% and the deviation in the Arctic is up to 1 ppm or 5%.
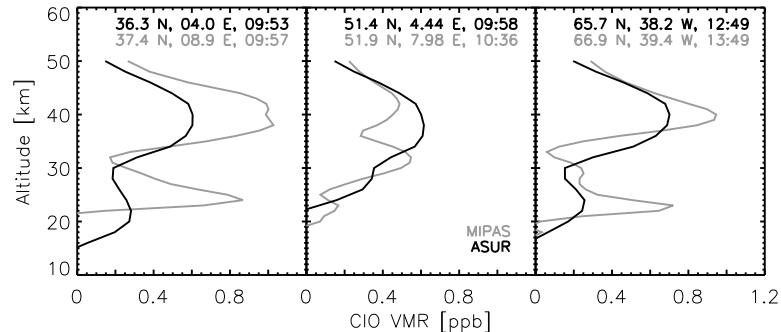
Figure 9.4: The profile comparison between ASUR and MIPAS ClO at specific measurements locations.

9.3 Chlorine monoxide

9.3.1 MIPAS

Results: There were not enough MIPAS measurements to compare with the ASUR ClO, at least for the campaign period. In addition, because of the lower sensitivity of the MIPAS profiles, only a few profiles were available to compare with the ASUR data. Moreover, after convolving with AKM, some negative values were still found in the lower stratosphere. So a detailed comparison was not possible with the restricted dataset. However, the data will be used for the validation purpose with a larger MIPAS dataset in future. The comparison of MIPAS and

ASUR ClO profiles at specific latitudes are shown in Figure 9.4. The profiles are not smoothed with the ASUR ClO kernels as it only demonstrates the capabilites of the sensors to observe the variations in the trace gas distribution and illustrates the possibilities of a future validation. The comparison looks very promising in the sense that the structures observed by both instruments are very similar.

9.4 Discussion

The deviation MIPAS-ASUR N$_2$O is systematic, which is clearly depicted in the shape of the Δ profiles (Figure 9.1). The values around 18 km are higher in the MIPAS and the values around 22 km are higher in the ASUR as well. Above 30 km the deviation is very small, around 5 ppb. However, the deviation is about 15% in general, except in the mid-latitude upper stratosphere. The initial validation by airborne, balloonborne and groundbased instruments shows that the MIPAS N$_2$O have a high bias in the UTLS (Upper Troposphere and Lower Stratosphere) region (Camy-Peyret et al., 2004). Hence, the deviation can be due to the problems in the MIPAS retrieval as it is very sensitive to clouds and aerosols in the UTLS. Since ASUR N$_2$O has a small high bias in the lower stratosphere (Greenblatt et al., 2002), that could also contribute to the differences. Nevertheless, the ASUR-MIPAS results are comparable with the results of Camy-Peyret et al. (2004).

Unlike the MIPAS data, the comparisons are performed in the tropics, mid-latitudes and in the Arctic between the SMR and the ASUR data. The deviations in the Arctic and the tropics are in the same direction, where the ASUR N$_2$O shows slightly higher values. However, the mid-latitude comparison yields quite good results as the deviation is very small. The high bias in the lower stratospheric ASUR N$_2$O, uncertainty in the atmospheric variations and the remaining noise in the SMR profiles can be the reasons for the offset between the profiles. It has also been noticed that the difference ASUR-SMR is in the accuracy range (30 ppb or 15%) of ASUR N$_2$O as well.

The deviation between ASUR and MIPAS HNO$_3$ in the mid-latitude is in the order of 0.2 ppb, where as in the high latitudes the difference is unidirectional for which the ASUR HNO$_3$ shows slightly higher values. The difference can probably be arised from the airmass variability. However, the difference is within 5% at all latitude sections, which is a very good agreement. Moreover, the deviation is well inside the accuracy (15%) of ASUR HNO$_3$.

9.5 Conclusions

The ASUR N$_2$O, HNO$_3$ and ClO observations during SCIAVALUE and EUPLEX are compared with the MIPAS and SMR measurements. The selection criteria for the comparisons is that the ASUR measurements that were performed in a ± 1000 km radius in ± 6 hours of the satellite measurements. The ASUR N$_2$O measurements in comparison with MIPAS and SMR show a deviation within 30 ppb or $\pm 15\%$, which is also inside the accuracy limit of the ASUR measurements. Hence, the ASUR N$_2$O in comparison MIPAS and the SMR produce promising results. The MIPAS and ASUR HNO$_3$ are in very good agreement, where the differences are within 5%. The initial comparison between ASUR and MIPAS ClO profiles show encouraging results for a future validation study.

10 The Bremen CTM: A new simple 3D model for stratospheric chemistry and transport studies

10.1 The model morphology

The Bremen CTM is a new three-dimensional chemical transport model, originally developed for studying the dynamics and chemistry of stratospheric ozone. A parameterized chemistry scheme is applied to account for the chemical state of stratospheric ozone in the model. Recently, a simulation setup for the trace species N_2O and NO_y was also incorporated. This chapter describes the general features of the model, transport processes, and the chemistry scheme used with the model. Table 10.2.1 gives a concise picture of the model setup.

10.2 Chemistry module

10.2.1 The linearized ozone chemistry, Linoz

Three-dimensional model calculations which include a large number of chemical reactions are computationally very expensive. In contrast, a parameterized chemistry scheme provides computationally effective (as it uses only a single tracer) and accurate simulation of the species concerned. Cariolle and Déqué (1986) and Prather et al. (1990) were the first to implement a simplified linearization of ozone chemistry in chemical transport models (CTMs) to calculate the ozone distribution in the stratosphere. Later, McLinden et al. (2000) developed an effective and accurate parameterization for the linearized ozone (Linoz) chemistry to be used for atmospheric models. The real strength of Linoz lies in its application to be employed in climate models and data assimilation models since it considerably reduces the time required for the calculations and storage space for post processing of the data. Estimation of cross-tropopause flux and simulations of a reasonable ozone gradient at the tropopause are the other potential applications of the scheme. Since it is a linearization of the ozone chemistry, Linoz does not mean to compete with full chemistry models. The scheme drives the model towards the photochemical balance not to the climatological state.

The ozone chemical tendency is calculated as a linear function of local ozone mixing ratio (μ), temperature (T), and the overhead ozone column density (cO_3) under the assumption that the key families like NO_y, Cl_y, Br_y and the long lived tracers like N_2O, CH_4, H_2O do not vary significantly from the mean distribution state. That is,

$$\frac{d\mu}{dt} = (P - L) \ [\mu, T, cO_3].$$

The ozone tendency is represented by P-L in *ppmv* per *seconds*, the square bracket stands for the functional dependence, and cO_3 is the overhead ozone column above the point under

Parameter	Specifications and Reference
Model grids	72×96
Horizontal resolution	$2.5°$ latitude $\times 3.75°$ longitude
Vertical resolution	1.5-2.0 km in the lower stratosphere
Vertical coordinate	Potential temperature (300-3000K)
Model time step	30 minutes (output at 12 UT)
Met fields	UKMO, Swinbank and O'Neill (1994)
Vertical transport	MIDRAD, Shine (1987)
Chemical advection	Second order moments, Prather (1986)
Ozone chemistry	Linoz, McLinden et al. (2000)
Rapid polar ozone loss	Sinnhuber et al. (2003)
N_2O chemistry	Olsen et al. (2001)
NO_y chemistry	Olsen et al. (2001)

Table 10.1: The general features of the Bremen CTM.

consideration. A first order Taylor expansion is then applied for the linearization,

$$\frac{d\mu}{dt} = (P-L)^m + \frac{\delta(P-L)}{\delta\mu}|_\delta(\mu - \mu^m) \quad + \quad \frac{\delta(P-L)}{\delta T}|_\delta(T - T^m)$$
$$+ \quad \frac{\delta(P-L)}{\delta cO_3}|_\delta(c - cO_3^m)$$

where the climatological values are represented by the superscript m and the subscript δ denotes the values of partial derivatives at μ^m, T^m, and cO_3^m. The scheme uses McPeters (1993) for ozone and column ozone, and Nagatani and Rosenfield (1993) for temperature climatologies.

Linoz consists of seven sets of coefficient tables calculated at 25 pressure altitudes (10 to 58 km in 2 km increment), in 18 latitude sections (-85°S to 85°N) for 12 months. The first four tables give the diurnally averaged climatological ozone tendency and the three partial derivatives to find the time constant. The time constant defines the photochemical relaxation time as a linearization for the loss. The rest of the tables give the ozone, the ozone column and the temperature climatologies respectively. The coefficients are mapped onto the CTMB grids and are interpolated to the model altitude layers to generate an effective set of seven tabulated coefficients exclusively for this model. Further details about Linoz can be found in McLinden et al. (2000).

10.2.2 Rapid polar ozone loss parameterization

Linoz does not include large scale non-linear perturbations beyond the climatological steady state. It is well known that the catalytic processes on the surface of the Polar Stratospheric Clouds (PSC) lead to the chemical destruction of ozone in the Arctic and the Antarctic lower stratosphere (Solomon, 1999; WMO, 2002). As the Linoz does not simulate an ozone hole (rapid loss of ozone) the CTM incorporates a simple parameterization. As a result, ozone is destroyed with a constant life time of 10 days whenever the temperatures are below the formation point of Nitric Acid Trihydrate (NAT) and solar zenith angles are below 85°. The param-

eterization has been validated in comparison with NyÅlesund ozonesonde data (Sinnhuber et al., 2003).

10.2.3 N_2O and NO_y chemistry

Simulations of N_2O and NO_y in the model are achieved by a photochemical parameterization derived by Olsen et al. (2001). The production of NO_y and loss of N_2O are computed from five pre-calculated coefficient tables which were calculated for 20 pressure altitudes (14 to 52 km off 2 km spacing), 18 latitudes (85°S to 85°N with 10° interval) and for 12 months. These coefficients are mapped onto the model grids and interpolated to the model vertical layers using the second order moments. The integration of the molecules takes 3 years to reach equilibrium because of their relatively long photochemical lifetime. The following describe the underlying chemistry processes and the tables that represent the reaction schemes.

R_1	$N_2O + h\nu \rightarrow N_2 + O(^1D)$	
R_2	$N_2O + O(^1D) \rightarrow N_2 + O_2$	
R_3	$N_2O + O(^1D) \rightarrow NO + NO$	
R_4	$NO + h\nu \rightarrow N + O$	
R_5	$N + O_2 \rightarrow NO + O$	$k = 1.5 \times 10^{-11} e^{-3600}/T$
R_6	$N + NO \rightarrow N_2 + O$	$k = 2.1 \times 10^{-11} e^{-100}/T$
R_7	$N + NO_2 \rightarrow N_2O + O$	$k = 5.8 \times 10^{-12} e^{-220}/T$
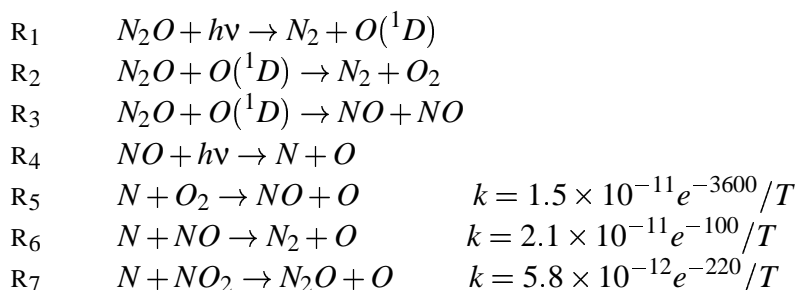
The rate constants and photolysis cross-section are taken from DeMore et al. (1997). The transmission through the molecular oxygen Schumann-Runge (SR) bands uses an opacity distribution function for each band as done by Fang et al. (1974). The reactions R_1 through R_3 describe the N_2O loss and NO_y production which depend on four factors, (a) the local ozone amount, (b) the overhead oxygen column, (c) the overhead ozone column and (d) the local temperature. All the dependent parameters are prescribed in the climatology. The following describes the tables and the relevant reactions.

C_1 : The daily mean N_2O loss frequency (R_1+R_2+R_3).

C_2 : The fractional yield of NO from N_2O loss (R_3) divided by the net loss (R_1+R_2+R_3).

C_3 : The 24 hour average NO photolysis frequency per NO_y molecule and it includes the diurnal average of the product of NO photolysis and the fraction of NO_y as NO. Thus, the production of atomic N is calculated in the model is the amount of NO_y times the frequency from the table C_3.

C_4 : Used to calculate the fraction of atomic N reacting with NO (R_6) or NO_2 (R_7) and thus destroying two NO_y molecules contrary to R_5 where, NO_y is regenerated. The coefficients in the R_4 are the ratio of the rates of R_6+R_7 to that of R_5 divided by mixing ratio of NO_y (μ_{NOy}).

C_5 : The fraction of NO_y loss that regenerates N_2O [$R_7/(R_6+R_7)$]. The reactions R_1 through R_3 describe the N_2O loss and subsequent NO_y production. About 90% of N_2O is photolyzed (R_1) and the rest reacts with odd oxygen atom in which $\sim$ 6% of the N from (R_3) N_2O converts into NO_y. The tables C_1 and C_2 are used to calculate the production of NO_y and loss of N_2O in the CTM. They depend only on photolysis frequencies of N_2O and O_3 and the rate coefficients for the reactions R_2 and R_3 and are independent of local amount of N_2O. The NO_y loss occurs through the reactions R_4 to R_7 and depends on the four factors described previously and the local abundance of NO_y itself. The coefficients C_4 and C_5 are independent of the local

NO$_y$ distribution assumed in the climatology. The loss frequency of NO$_y$ is non-linear in its abundance and is calculated as,

$$L_{NO_y} = \frac{2 \times C_3 \times (C_4 \times \mu_{NO_y})}{(1 + C_4 \times \mu_{NO_y})}.$$

10.3 Discussion and Summary

The limitations of the chemistry scheme: The chemical module for O$_3$, N$_2$O and NO$_y$ is derived from the current knowledge of photochemical mechanisms, cross-sections, climatologies and rate constants (DeMore et al., 1997; Nagatani and Rosenfield, 1993; McPeters, 1993). Apart from the limitations of the linearizations, the uncertainty in the above given quantities are also affected by the simulations of the trace gases [for e.g., changes from DeMore et al. (1997) to Sander (2003)]. The upper stratospheric 'ozone deficit' problem is an example, which is common to most models that use DeMore et al. (1997) reaction rates because of the uncertainties in the rate constants. Previous studies with the Linoz calculations have shown that (a) error in the simulated ozone is about 10-20%, (b) the upper stratospheric values underestimate the observations by 10-20%, (c) simulated results in the tropics underestimate the observed values by 0.5-1.0 ppmv at the peak mixing ratio altitudes [this difference is increased if the ozone column feedback is not included in the model since the column pushes back the ozone into the climatological state as a 'self healing' processes (Brasseur and Solomon, 1984)] and (d) the calculated ozone is slightly reduced in response to warmer temperature climatologies. (e) For N$_2$O, the VMR simulations are quite sensitive to transport in the model, the tropical upwelling in particular. This in turn has a dominant impact on the mixing ratio values and the lifetime of the molecule in the model. (f) The meteorological analyses have a profound impact on the location and magnitude of NO$_y$ maxima as well.

The advantages of the chemistry scheme: The scheme provides simple but accurate calculation of the trace gases with negligibly small CPU (Central Processing Unit) use, which is particularly useful for long term trend analysis with chemistry, climate and data assimilation models. The chemistry scheme has been very much successfull in estimating ozone chemical propagation (Prather et al., 1990), calculation of ozone loss (Sinnhuber et al., 2003), cross-tropospheric flux (McLinden et al., 2000), N$_2$O and NO$_y$ budget and lifetime analyses (Olsen et al., 2001), stratospheric NO$_2$ trends (McLinden et al., 2001), stratosphere-troposphere mass exchange (van Noije et al., 2004), ozone fore/hindcastes (McCormack et al., 2004), etc. The Linoz also allows on-line calculation of ozone columns and photolysis/heating rates.

Summary The Bremen CTM uses parameterized chemistry derived form the 'current' understanding of photochemical mechanisms, reaction rates, rate constants supplemented by a set of climatological values with certain assumptions as constraints. The schemes try to incorporate all the possible current knowledge to simulate the tracers realistic and accurate. Incorporation into GCMs and CTMs to perform long term integrations to carry out trend analyses, with negligibly small CPU use, is the main advantage of the parameterized chemistry schemes used in the model.

11 Evaluation of chemistry and transport processes in the Bremen CTM.

The quality of the ozone, N_2O and NO_y simulations from the Bremen CTM *are evaluated in this chapter. The chemistry employed and the transport processes applied in the model are critically analyzed with the help of measurements and other model calculations.*

11.1 Data analyses

Ozone profile measurements from SHADOZ (Thompson et al., 2003a,b), NDSC (Logan, 1999), HALOE (Russell et al., 1996), and POAM-3 (Randall et al., 2003) are used for a detailed validation of the simulations. In addition, three climatologies: The KNMI (Fortuin and Kelder, 1998), HALOE v18 (Russell et al., 1996) and IUP UB (Lamsal et al., 2004) are exploited as well. The N_2O simulations are examined with ASUR, ATMOS-3 (Abrams et al., 1996), CLAES (Roche et al., 1996), CRISTA-1 (Riese et al., 1997) and CRISTA-2 (Riese et al., 2002) measurements and the SLIMCAT, the UCI (McLinden et al., 2000), and the UCI GISS (Olsen et al., 2001) simulations. It should be noted that the same chemistry scheme has been used in the CTMB and the UCI models. Transport in UCI GISS is driven with a single year of meteorological analyses from the GISS middle atmosphere GCM, which are recycled annually to steady state. So the model output does not represent any particular year as noted from the meteorological fields. The comparison of the CTMB results with the SLIMCAT simulations (Tian and Chipperfield, 2004) are also interesting since the models use similar transport schemes. The NO_y comparisons make use of Shia et al. (1998) measurements and UCI GISS and the UCI simulations. The specifications of the data are given in Table 11.2 and Table 11.2.

11.2 Evaluation of the Linoz chemistry

Figure 11.1 shows the comparisons of the zonally averaged monthly mean ozone simulations with three different ozone climatologies, the KNMI, the HALOE and the IUP UB for January, April, July and October 2002. Qualitatively, the model reasonably imitates the lower and upper stratospheric values and fairly reproduces the latitudinal gradients. There are high mixing ratios 'tongues' extending from mid to high latitudes at southern and northern latitudes in certain months (for eg: April). A small difference is found in the tropical latitudes where the simulated mixing ratios underestimate the climatological values by $\sim 10\%$. This difference is the largest with the Bremen climatology. It is of special importance that this climatology is created from the measurements made during the recent years (1991-2002). So the climatology is a more realistic representation of the current state of the stratospheric ozone volume mixing ratio distributions.
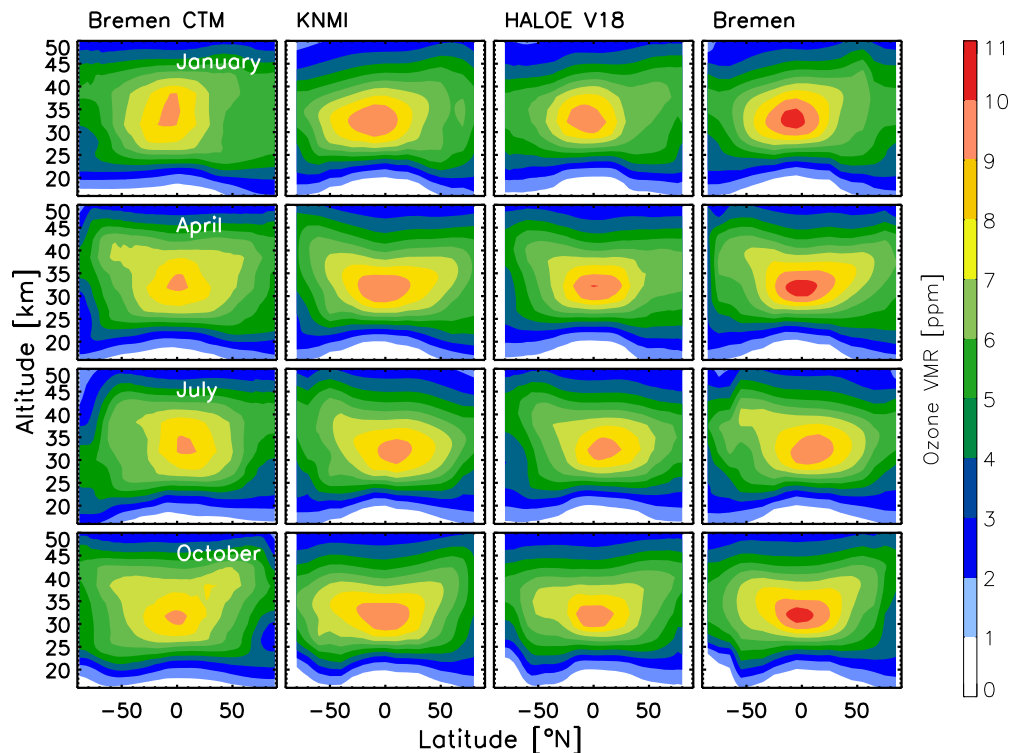
Figure 11.1: The zonally averaged monthly mean CTMB ozone is compared with the KNMI, the HALOE, and the Bremen climatologies.

In order to examine the difference in the tropical latitudes closely, a large number of the ozonesonde observations are compared with the simulations. A number of ozonesonde measurements from the SHADOZ and the NDSC stations were selected for the comparison. Since the sonde data are good only up to 30 km in general, a height barrier of 30 km is set. The ozonesonde measurements which were observed below 30 km are not selected for this analysis as well. The data are then binned to 50 m and interpolated up to 30 km. The names, coordinates and the number of profiles for comparison are listed in Table 11.2 and Table 11.2. Since there were no measurements in fall 2002, the comparison is made for fall 2001 for the Nairobi ozonesonde measurements. As the maximum altitude coverage by ozonesonde measurements is up to 30 km, satellite measurements (POAM-3 and HALOE) are also used to examine the quality of the middle and upper stratospheric ozone simulations. At each latitude section 40 HALOE profiles are averaged. To be consistent with, the ozone profiles are analyzed from 20 km since some of the tropical profiles do not extend further down. The simulated data are then interpolated to the co-ordinates of the sonde/satellite measurements for the measurement days. As there were no striking seasonal patterns, the data are presented for the complete observation period.

The compact and summarized picture of the analysis and the results are shown in Figure 11.2. The POAM-CTMB deviation is about -0.5 to 0.3 ppm or $\pm$ 6% for the 313 instances at 20-50 km. The difference between the HALOE and the CTMB profiles is about -1.0 to 0.7 ppm or -20 to 10% in the same altitude range for the 960 coincidences. The SHADOZ-CTMB difference in the tropics is up to 1.2 ppm or -20 to 10% above 20 km. Whereas, the simulations always underestimate the mid-latitude NDSC sonde measurements by 0.3 ppm or up to 15% at 20-30 km. There are a few common features like, (a) the simulations overpredict the upper stratosphere (with peak at 44 km) and the lower stratosphere measurements. (b) The

Measurements	Time	Molecule
Airborne		
ASHOE/MAESA	Nov 1994	O_3, NO_y
ASUR	Sep 2002, Feb, Mar 2003	O_3, N_2O
Groundbased		
SHADOZ	2002 and Jan - Mar 2003	O_3
NDSC	2002 and Jan - Mar 2003	O_3
Spaceborne		
ATMOS-3	Nov 1994	N_2O
CRISTA - 1	Nov 1994	N_2O
CRISTA - 2	Aug 1997	N_2O
HALOE	2002 and Jan - Mar 2003	O_3
POAM	2002 and Jan - Mar 2003	O_3
Climatology	Not applicable	
CLAES		N_2O
HALOE V18		O_3
IUP UB		O_3
KNMI		O_3
Models		
UCI GISS	2002	N_2O, NO_y
SLIMCAT	Sep 2002, Feb, Mar 2003	O_3, N_2O
UCI	Not applicable	N_2O, NO_y

Table 11.1: The measurements, model results and climatologies used for the validation of the CTMB simulations.
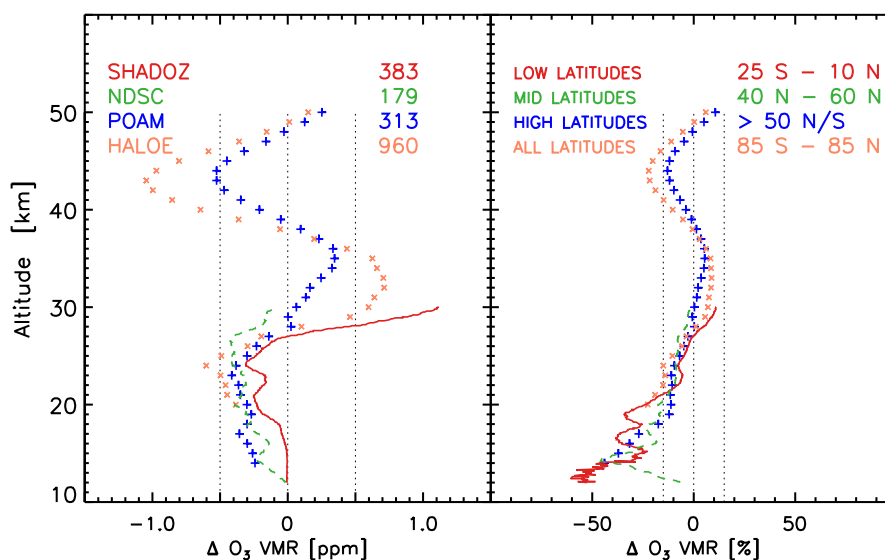
Figure 11.2: The deviation measurements-CTMB ozone simulations is shown for the different datasets used in the comparison. The numbers indicate the number of profiles averaged for each dataset.

Sensors	Lat, Lon	No: Profiles
SHADOZ		
Irene	25.90°S, 008.22°E	31
Suva	18.13°S, 178.40°E	22
Am. Samoa	14.23°S, 170.56°W	46
Ascension	07.98°S, 014.42°W	46
Natal	05.42°S, 035.38°W	52
Malindi	02.99°S, 040.19°E	10
Nairobi	01.27°S, 036.80°E	43
San Cristobal	00.92°S, 089.60°W	45
Kuala Lumpur	02.73°N, 101.70°E	23
Paramaribo	05.81°N, 055.21°W	45
NDSC		
Hohenpeissenberg	47.80°N, 011.02°E	127
De Bilt	52.10°N, 005.18°E	52
Space-borne		
ATMOS-3	00-60°N, 60-80°S	143
CRISTA - 1	60°S - 90°N	457
CRISTA - 2	90°S - 90°N	1434
HALOE	85°S - 85°N	240
POAM3	≥ 50°S/N	313

Table 11.2: The measurements used to validate the CTMB simulations. The sensors, latitudinal coverage, and the number of profiles used for the comparisons are also listed.

simulations underestimate the middle stratosphere measurements, which is maximum at the altitude of maximum ozone volume mixing ratio. (c) Considering the Δ (measured-calculated) profiles, the lowest deviation (in %) is found in the middle stratosphere.
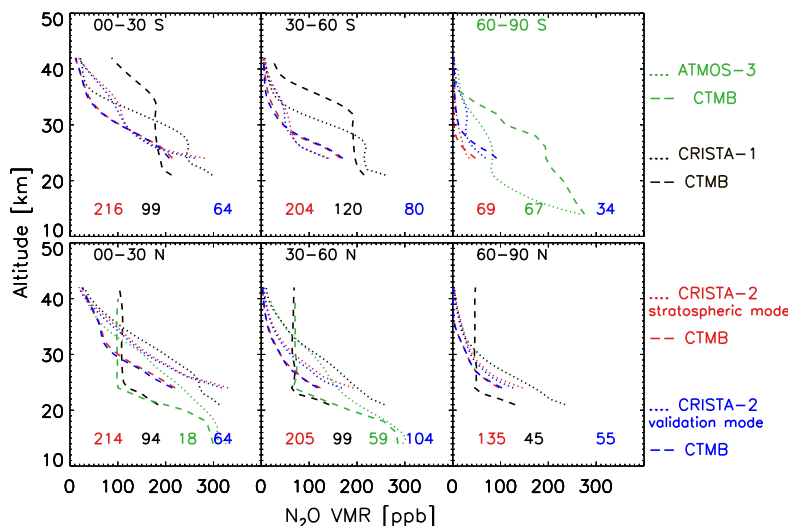
Figure 11.3: The CTMB N_2O profiles are compared with ATMOS-3, CRISTA-1 and CRISTA-2 measurements. The latitude sections and the number of profiles averaged in each section are also scripted in respective color codes.

11.3 Investigation of N$_2$O chemistry and transport in the model

Figure 11.3 shows the comparison between the ATMOS-3 and CRISTA-1 N$_2$O measurements with the CTMB simulations. Both missions took place in the same month with a difference of a few days. So the CRISTA-1 comparison also give an opportunity to check the consistency of the simulations and examine the validity of the comparison between CTMB and ATMOS-3. In the northern hemisphere (NH) the simulations underestimate the measurements in the the lower and middle stratosphere and overestimate the measurements in the upper stratosphere. Moreover, the model profiles show constant values right from 25 km upwards. The difference between the measurements and the simulations reduces with the latitude towards the northern pole. Whereas in the southern hemisphere (SH) the model profiles overestimate the measurements. The profiles show a high elevation in the southern high latitudes too. Hence, the CTMB simulations in comparisons with both the ATMOS and the CRISTA-1 measurements show a similar pattern. Figure 11.3 also shows the comparisons of the CTMB N$_2$O simulations with the CRISTA-2 measurements taken in the stratospheric and validation observation modes. The simulated profiles underestimate the NH measurements, though the difference is getting abated with latitude. In the SH, the calculations overpredict the lower stratospheric and underpredict the middle stratospheric measurements.

Figure 11.4: The zonally averaged monthly mean N$_2$O data from the CTMB simulations for year 2002 are compared with the CLAES climatology and the UCI GISS and the UCI model simulations. The white vertical dashed line in CLAES plots show the transition region from negative to (interpolated) positive values.

Figure 11.4 compares the monthly mean simulations of N$_2$O from CTMB with the CLAES climatology, the UCI GISS and the UCI model simulations. Though the CTMB simulations

capture the latitudinal and seasonal distributions reasonably, the simulated mixing ratios are relatively smaller in the lower stratosphere. In addition, a tongue like structure is extending to the southern latitudes, which is absent in the CLAES and in the other model (UCI and UCI GISS) simulations. This is very evident at 225-250 ppb level. A high VMR pocket is formed in the CTMB calculations in the high northern latitudes in July. In January, elevated VMR levels (at 125-150 ppb) are found in the southern latitudes, which is also slightly different from the CLAES and the other model simulations.
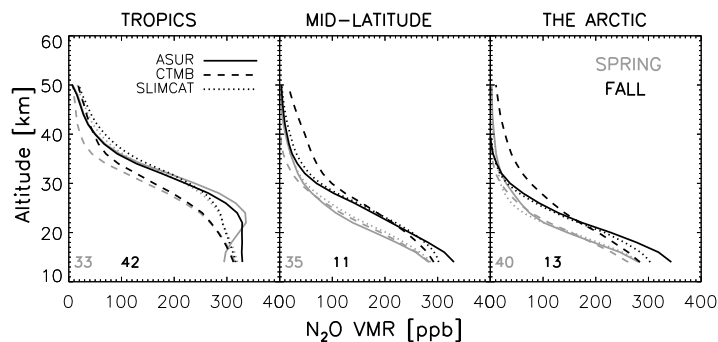
Figure 11.5: The simulated N_2O profiles from CTMB are compared with SLIMCAT and ASUR profiles in fall 2002 and spring 2003 seasons at different climatic regimes. The number of averaged profiles in each region is noted at the bottom of the respective plots in the same colour code. The profiles are reduced into ASUR vertical resolution to compare together.

Figure 11.5 shows the comparison among the ASUR measurements, the CTMB and the SLIMCAT simulations. Since both models use the similar transport scheme, the comparisons between the model results have a special significance. The tropical and mid-latitude CTMB profils always underpredict the measurements and the SLIMCAT simulations. Though the Arctic lower stratospheric mixing ratios underestimate, the middle and upper stratospheric values overestimate the measurements and the SLIMCAT results. There is a tendency in CTMB to simulate relatively high values in the upper stratosphere. Though there is hardly any seasonal difference in the tropics and mid-latitudes, the spring to fall difference in CTMB is very evident in the high latitude profiles. Hence, the comparison affirm that the simulated tracer mixing ratios with CTMB are slightly smaller. Since the transport scheme is similar, the differences in the chemistry scheme (uncertainties in the reaction rates used), the model resolution together with the meteorological data can be reasons for the lower values in the simulations.

11.4 NO_y simulation and impact of meteorological analyses on the calculation

Figure 11.6 compares the monthly mean NO_y simulations for 1998 and 2002 with the UCI GISS and the UCI model calculations. Since NO_y in the model is produced from N_2O, the simulations also give a chance to diagnose the coupled N_2O-NO_y chemistry in the model. The production of NO_y from N_2O is very quick at 35-40 km in the tropics. It is transported poleward and downward from the source region. The transport and continued production results into a latitudinal gradient, which is prominent in the lower stratosphere. Reaction with atomic nitrogen above 40 km and transport down to the troposphere are the significant loss
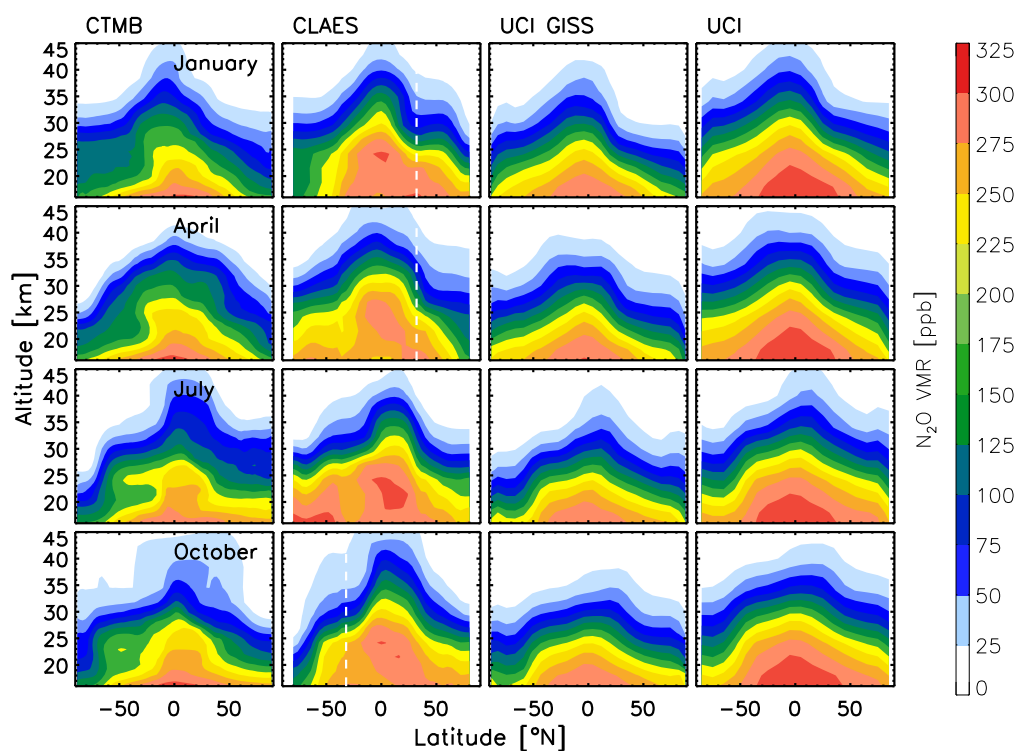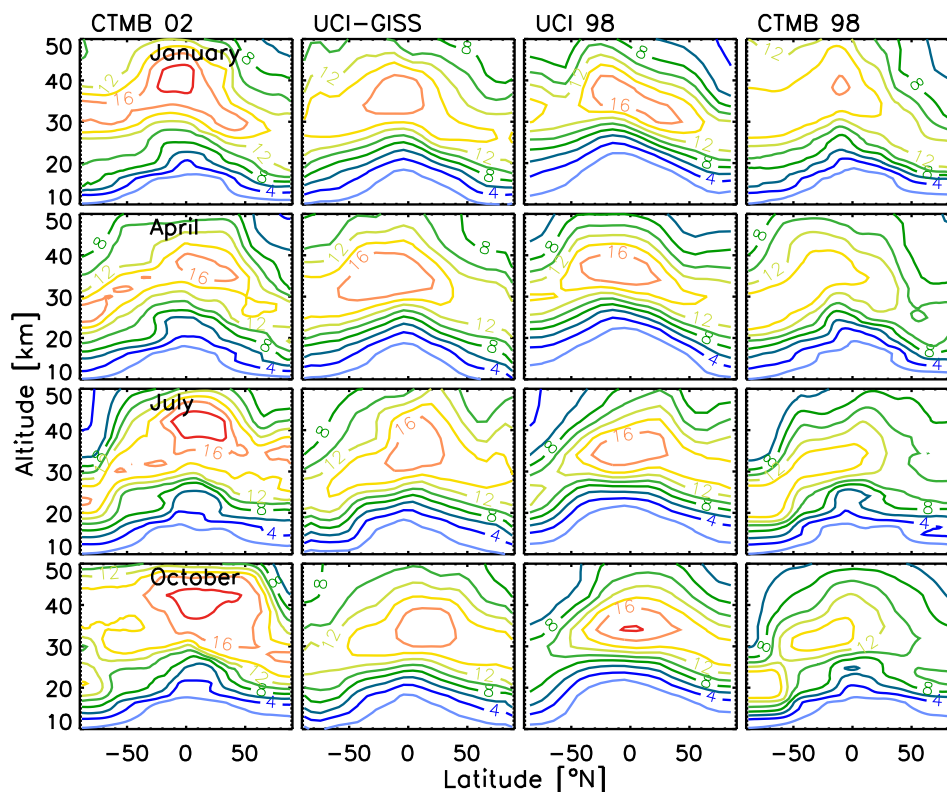
Figure 11.6: The zonally averaged monthly mean NO$_y$ data from the CTMB simulations for 1998 and 2002 are compared with the UCI GISS and the UCI model simulations.

processes. Mixing with low latitude NO$_y$ as well as the downward transport produce vertical gradient in NO$_y$ profiles in the stratosphere. Since denitrification can make a strong vertical and horizontal gradient in NO$_y$ profiles, the high latitude mixing ratio is strongly influenced by this underlying processes. Airmass descent at high latitudes from mesosphere (and even from thermosphere) makes mixing ratios little higher in the upper and middle stratosphere, which is apparent in the simulations for the winter months in both hemispheres.

The CTMB 98 NO$_y$ simulations are comparable with the UCI simulations. However, the CTMB simulations quantitatively overestimate the lower stratospheric and underestimate the middle stratospheric UCI calculations, especially at the altitude of maximum mixing ratios. Furthermore, the high values simulated in the upper stratosphere by CTMB in certain months are absent in the UCI calculations (for e.g., January for the southern high latitudes and July for the northern high latitudes upper stratosphere). As compared to the UCI simulations, the agreement between the CTMB 98 and UCI GISS are better and consistent. The CTMB 98 results well reproduce the UCI GISS simulations. Nevertheless, the absolute difference is higher than those of the UCI calculations, so that the CTMB 98 underestimate the mixing ratios with altitude. Though the shape and gradients of the mixing ratio distribution are similar for the CTMB 02 and the UCI GISS simulations, the difference between the absolute values has no common trend unlike the CTMB 98 and UCI GISS simulations. In certain seasons, the CTMB 02 overestimate the UCI GISS simulations (e.g., September) and in some other seasons the CTMB 02 underestimate the UCI GISS calculations (e.g., April). The same chemistry scheme in the models indicate that the discrepancies might be contributed by the differences in the wind fields used together with the differences in transport in the models. Again, a noted dif-

ference is found between the CTMB calculations for the years 1998 and 2002. It is unlikely that the NO_y mixing ratios to be changed that dramatically within the time span of four years from 1998 to 2002. Since the meteorological fields are the only change in the model input domain, the analyses are the apparent cause of the drastic change in the simulations. This experiment attests that the meteorological analyses used for the model runs have great impact on the simulations.
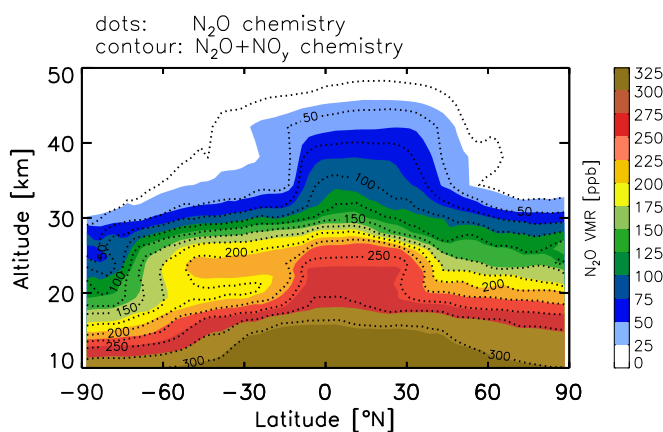
Figure 11.7: The zonally averaged N_2O data from the CTMB simulations for 04 September 2002. The color filled contours show the results from the simulations with the N_2O and NO_y chemistry run and the dot contours show the results from the N_2O only chemistry run.

11.5 Influence of NO_y on the calculations of N_2O

Although N_2O is necessary to simulate NO_y, N_2O can be calculated with and without NO_y in the model. Figure 11.7 shows the N_2O simulations including and excluding NO_y in the chemistry scheme in the model. The tropical isopleths are slightly higher (in the order of 1-2 km) in the N_2O only run. Though the elevated isopleths can be seen throughout the latitudes for this particular run, this is more clear and more affected in the tropics. Since NO_y is calculated from N_2O, a small amount of NO_y is converted back into N_2O as well (refer table C5 listed in the previous chapter). The NO_y excluded run omits the conversion of NO_y to N_2O, which eventually results into the difference.

11.6 N_2O-NO_y correlations: Implications for the chemistry scheme

Long-lived tracers exhibit a compact relationship in the stratosphere (Plumb and Ko, 1992). Such relationships are extensively used to diagnose model calculations. The photochemical lifetime of N_2O and NO_y are longer than the horizontal transport time in the lower and middle stratosphere. So the constituents show a very robust correlation in the stratosphere. They are negatively correlated and show a linear relationship up to 50 ppb of N_2O. For smaller values of N_2O the relationship turns into a curvilinear form as the lifetime of both molecules shortens
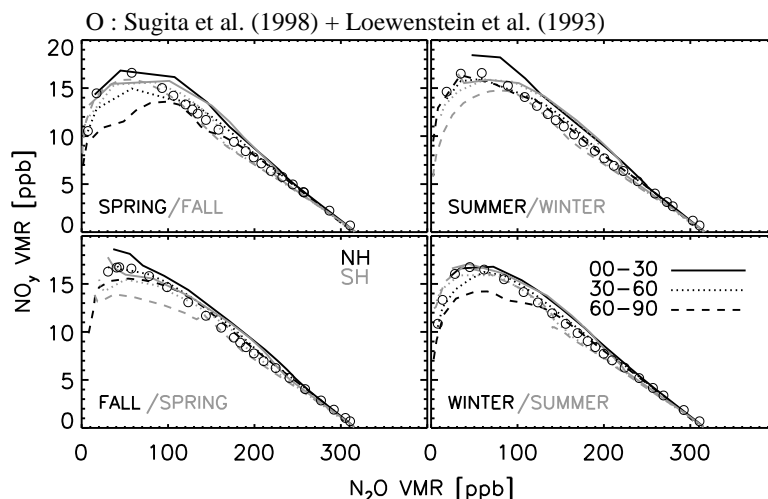
Figure 11.8: The correlations derived from the zonally and seasonally averaged N$_2$O and NO$_y$ data from CTMB simulations for the year 2002. The correlation fit in circles represent the combined form of AASE and ATMOS-3 N$_2$O and NO$_y$ correlation for mid and high latitudes.

in the upper part of the stratosphere (Loewenstein et al., 1993; Sugita et al., 1998; Sankey and Shepherd, 2003).

The Airborne Arctic Stratospheric Expedition (AASE) measurements showed a strong correlation between these two molecules. According to Loewenstein et al. (1993) the calculated reactive nitrogen,

$$[NO_y^*] = 20.7 - 0.0644[N_2O]. \tag{11.1}$$

The square bracket stands for VMR in ppb. The limits of the equation are (a) valid only above 220 *ppbv* of N$_2$O and (b) valid only for the latitudes between 22°N and 90°N because of the measurements were performed within the latitude band. Recently, Sugita et al. (1998) extended the equation up to the upper stratosphere by fitting a 4th order polynomial,

$$[NO_y^*] = 5.71 - 2.28\mu + 11.8\mu^2 - 2.14\mu^3 - 1.04\mu^4 \tag{11.2}$$

where, $\mu = log_{10}([N_2O])$ and the square bracket stands for the mixing ratios in ppb. This fit is derived from the ATMOS-3 data for a latitudinal range 39°-49°N for 2 to 220 *ppb* of N$_2$O. Kondo et al. (1999) confirmed the validity of the equation with the mid-latitude (39°N) balloon data. The relationship is investigated here with CTMB simulations in a chemistry perspective.

Figure 11.8 illustrates the N$_2$O-NO$_y$ correlations deduced from the CTMB simulations for the year 2002. The data are analyzed in season-wise as spring (March, April, May), summer (June, July, August), fall (September, October November) and winter (December, January and February). The profiles are averaged over different climatic regimes as the tropics (0-30), the mid-latitudes (30-60) and the highlatitudes (60-90) as well. The circles in the figure represent the combined form of the aforementioned equations (hereafter LS-fit).

The correlation curves in the tropics are seem to be slightly elevated and this can be due to the higher values in N$_2$O and NO$_y$ since the equation considered the latitudes northwards of 22°N only. The high latitude profiles, the southern hemispheric profiles in particular departs slightly from the LS-fit. Furthermore, the profiles, which are slightly away from the fit is in the winter-spring hemisphere. Since the shape of the correlation diagrams is severely affected by the denitrification and mixing process, the high latitude descent and mixing are the possible
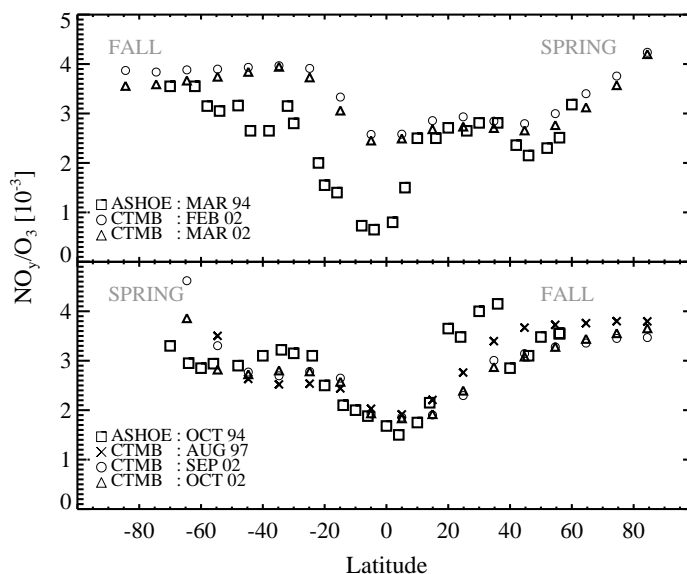
Figure 11.9: The NO_y - O_3 correlation derived from CTMB compared with ASHOE/MAESA data for different years.

reasons for this feature (since the model run is not included the denitrification process). Also, the slopes are comparable to the ones shown in Olsen et al. (2001). Hence, the N_2O-NO_y chemistry in the model is reasonably represented.

11.7 NO_y-O_3 correlations: Representation of transport barriers

Since the lifetime of NO_y and O_3 is very long and comparable to each other in the lower stratosphere, the molecules are primarily under dynamical control (Brasseur and Solomon, 1984). The mixing ratios of both molecules increase with altitude and have the maximum values around 35-40 km, the maximum in the tropical stratosphere. Both molecules show significant poleward latitudinal gradients with average NO_y increasing by nearly an order of magnitude (around 20 km) (Fahey et al., 1996). Further, such a property results into a correlation of both molecules, which is very compact in the lower stratosphere. In addition, the correlation is not changed with the mixing of air which contains relatively small values of NO_y and O_3 (Murphy et al., 1993).

Figure 11.9 examines the NO_y/O_3 ratio derived from the model at 20 km. As the CTMB calculations are performed for the years 1997 and 2002, whereas the ASHOE/MAESA measurements were taken in 1994. The data simulated for the ASHOE/MAESA year were not good enough (because of the inaccurate met analysis) and were avoided. The ASHOE/MAESA NO_y/O_3 data have been taken from the work of Shia et al. (1998). The CTMB data are taken from the zonally averaged monthly means from the years considered and have been arranged in 10° latitudinal bins over 89°S to 89°N. The months considered are February, March (upper panel) and August, September and October (lower panel). So the data can be used to make a qualitative assessment on the nature of the slope produced by the relationship between the molecules.

Latitudinal gradients: The NO_y/O_3 ratio is very low in the tropics and can be due to the *in*

situ O$_3$ production there [see Fahey et al. (1996); Avallone and Prather (1997) for the details about the discussions on how the ozone production influence the ratio in the inner tropics] rather than low NO$_y$ (Murphy et al., 1993), although the tropical ozone production doesn't have a sharp edge (Brasseur and Solomon, 1984). A latitudinal gradient is observed around 20°, which indicates a clear separation between the two regions, the subtropics and the mid latitudes. This gradient in the NH is sharper in both seasons than in the SH, which is consistent with previous observations too [e.g., Fahey et al. (1996)]. The latitudinal gradient at the edge of the tropics points out that the airmasses are composed differently and mixing across the region is weak. The high gradient region is called the subtropical barrier and is usually present between 10° and 22° of latitude (Murphy et al., 1993) on both sides of the equator, which indicates the edge of the tropics. Away from the tropics, the ratio increases towards the poles. The mid-latitude ratios are relatively constant due to the planetary wave mixing of mid-latitude airmasses. In addition, significant sources or sinks of either species absent in the midlatitude lower stratosphere. The model reproduces the gradients fairly, especially in the fall. In addition, the latitudinal features discussed in the previous studies (Murphy et al., 1993; Keim et al., 1997; Fahey et al., 1996) are well reproduced by the model.

Seasonal features: A characteristic seasonal difference is observed in the NO$_y$/O$_3$ ratio values. According to the Figure 11.9, one of the profound differences is the NH poleward movement of the subtropical edge between the spring and the fall. Interestingly, the replacement of the location of the gradient is nominally consistent with the seasonal location of the tropical upwelling region (Rosenlof, 1995; Appenzeller et al., 1996). The NO$_y$/O$_3$ ratio is higher in spring than that in fall, especially at mid and high latitudes. This is also consistent with the ozone annual cycle, which has the maximum column density in spring and the minimum in fall. The latitudinal variability of the NO$_y$/O$_3$ ratio outside the tropics is small in the spring as compared to the fall values. According to Rosenlof (1995), latitudinal gradients of the ratios of the long-lived stratospheric species are expected to be small in spring due to increased wave activity, NH in particular. These seasonal patterns can also be found on both sides of the equator in each season and are consistent with previous studies (Murphy et al., 1993; Fahey et al., 1996) as well.

11.8 A quick diagnose of vertical transport

It has already been shown that the comparatively (compared to the measurements) lower mixing ratios in the lower stratosphere is a common feature of the N$_2$O simulations, which is a problem in most models (Park et al., 1999; Hall et al., 1999). Moreover, the models that use the UKMO windfields to force the runs calculate relatively smaller values as well (Chipperfield, 1999; Davies et al., 2003). However, studies have shown that the inaccuracies in the model transport have significant effect on the simulated chemical structure of the stratospheric species like N$_2$O, Cl$_y$ (Park et al., 1999; Hall et al., 1999; Douglas et al., 1999; Waugh and Hall, 2002). This study also shows that the transport in CTMB is reasonably represented. The problem with the CTMB simulations is here is shallow latitudinal gradients and lower mixing ratios, especially in the tropical lower stratosphere. Should the N$_2$O isopleths can be elevated then reasonable mixing ratios and thus relatively good latitudinal gradients can be produced. It is possible to elevate the tracer mixing ratios by simulating with increased heating rate in model. As the vertical transport in the model is calculated form the diabatic heating rate us-

ing the MIDRAD radiation scheme, the increased heating will also increase the transport in the vertical direction. Since N_2O is a tracer of airmotions, any change in the vertical transport will also reflect in its distribution. So a few model runs are performed with altered heating rates in the model.
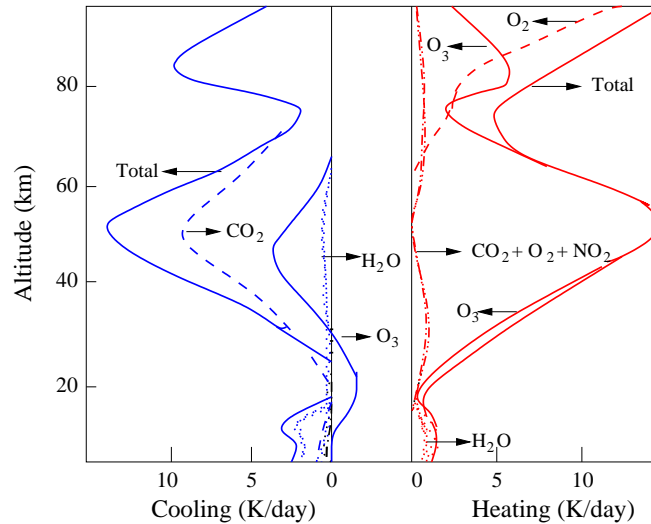
Figure 11.10: The short-wave heating and long-wave cooling by various trace gas in the standard atmosphere, reproduced from London (1980).

It should be noted that this heating rate tests may not be either the ideal or an accurate way to diagnosis the vertical transport in a model. There may be other methods to check the transport processes in the model. So this study aims at checking the N_2O profiles simulated with the increased heating rates in the model with an assumption that the additional heating in the model increases the mixing ratios. It also discusses the model run results in a transport point of view and critically debate validity of the test.

The heating rate (HR) can be defined as the diabatically induced temprature change per unit time (= day). Heating in the middle atmosphere is primarily through the absorption of ozone in Hartely (200-310 nm)-Huggins band (310-350 nm, weaker than Hartely band) and Chappuis band (450-750 nm, very week compared to other bands) in the visible region of the spectrum. In the upper atmosphere, heating due to the absorption in the Shumann Runge Continuum (125-175 nm) and Schumann Runge bands (175-205 nm) dominate. Although there are other trace gases like CO_2 and H_2O that heat the atmosphere up, their contribution is comparatively small. Also, the heating by ozone itself is comparable to the net heating by all the constituents in the middle atmosphere. The cooling in the middle atmosphere is mainly due to radiative emission of CO_2 in the $15\mu m$ band. Ozone in the lower stratosphere and H_2O in the upper stratosphere also play a significant role in the cooling of the respective altitude regions. The model has incorporated the solar heating rates (in the shortwave) due to ozone and diatomic oxygen. This should be reasonable for the heating rate part in the model as the ozone heating is more or less equal to the total heating rates. Hence, the solar heating side is well represented in the model. The thermal infrared heating (cooling effect, long wave cooling) by CO_2 in $15\ \mu m$, ozone in the $9.6\ \mu m$ and H_2O are also considred. Since these three molecules are the principal components of the cooling mechanism in the middle atmosphere, the infrared cooling is also

well represented in the model. The heating and cooling by various atmospheric gases in the middle atmosphere for the standard atmosphere is shown in Figure 11.10.

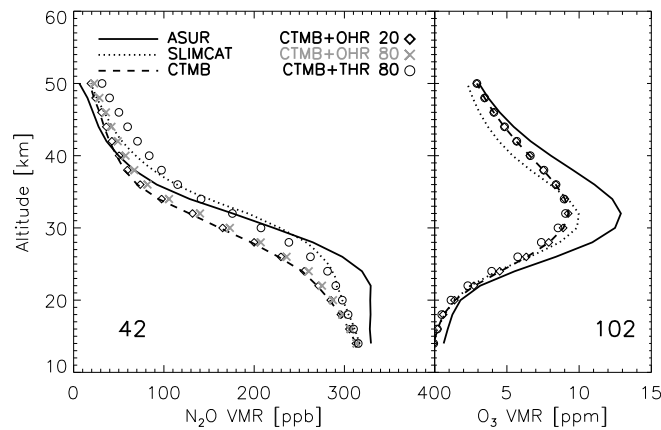Figure 11.11: TheCTMB N_2O and O_3 simulations are examined with the increased net and ozone heating rates in the model. The profiles are averaged over the tropical latitudes from $5°S$ to $30°N$ and are reduced to ASUR vertical resolution in order compare with the measurements. The number of profiles averaged in each sections are noted at the bottom of the figures.

The additional model runs have been performed with increased diabatic heating rates in the model (heating rate term has multiplayed by a certain factor). The experiment was conducted with 20%, 40%, 60% , 80% and 100% increment in the net heating rate (THR). Since the ozone heating itself is comparable to the THR in the middle atmosphere (see Figure 11.10), the ozone heating rates (OHR) in the model are also increased for testing the sensitivity of the transport in the model. This is achieved by increasing the ozone VMR in the model by multiplying the VMR term by 1.2 (20%) and 1.8 (80%). Together with the additional heating in the short wave radiation (dominant at low latitudes), the cooling by long wave radiation (dominant at high latitudes) has also been observed in the simulated results. The increment in the heating rate has resulted in an increased upwelling in the tropics and an increased airmass descent at high latitudes in the simulations. Among the tests the simulation with 80% (heating rate term has been multiplayed by 1.8) increment in the heating rates showed reasonably good latitudinal gradients in comparisons with the ASUR measurements and the SLIMCAT simulations with the latitude. So this discussion further examines these results.

Figure 11.11 shows the results of the tests for the tropical latitudes. Tests with THR 80% and OHR 20% and 80% are shown in the profiles. Among the tests (with THR 20%, 40%, 60%, 80% and 100% and OHR 20% and 80%) the simulation with 80% increment in the heating rates showed reasonable N_2O gradients with the latitude and comparable to the measured ones. Though ozone plays an important role in heating and cooling of the stratosphere, the increment in the O_3 VMR to augment its effect on heating/cooling did not elevate/suppress the tracer isopleths. Also, the difference between the 20% and 80% increment results are not considerably apart. Because of the additional heating throughout the latitudes, especially in the tropics, the airmass has been transported to higher altitudes (directly proportional to the heating in the tropics). Hence, among the tests 80% increment in THR results are most comparable to the ASUR and the SLIMCAT profiles. However, the ozone VMRs show a negative effect to this heating rate test. As the THR is increased ozone is decreased slightly at tropical latitudes below 30 km. It can be due to the additional heating in the model since the Linoz

simulations slightly reduce the mixing ratios for warmer temperatures. Since the lower stratospheric values are slightly higher in CTMB, this reduction in ozone is a promising result. The OHR tests did not show any significant change from the earlier simulations.
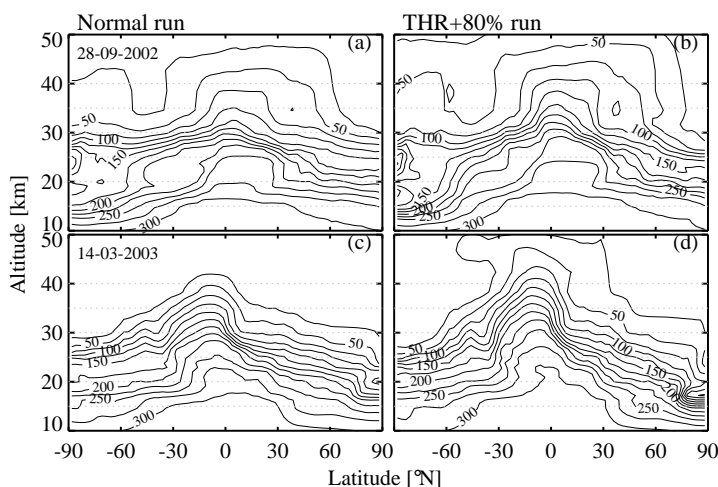
Figure 11.12: The zonally averaged N_2O profiles simulated with the control run and the net heating rate run (THR+80%) for 28 September 2002 and 14 March 2003.

Figure 11.12 compares the N_2O simulations with the increased heating rate with present run (control run) for 28th September 2002 and 14th March 2003. Due to the additional heating the isopleths are elevated throughout the latitudes in September and predominantly in tropical latitudes in March. The latitudinal gradients are sharpened in both seasons as well. The higher airmass descent in the mid and high latitudes with the heating rate run is another noted difference, especially in the souther hemisphere.

11.9 Discussion

The difference in the measured and the calculated ozone is consistent and systematic throughout the seasons, indicating a characteristic feature of the model chemistry. Prather et al. (1990) found that the tropical ozone simulated by the parameterized chemistry underestimated the observations by 14%, especially between 10 and 50 mbar. They suspect that the discrepancies might come from the chemistry module or from the rapid tropical upwelling in the model. According to McLinden et al. (2000), the Linoz chemistry underpredicts tropical mixing ratios by 0.5 to 1.0 ppm around 35 km. A recent study by McCormack et al. (2004) also showed that the model calculations with the Linoz scheme underpredict the ozone measurements above 10 hPa. Thus, the difference found in the middle stratosphere is consistent with the previous studies as well.

The uncertainties in the measured profiles are 17% between 1.0 and 0.2 hPa and 30% at 100 hPa for HALOE ozone, $\leq$ 5% for the ozonesondes, and 10% for the POAM ozone between 13 and 40 km. Hence, comparing these figures with the bias in the simulations, the discrepancies between the measurements and the model calculations are within the uncertainties of the measurements. It should be noted that the accuracy of the calculated profiles may vary with models (in accord with the model transport, meteorological analyses used, model resolution etc.). The study by McLinden et al. (2000) showed a difference up to 10% in Linoz based calculations

for different models, which is evident in the comparisons of McCormack et al. (2004) as well. In their study, the Linoz model produced very low mixing ratios above 10 hPa, in particular. So the comparions with the measurements in turn produced bad agreement at these altitudes. However, in this study, it shows that the Linoz module with the Bremen CTM is in good shape and the simulations can be used for scientific studies in the upper stratosphere . The reason for the remaining difference between the measured and the simulated values can be due to overestimation of the background ozone VMRs in the model (McCormack et al., 2004). The old reaction rates (more than 12 years old) and climatologies (more than 7 years old) used for the parameterization could also contribute to the discrepancies. The temperature climatology is an important aspect in this context since the Linoz based simulations underestimate measurements for temperatures warmer than the climatology used in it, which is particularly significant in the tropics (McLinden et al., 2000).

The accuracy of the UKMO data matters the quality of the simulations very much, in the beginning of its operational analyses period (1991) in particular. The N_2O simulations for the ATMOS and CRISTA-1 observation periods (1994) were not good with the UKMO data. However, the calculations improved for the CRISTA-2 period in 1997. The simulations performed to compare with the CLAES climatology, the other model calculations (2002) and for the ASUR observations (2002 and 2003) show signs of further improvements. Hence, the N_2O shows a gradual and constant improvement in the simulations. Since the only change in the input for the simulations is the analyzed wind fields, the problems or inaccuracies in the analyzed wind fields are the reasons for the large difference in the calculations. The huge differences in the CTMB NO_y simulations between the years 1998 and 2002 in comparisons with UCI calculations corroborate this postulation. The UCI N_2O simulations look more realistic and more comparable to the measurements than the UCI GISS simulations. Since the models are basically similar, the analyzed winds can be the reasons for the large interannual difference in the mixing ratios simulated by these models as well. The study reveal that the impact of meteorological analyses on the simulations of stratospheric NO_y is very much greater than that of the N_2O calculations. There is a seizable role for the analyzed wind fields in deciding the altitude of the NO_y mixing ratio maxima, which is an affirmation of an earlier study by Olsen et al. (2001) too. However, it is very difficult to quantify to what extent the calculations are influenced by the meteorological analyses as the chemistry and transport also play a pivotal role in the calculations. The comparison between the models applying the same chemistry but different meteorological fields (UCI and CTMB) shows that the windfields and the model transport make the difference in the simulated results. The simulated results from the models using the similar transport scheme and different wind analyses and chemistry scheme (SLIMCAT and CTMB) suggest that the difference might come from the met analyses or from the chemistry.

The above discussion draws some hints about the reasons for the differences between the CTMB simulations and the measurements. Taking the comparison among SLIMCAT, UCI, UCI GISS and CTMB into account, the forcing (inaccurate) wind fields might be one of the reasons to calculate relatively smaller values (flat contours) in the lower stratosphere (Davies et al., 2003; Olsen et al., 2001; Chipperfield, 1999; Waugh, 1996). The nature of the model transport (or inaccuracies in the model transport) could be the additional reason to simulate the lower N_2O values as shown by the comparison among CTMB, UCI and UCI GISS (Olsen et al., 2001; Hall et al., 1999; Park et al., 1999). The uncertainties in the chemical reaction rates used in the chemistry schemes in the models could also contribute to the differences as shown by the comparisons among the models UCI, UCI GISS, SLIMCAT and CTMB. Resolution of the

models were different from each other, which could also contribute to the differences among the model (CTMB, SLIMCAT, UCI, and UCI GISS) simulations.

The increased heating rate elevates (simulates comparatively higher values) the N_2O isopleths in the tropics and suppress (simulates comparatively lower values) the isolines in the high latitudes. Though the lower stratospheric values are still slightly smaller as compared to the observations, the gradients are fairly represented and the subtropical gradients are sharpened. In addition, the southern mid and high latitude values are decreased with the additional heating in the model. The reduction of N_2O in the southern latitudes is particularly important as the simulated values in comparison with measurements were higher at these latitudes, which caused a north-south assymmetry in the simulations (in the control run). Moreover, the reduction in ozone below 30 km is also encouraging since the CTMB ozone has a high bias in that region.

The reason for the increased heating rate can be explained by the nature of the tracer isopleths simulated by the model. Theoretically, the slope exists as a balance between the zonal mean advection by diabatic circulation (slope steepening effect) and an effective meridional diffusion or eddy mixing (slope flattening effect) (Plumb and Ko, 1992) [The flattened tracer isopleth depicts the model is a global 'diffuser' (Hall et al., 1999; Park et al., 1999)]. The significant mechanism that leads to the slope steepening effect is the diabatic or similar meridional circulation [see Guthrie et al. (1984) and Mahlman et al. (1986) for examples]. This implies that the model needs additional diabatic heating to elevate the N_2O isopleth in the tropics. In other words, the model needs more heating in the tropics. Furthermore, a recent work by Olsen et al. (2001) compared N_2O simulations from three different models using the same chemistry (that used in CTMB). Only one model reproduced the observed tracer gradients reasonably in the stratosphere. The study concluded that the tropical upwelling was weaker in the other models and hence, they failed to simulate reasonable tracer gradients. Nonetheless, this does not mean that the tropical upwelling in the model is weaker.

The calculated N_2O with the increased heating rate compares better with the observed and the SLIMCAT latitudinal gradients, which was the main concern for the simulations in the low latitudes. So the experiment shows that the current model setup demands additional dynamical drive to simulate reasonable tracer gradients. Nonetheless, the high values simulated in the mid and high latitude upper stratosphere in September and the higher (increased) diabatic descent in the high latitude lower stratosphere suggest that the increased heating rate run is not a permanent solution to increase the simulated mixing ratios and thus to calculate reasonbale latitudinal gradients.

11.10 Conclusions

In order to evaluate the ozone simulations with the Linoz photochemical module, the ozone measurements from high resolution ozonesondes (SHADOZ and NDSC) and validated satellite sensors (HALOE and POAM) are compared with the Bremen CTM calculations in addition to three different climatological analyses (KNMI, HALOE and IUP Bremen). All the data are analyzed for 2002 and 2003 and are averaged over the seasons. The model calculations reproduce the measured vertical, seasonal, and latitudinal ozone distributions very well. It is found that the simulations with Linoz are slightly biased. The model calculations overestimate the measurements in the lower stratosphere up to 0.5 ppm or 20% above 20 km, depending on altitude

and the measurement sensor. The upper stratospheric calculations are also on the higher side up to 0.6 ppm or 15%, which is the highest at 44 km. The high difference in percentage at the upper and the lower stratosphere is due to the lower absolute values of ozone at these altitudes. The difference in the middle stratosphere is in the opposite direction, for which the simulations underestimate the measurements up to 1.2 ppm or 9%. Tests with N_2O simulations, NO_y/O_3 and N_2O/O_3 correlation analyses (not shown) reveal that the transport in the model is reasonable. Therefore, the bias is coming from the ozone chemistry parameterization. The overestimation of the background ozone VMR might be one of the reasons for the bias in the Linoz based calculations. The 'current knowledge' of the atmosphere (the photochemical data, climatologies of relevant molecules, and the mixing ratio distribution of the involved chemical families) used for the Linoz parameterization could also contribute to the discrepancies between the measurements and the simulations. In consideration with the measurement uncertainties and the standard deviation of the compared profiles, a reasonable agreement is found between the measured and simulated profiles. Thus, the linoz based ozone simulations are accurate enough to study most aspects of the chemistry and dynamics in the stratosphere.

The N_2O and NO_y simulations prove that the quality of meteorological analyses has a great impact on the simulations of these gases. A gradual improvement in the calculations is apparent throughout the years (from 1991 to 2003). The model simulations reasonably reproduce the measured vertical, latitudinal and seasonal variations in accord with chemistry and transport in the stratosphere after the year 1997. However, the simulated N_2O mixing ratios are slightly lower in the lower stratosphere. The inaccuracies in the model transport, meteorological analyses, coarse/differences in the model resolution and the uncertainties in the chemical reaction rates can be the reasons for the reason for the differences (or the lower values) in the CTMB calculations. The NO_y simulations in the model look very promising and are comparable with the measurements and the UCI GISS and the UCI calculations. The dramatic inter annual variability of the simulated NO_y mixing ratio and changes in the altitude of peak mixing ratios suggest that the NO_y calculations in the model is greatly affected by the meteorological analyses. The NO_y included chemistry in CTMB has little influence on the simulations of N_2O. Slightly elevated isopleths (relatively higher mixing ratios) throughout the latitudes are simulated without the NO_y in the model due to the omission of the conversion of NO_y into N_2O in the model (which implies an additional source of N_2O in the stratosphere). The simulated N_2O-NO_y correlation curves in comparison with observations indicate that the parameterized chemistry of the molecules in the model is well represeted. The simulations reasonably reproduce the measured latitudinal and seasons NO_y/O_3 variations. The barriers of tracer transport are not well represented in the model. However, the simulated results in comparisons with the measurements suggest that the transport processes in the model is reasonable to simulate observed stratospheric chemical and dynamical structures.

As an attempt to simulate reasonable N_2O latitudinal gradients, a few additional CTMB runs were performed with increased heating rates in the model. The additional heating with 80% increment helped to simulate reasonable mixing ratios and comparable latitudinal gradients as compared to the SLIMCAT and the ASUR. In addition, the runs reduce the N_2O discrepancies in the southern mid and high latitudes and ozone high bias in the lower stratosphere. The experiment indicates that the model needs additional dynamical drive to produce reasonbale N_2O simulations in the stratosphere. Since the simulated results still show some differences with the measurements, the additional heating in the model is not a permanant setup to solve the problem.

12 Seasonal and latitudinal variation of stratospheric trace gases: Measurements and model calculations

Previous chapters discussed about the ASUR trace gas retrievals and the validation of CTMB simulations. The latitudinal, longitudinal and seasonal variations of the ASUR O_3, N_2O, HCl, and HNO_3 measurements during the SCIAVALUE campaign are discussed in this chapter. The measured features are interpreted with the help of SLIMCAT and CTMB. The measurements are tapped to diagnose the simulations as well.
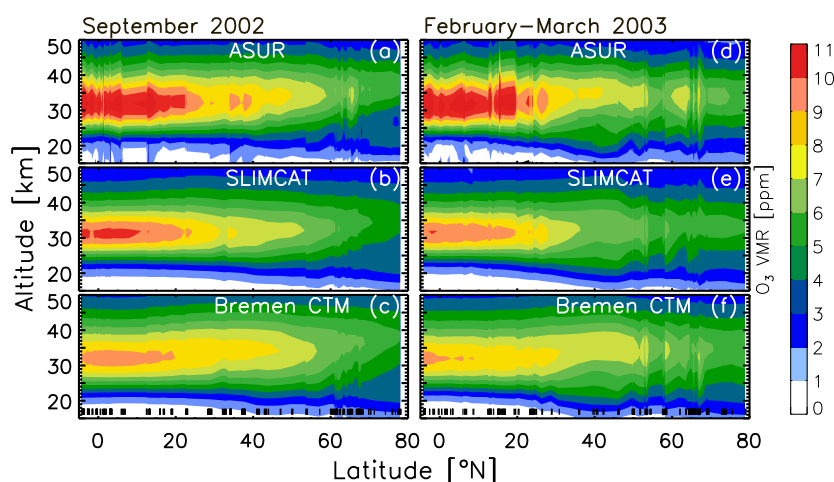
Figure 12.1: The contour plot of O_3 vertical profiles of ASUR, SLIMCAT and CTMB as a function of latitude for September 2002 and February-March 2003. The black signs on the bottom of the plot indicate the position of the aircraft during the measurements.

12.1 Ozone

12.1.1 Latitudinal variations

Figure 12.1(a) summarises the ASUR ozone measurements for the September 2002 deployment. The variations around 65°N are due to longitudinal variations of ozone (these will be discussed in Section 12.1.2). The equatorial and the tropical latitudes record high mixing ratios of about 11 ppm around 33 km which gradually decreases towards the mid and high latitudes. The rising altitudes of maximum volume mixing ratio (AMV) gives the so-called banana shape (Rasch et al., 1995) in the ozone distribution. Since ozone production is effective in the tropical middle stratosphere and is transported to high latitudes with the meridional transport, the

93

observed features are consistent with photochemistry and stratospheric transport processes. Figure 12.1(b) shows the SLIMCAT calculations for September 2002. The general behavior of the latitudinal distribution of ozone described previously for the ASUR measurements is reproduced by the model. Fine structures like the upward slope in the contours around 33°N are even represented in the model. Figure 12.1(c) shows the CTMB results for September 2002. The observed latitudinal features are well reproduced by the model.

Figure 12.1(d) depicts the ASUR ozone measurements in the winter/spring deployment and the SLIMCAT ozone for the same time period is shown in Figure 12.1(e). The main features of the latitudinal variations are found as in the fall measurements, but some seasonal differences in the distribution are evident (these will be discussed in Section 12.1.3). Figure 12.1(f) shows the Bremen CTM run for the winter/spring season. The observed latitudinal distribution is well represented in the calculations.
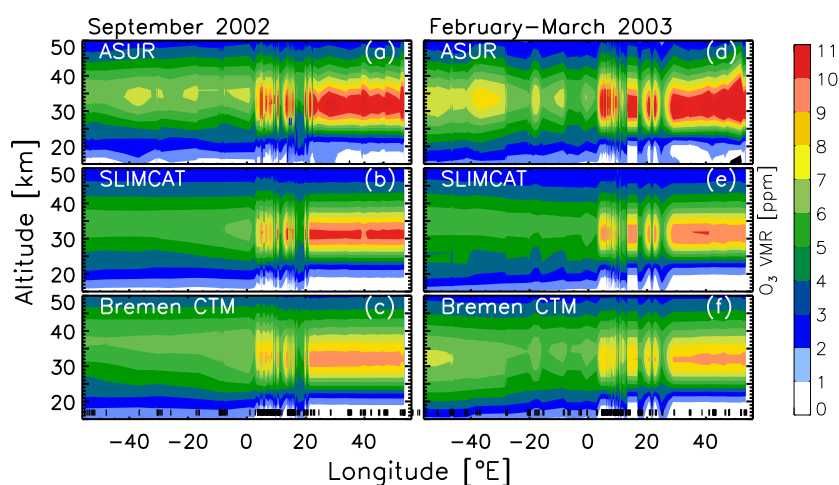
Figure 12.2: The longitudinal distribution of stratospheric ozone measured by the ASUR sensor in September 2002 and February/March 2003 are compared with the SLIMCAT and the CTMB simulations. The black signs on the bottom represent the measurement co-ordinates.

12.1.2 Longitudinal variations

The longitudinal variations in the trace gas mixing ratios are primarily due to the effect of global scale stationary waves (1 and 2). In addition, low and high pressure systems and the polar vortex dynamics can also induce changes in VMRs along the longitudinal plane. Figure 12.2 compares the longitudinal variations of stratospheric ozone measured by ASUR with the SLIMCAT and the CTMB simulations for the SCIAVALUE measurement points (not at a latitude in particular). The longitudinal survey around 65°N is shown from 60°W to 0°E. These were the flights from Kiruna (Northern Sweden) to Kangerlussuaq (Greenland) and back to Keflavik (Iceland). The variations from 0°E to 20°E are due to the latitudinal measurements/variations. Though the flight from Yaounde (Cameroon) to Mahé (the Seychelles) is a longitudinal survey, there is hardly any variations. This can be due the effect of zonal winds in the tropics as they can smear out the longitudinal variations. The models are very good in imitating the measured variations.

12.1.3 Seasonal variations

One of the noted differences between the seasonal VMR distributions is the airmass descent at the high latitudes in the spring, which is apparent when following the 3 and 4 ppb isolines from 60°N ownwards. These seasonal signature are also imprinted with the higher values in the MPV (not shown here). Thus, the high latitude lower stratospheric ozone abundance is influenced by the seasonal cycle of stratospheric transport (Ko et al., 1989; Rosenlof, 1999). In fall the high VMRs ($\geq$9 ppm) are extended up to 40°N in ASUR, whereas in the spring the same values are noted only up to 30°N. The simulations also show high values in the tropics in the fall as compared to the spring mixing ratios. However, the values in the ozone source region in the tropical stratosphere is more reasonably reproduced by SLIMCAT than CTMB.It should be noted that the upper stratospheric simulations by SLIMCAT underpredict the measurements and the CTMB calculations.
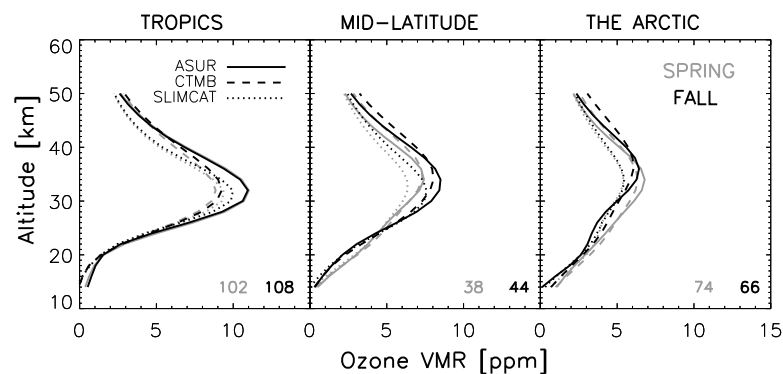
Figure 12.3: The O_3 vertical profiles from ASUR measurements compared to SLIMCAT and CTMB ozone simulations. The numbers on the bottom of the figures represent the number of averaged profiles in each latitude section and the color codes indicate the respective seasons as shown by the legend.

Figure 12.3 illustrates the ozone profile comparison at different latitude sections for the two seasons. The latitude sections are defined as 5°S to 30°N for the tropics, 30°N to 60°N for mid-latitudes and 60°N to 90°N for the Arctic or high latitude . The same definition is used elsewhere in the chapter for referring the climatic regimes. In the tropics the seasonal variation is not pronounced in the ASUR ozone, whereas the models show slightly higher values in the fall. Although the mixing ratios at AMV in the mid-latitude region show higher values in the fall, the lower stratospheric VMRs are higher in the winter/spring for both the measurements and the model simulations. In the Arctic, VMRs in the winter/spring season is higher except in the upper stratosphere, where the reversal found around 38 km. The middle stratospheric ozone low bias in the CTMB and the upper stratospheric ozone 'deficit' in the SLIMCAT are also revealed. Though there are slight differences (in VMR) among the measurements and the simulations, the calculations capture the details of the latitudinal and seasonal variations very well.

Figure 12.4: Same as Figure 12.1, but for N_2O.

12.2 N_2O

12.2.1 Latitudinal variations

Figure 12.4 illustrates the ASUR N_2O observations during the fall deployment. High mixing ratios are noted at the tropical low altitudes indicating their tropospheric origin (young air) and the tropical upwelling (Hall and Plumb, 1994). The high tropical mixing ratios give rise to steep horizontal gradients (Mahlman et al., 1986; Holton and Ch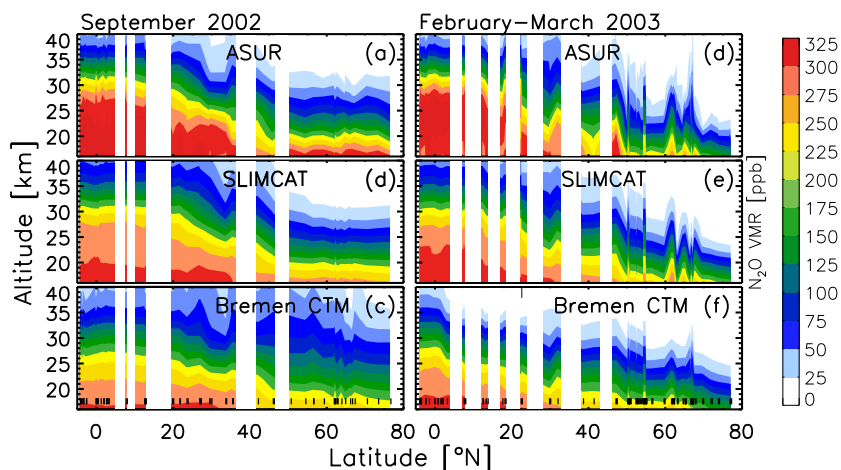oi, 1988). The mixing ratios decrease with increasing altitude and latitude. A sharp gradient seen around 30°N likely to be caused by the subtropical barrier (Murphy et al., 1993; Minschwaner et al., 1996; Mote et al., 1996; Volk et al., 1996; Avallone and Prather, 1997; Plumb and Eluszkiewicz, 1999). Another sharp gradient present at the mid latitudes around 45°N, is separating the air from mid and high latitudes (Rosenfield and Schoeberl, 1986). However, the gradients cannot be regarded as strength of the mixing barriers (Nakamura and Ma, 1997). The tracer isopleth (same VMR level) is elevated at the low latitudes and crest fallen at the high latitudes because of the nature and influence of the meridional circulation (Plumb and Ko, 1992; Plumb, 2002). Along the quasi-horizontal surfaces at the mid latitudes the isopleth is flat due to wave mixing (Randel et al., 1993). N_2O has an exponential decay with altitude in the stratosphere due to photolysis (Holton, 1986). The SLIMCAT calculations for the September deployment is shown in the Figure 12.4(b). The general features observed by ASUR are also reproduced by the model quite well. The calculated values are slightly lower in the tropical lower stratosphere. The CTMB calculations for the same time period is depicted in Figure 12.4(c). As seen from the observations and from the SLIMCAT simulations, the model reproduces the measured features reasonably. However, the calculations show slightly lower values in the tropical lower stratosphere and higher values in the mid and high latitude upper stratosphere.

Figure 12.4(d) shows the observed N_2O VMR in the winter/spring season. The main latitudinal behavior is the same as discussed previously. Both the subtropical and the high latitude gradients are steeper in the spring. The SLIMCAT run for the same time period is given in Figure 12.4(e). The gradients are well reproduced and the mixing ratios are comparable. Figure 12.4(f) shows the CTMB results for the same time period. The observations show high mixing ratios at a latitude from 5°S to 20°N, whereas in the model, the area is reduced from 5°S to 3°N, which is a noted difference between the measurements and the calculations. The
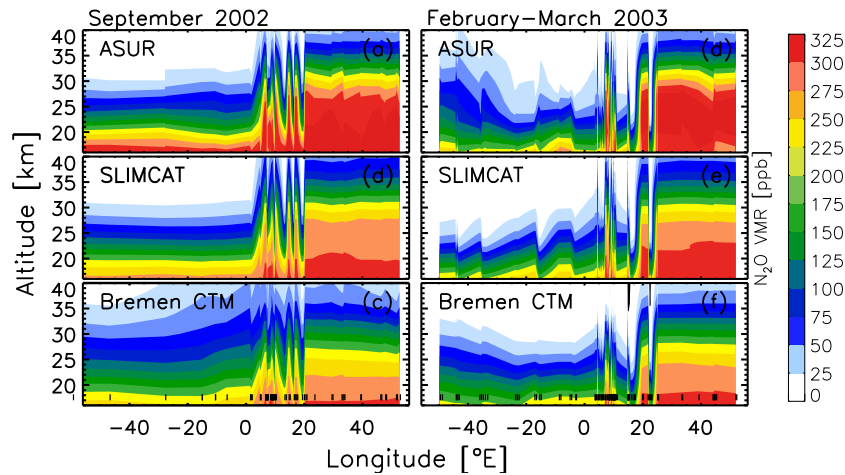
Figure 12.5: Same as Figure 12.2, but for N$_2$O.

simulated gradients separating the low, mid and high latitudes (subtropical and polar vortex mixing barriers respectively) are not as steep as observed, which is another prominant discrepancy. The seasonal variations will be discussed in Section 12.2.3.

12.2.2 Longitudinal variations

Figure 12.5 compares the measured longitudinal variations with the SLIMCAT and the CTMB calculations. As discussed in Section 12.1.2, the variations from 60°W to 0°E are due to the high latitude longitudinal survey around 65°N. The latitudinal variations are shown by the ripples in contours from 0°E to 20°E. The variations in the tropics (20°E to 60°E) are not pronounced because of the effect of zonal winds. The SLIMCAT simulations reproduce the measured longitudinal variations very well. The given input initial climatology has no longitudinal variation in CTMB. As the model needs about 3 years to get adjusted for simulating the N$_2$O distribution, the long run also reduces the influence of the initial profiles on the final results of the model. However, the model is successful in imitating the observed longitudinal variabilities.
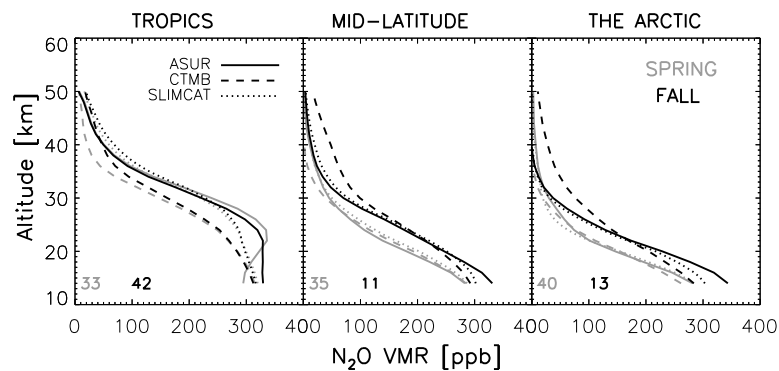
Figure 12.6: Same as Figure 12.3, but for N$_2$O.

12.2.3 Seasonal variations

Since N_2O is a tracer, a more profound seasonal difference in mixing ratio is expected. As planetary wave activity is higher in winter, the subtropical gradient is also steeper in winter (Hirota and Shiotani, 1983; Randel, 1988; Dunkerton, 1989). The observed gradients clearly show the seasonal cycle of the steepness in the subtropical gradient. The observations also show the airmass subsidence at the high latitudes during the winter/spring season with relatively small mixing ratios (Figure 12.4). Since the stratospheric transport is higher in winter, an increased tropical upwelling and an increased high latitude descent are apparent in both the measurements and in the calculations (Rosenlof and Holton, 1993; Holton, 1995; Rosenlof, 1995; Appenzeller et al., 1996). The diabatic descent at the high latitudes is estimated to be roughly about 4-6 km as following the N_2O isopleths. The seasonal variations (the difference in the tropical upwelling and the high latitude descent) are clearly seen in the longitudinal distributions of the molecule as well (Figure 12.5). The SLIMCAT and the CTMB calculations reasonably reproduce the observed seasonal features. However, the SLIMCAT calculation matches better with the observations as the gradients and VMRs are closer to the measurements.

Figure 12.6 illustrates the nitrous oxide profile comparisons at different climatic regimes. In the spring the ASUR mixing ratios at the tropical latitudes are slightly higher in the lower stratosphere, indicates the high tropical airmass uplift in winter/spring season. However, in the upper stratosphere the fall values seem to have higher values. At the mid and high latitudes the fall mixing ratios are higher than those of the winter/spring due to increased stratospheric transport. The modeled profiles are consistent with the latitudinal and seasonal pattern of the measured profiles.
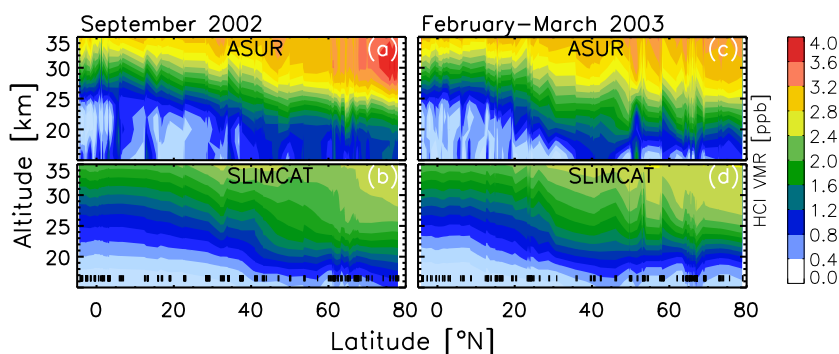
Figure 12.7: Same as Figure 12.1, but for HCl.

12.3 HCl

12.3.1 Latitudinal variations

Figure 12.7(a) depicts the observed HCl mixing ratios in the fall. Since HCl is a quasi-inert tracer in the stratosphere, its distribution partially depends on dynamics of the region (Rasch et al., 1995). A rapid increase in Cl_y mixing ratios with height is found in the lower stratosphere where photolysis of chlorine source gases is the most efficient. So a similar pattern is expected for HCl mixing ratios with the stratospheric altitudes as it is one of the reservoir gases of chlorine in the stratosphere. Since the photolysis is very efficient in the tropics, the

mixing ratios are very small near the tropopause and increase with altitude. The SLIMCAT simulations are in agreement with the measured variabilities in HCl distributions, as shown in Figure 12.7(b). Though there some discrepancies between the measured and the calculated values, the differences are within the accuracy of the measurements.
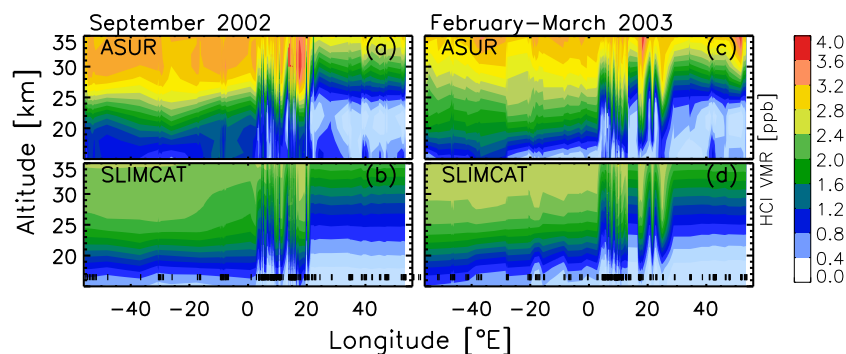
Figure 12.8: Same as Figure 12.2, but for HCl.

Figure 12.7(c) illustrates the measured HCl mixing ratios in the winter/spring period and the model calculations for the corresponding period are shown in Figure 12.7(d). The observed latitudinal features are similar to those observed in the fall. The seasonal variations in the measured HCl distributions will be discussed in the following sections.
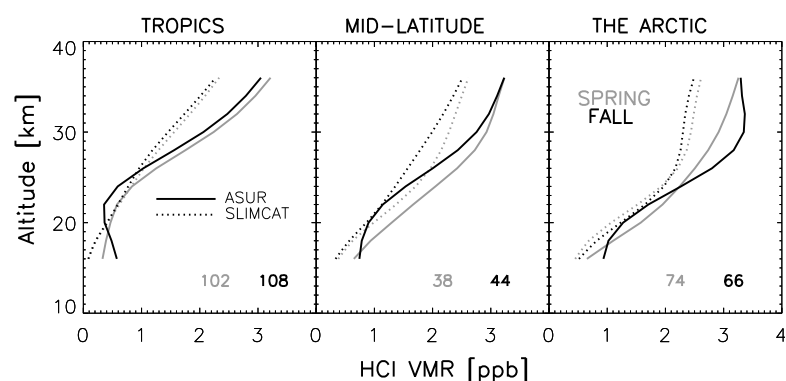
Figure 12.9: Same as Figure 12.3, but for HCl.

12.3.2 Longitudinal variations

As discussed previously for other molecules, the longitudinal scan has been performed for this molecule as well. So the features and the inhomogeneity in the mixing ratios around 60°N (Figure 12.7) is due to the same longitudinal observations in the Arctic. A detailed structure of the longitudinal variation of the measured HCl is shown in Figure 12.8. The variations around 10°E is, however, due to the latitudinal measurements. The measurements from 60°W-0°E and 30°E-60°E are the Arctic and the tropical longitudinal measurements respectively. The model is successful in capturing the observed variations in every detail.

12.3.3 Seasonal variations

As the seasonal patterns are hardly visible in Figure 12.7, the profile comparisons with respect to the climatic regimes will be exploited. Figure 12.9 shows the profile comparison between the measurements and the calculations at different latitude regions. The seasonal difference in the tropics is relatively weak. The mid-latitude and the Arctic profiles exhibit a considerable seasonal difference. The tropical and mid-latitude profiles in the spring show higher values than those of the fall. However, in the Arctic the simulated and the measured profiles are in an offset, showing the opposite seasonal structures. In SLIMCAT, the spring values are smaller than the fall values, whereas in ASUR the spring values are higher in the lower stratosphere and lower in the middle stratosphere.
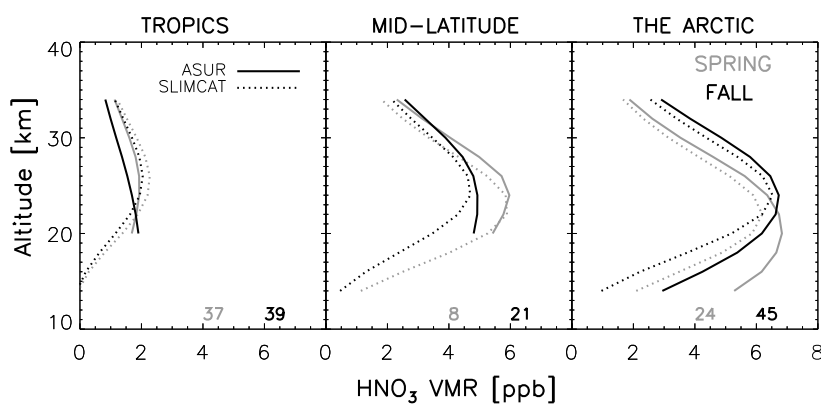
Figure 12.10: Same as Figure 12.3, but for HNO_3.

12.4 HNO_3

12.4.1 Latitudinal variations

Figure 12.10 shows the comparison between the ASUR and the SLIMCAT HNO_3 in the tropics, mid-latitudes and in the Arctic. Since photolyses of the molecule is very strong in the tropics, little HNO_3 is found there. The mixing ratio has its maximum around 25 km in the stratosphere. It increases with latitude as the intensity of the photolyses decreases. The highest VMR usually occurs in high latitude lower stratosphere in winter/spring season [eg: Santee et al. (2004)]. The observed profiles are consistent with the aforementioned features of the latitudinal distribution of the molecule. The SLIMCAT calculations reasonably reproduce the latitudinal variations with the seasons. However, the SLIMCAT mixing ratios are smaller as compared to the measured values, especially in the mid and high latitudes. Nevertheless, the difference is restricted to the lower stratosphere, below 20 km in particular. A systematic deviation is found in the lower stratosphere, where the ASUR HNO_3 overpredicts the calculations in the order of 0.5 to 1 ppm.

12.4.2 Seasonal variations

The seasonal difference in the tropics is very small. However, the observed mixing ratios in the spring are slightly higher than the fall values, which is more pronounced at the altitudes of maximum VMRs. The spring observations show higher values up to 30 km in the mid-latitudes. However, above 30 km the fall observations show higher mixing ratios. The simulated results agree well with the observed features and the VMRs are comparable at the low and mid latitudes. A significant seasonal difference is found in the high latitude, where the observed mixing ratios are higher in the fall, above 22 km. Below which (22 km) the spring measurements show higher values. The calculated mixing ratios are in good agreement with these features. Nevertheless, the SLIMCAT values are slightly lower as compared to the ASUR VMRs.

12.5 Discussion

Though the lower and upper stratospheric values of the ozone measurements are in good agreement with the simulated profiles, the middle stratospheric observations are in a small offset with the simulations. This is the region where both photochemistry and dynamics dominate the variations in ozone concentrations (Sinnhuber et al., 1999; Solomon, 1999; Staehelin et al., 2001). The difference in the middle stratospheric simulations in CTMB with ASUR is about 10%. Calculations with Linoz model have a low bias of about $\sim$9% in the middle stratosphere. The differences found in this comparison are also in the same range and hence, it re-affirm the limitation of the linearized ozone chemistry. The reason for the low bias has been discussed in the previous chapter on the model evaluation. It should be noted that the ASUR high bias (12%) has been subtracted from the measurements presented in this study.

The ozone profile comparisons show that the SLIMCAT profiles in the spring and in the fall have no considerable difference in the high latitude, whereas the ASUR and the CTMB profiles show the seasonal variations. So the SLIMCAT chemistry might have a problem in capturing the seasonal difference in that detail. It could also be due to inadequate representation of spring time ozone chemistry, heterogeneous reactions and ozone loss in SLIMCAT. Furthermore, the SLIMCAT calculations also show the 'upper stratospheric ozone deficit', which is common to most CTMs due to the inaccuracies in the chemical reaction coefficients [especially those use the reaction constants from DeMore et al. (1997)]. The ASUR ozone shows no seasonal difference in the tropics, while the models show high values at the AMVs of ozone in the fall. This is an interesting issue that demands further comparisons, which is a future work.

The CTMB calculations for N_2O show small differences to the observations and even to the SLIMCAT results (both model use the similar transport scheme). The gradient in the VMR values between the tropics and mid-latitude is more gentle in the CTMB simulations. This seems to be a problem in some stratospheric chemical transport models, failing to reproduce the transport properly (Hall et al., 1999; Park et al., 1999; Waugh and Hall, 2002). Shortcomings of the analyzed wind fields in the tropical lower stratosphere can be another reason (Waugh, 1996) for this offset. The simulated N_2O mixing ratios are smaller in the lower stratosphere, in the tropics in particular. Studies have shown that the simulations with the UKMO analyses produce slightly lower mixing ratios in the lower stratosphere as compared to the measurements (Chipperfield, 1999; Davies et al., 2003). Inaccuracies in the model transport and uncertainties

in the chemical reactions rates (used in the parameterized chemistry scheme) together with in-accuracies in the UKMO analyses can be the reasons for the offset/lower VMRs in the CTMB N_2O (Douglas et al., 1999; Hall et al., 1999; Park et al., 1999; Olsen et al., 2001). Neverthe-less, it is very promising that CTMB has reasonably reproduced the latitudinal, longitudinal and seasonal patterns of the N_2O distribution with its coarse resolution. The higher resolution and the quality of ECMWF winds enable SLIMCAT to perform better than CTMB and thus to come up with good agreement with the observed features.
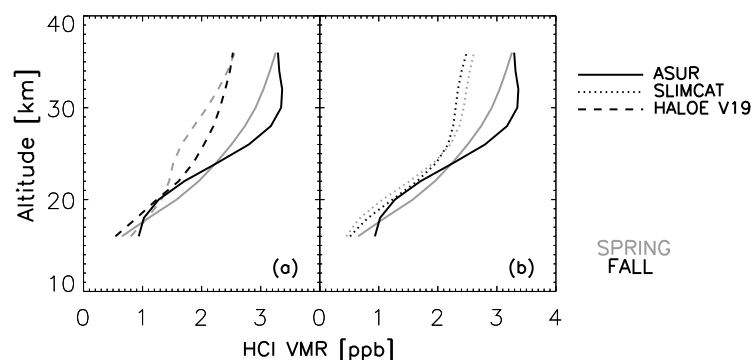
Figure 12.11: The HCl vertical profiles in the Arctic from (a) ASUR and HALOE V19 and (b) ASUR and SLIMCAT are compared for the fall and the spring seasons. The ASUR and SLIMCAT profiles are the same as shown in Figure 12.9.

At the high latitudes the calculated and the measured HCl values are slightly different. In order to test the origin of the discrepancy in the Arctic profiles the HALOE V19 (Russell et al., 1996) profiles are used. The profiles are taken for the latitudes between $60°N$ and $79°N$ in order to match the ASUR observation co-ordinates. The number of profiles averaged for the HALOE mean profiles are 25 for each season. So the profiles are taken from the same months and within the same latitude band. This seems to be reasonable for a qualitative analyses of the nature of the seasonal HCl distribution in the Arctic.

Figure 12.11(a) shows the results of the comparison between the ASUR and the HALOE profiles. It shows that the HALOE mixing ratio has relatively higher values in the lower strato-sphere and lower values in the middle stratosphere in the spring. Thus, the HALOE obser-vations are in agreement with ASUR measurements. With respect to the high bias (about 10-15%) in ASUR (von König, 2001) and low bias (10-15%) in HALOE in the similar scale (Russell et al., 1996), the mixing ratios are comparable as well. It points out that the SLIM-CAT simulations must have some problems in this latitude region. In addition, although the agreement of the HNO_3 profiles above 25 km at the low and mid-latitude is good, the high latitude lower stratospheric simulations have a low bias of about 0.5 to 1.0 ppb in SLIMCAT. Winter/spring values are highly influenced by the de/re-nitrification in the lower stratosphere. Since the SLIMCAT run was without the 'denitrification scheme', this could be reason for the differences in HCl and HNO_3 in the Arctic.

12.6 Conclusions

A new set of stratospheric trace gases measurements that were observed during the SCI-AVALUE campaign are presented. (a) The trace gases measured by the ASUR sensor during

the SCIAVALUE covering a latitude from 5°S to 80°N show tangible vertical, latitudinal and seasonal variations of O_3, N_2O, HNO_3 and HCl molecules. The models reasonably reproduce the latitudinal and seasonal features of the measured stratospheric ozone. There are slight discrepancies among the ASUR measurements, the SLIMCAT and the CTMB calculations. The calculated ozone in the CTMB is negatively biased about 9%. Since CTMB ozone with Linoz model is negatively biased in the middle stratosphere about 10%, the comparison re-iterate the limitation of the Linoz scheme. (b) The SLIMCAT shows the upper stratospheric deficit problem in the simulations. The uncertainty in the chemical reaction rates can be the reason for the problem with the SLIMCAT. (c) The seasonal and latitudinal distribution of the measured N_2O mixing ratios are well reproduced by the model calculations, SLIMCAT in particular. However, the CTMB N_2O isopleths are relatively flat (lower mixing ratios and relatively flat latitudinal gradients) in the lower stratosphere. This offset can be due to the inaccuracies in the model transport, the meteorological analyses and the uncertainties in the chemical reaction constants. The comparisons indicate that the transport in the models is still to be improved to simulate reasonable tracer gradients. (d) The low and the mid latitude HCl and HNO_3 observations are reasonably reproduced by the SLIMCAT simulations. However, the HCl simulations show an opposite (to the measurements) seasonal trend and the HNO_3 calculations show a low bias in the Arctic lower stratosphere. These deviations might be the result of the SLIMCAT rum without the 'denitrification' scheme. (e) The absence of the seasonal variations in the tropical ASUR measurements and in the Arctic SLIMCAT simulations demand further investigations, which is a future task.

13 Stratospheric transport in ASUR measurements

Representation of various features of stratospheric transport in the ASUR measurements are discussed in this chapter. The SLIMCAT and the CTMB simulations are used for the interpretation of the measured features.

13.1 Tropical upwelling

The diabatic processes and planetary wave activities in the troposphere lift the airmasses upward in the tropical inter tropical convergence zone across the tropopause. This upward motion of the airmasses are termed as the tropical upwelling. Atmospheric constituents enter the stratosphere through this region. Abundance of these constituents in the stratosphere greatly depends on the strength of the tropical upwelling.
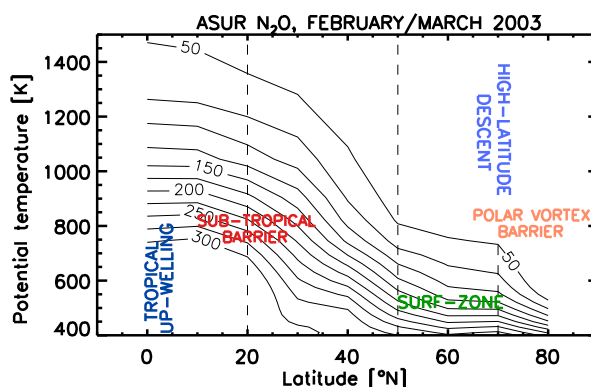
Figure 13.1: Measurements of N_2O during the SCIAVALUE 2003 deployment. The important transport features associated with winter/spring stratosphere are also noted.

Figure 13.1 is the N_2O distribution in the stratosphere as seen by the ASUR sensor during the SCIAVALUE 2003 deployment. The data are binned to 10° latitude. The tropical data (up to 30°N) belong to February (winter) and the rest belong to March (spring) seasons. The elevated contour levels in the tropics show the region of massive upwelling, where the large-scale ascent of tropical airmasses lift the isopleths up with its (near) tropospheric mixing ratio. Planetary wave activities make the mid-latitude lower stratospheric surfzone relatively flat, where gradients in the tracer mixing ratios with latitude are relatively constant (flat) as compared to the steep gradients at the latitudes of eddy mixing barriers in the subtropics and in the polar vortex regions. The gross diabatic descent and the polar vortex processes produce the low mixing ratio values at the high latitudes. Thus, the prime dynamical features are clearly represented in the N_2O volume mixing ratio distribution in the winter/spring stratosphere.
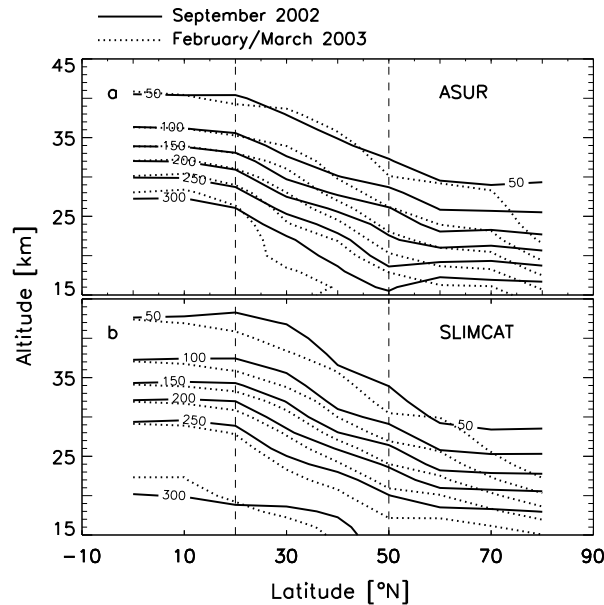
Figure 13.2: Contour plot of (a) ASUR and (b) SLIMCAT N_2O vertical profiles as a function of latitude in September 2002 (fall) and February/March 2003 (winter/spring) seasons.

13.1.1 Seasonal variations in tropical upwelling

Figure 13.2 compares the N_2O observations with the SLIMCAT simulations. Since N_2O has no known sources in the stratosphere, it enters the tropical stratosphere through the upward branch of the tropical Hadley cell. As it is a tracer the lower stratospheric abundance changes only with changes in the upward lift of the airmasses. So for a given altitude in the lower stratosphere, if mixing ratio of the molecule changes with seasons implies that the airmass uplift at these latitudes changes with seasons as well. The figure shows that the lower stratospheric spring time mixing ratios are higher than those of the fall. It proposes that the tropical upwelling is higher in the winter as compared to the fall. This seasonal difference has been proved by many studies with radiative calculations, mass flux estimations and trace gas ascent rates (Solomon et al., 1986; Holton and Choi, 1988; Dunkerton, 1991; Rosenlof and Holton, 1993; Rosenlof, 1995; Appenzeller et al., 1996; Rosenlof, 1999; Niwano et al., 2003). The tropical measurements by ASUR in the fall were around the equinox period and the spring measurements were one month before the equinox. The vertical component of effective transport velocity (ω) calculated from N_2O in Holton and Choi (1988) shows that, the ω has a small upward velocity during the solstice in the summer hemisphere (Solomon et al., 1986; Holton and Choi, 1988; Dunkerton, 1991; Scott, 2002b) and downward velocities during the equinox at the equatorial latitudes. Their study also found that the equinox case is at its best in the March N_2O, which is observed in this study too. The equinox measurements (September 2002) show lower tropical upwelling (because of smaller upward thrust in the equatorial/tropical region) than the near-equinox (February/March 2003) observations.

Figure 13.3 depicts a close look at the seasonal difference in the tropical upwelling. The difference in the upwelling altitude is calculated as follows. The N_2O VMR at a specific altitude (the altitude at which the tropospheric mixing ratio just vanishes in the tropical ASUR/SLIMCAT profiles) in the fall is taken as the reference VMR. The altitude of occurrence of the same reference VMR in the winter profile is then marked. The difference between the two altitudes (altitude of the reference VMR in the fall and the altitude of occurrence of
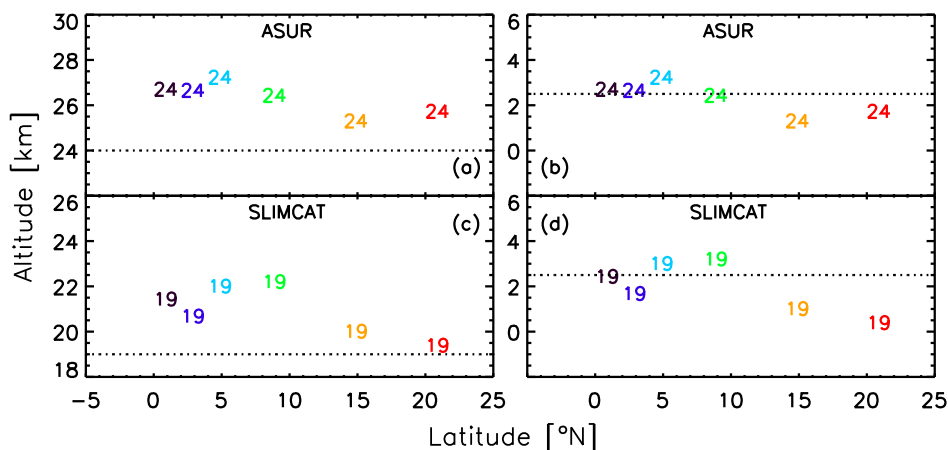
Figure 13.3: Seasonal variation in the tropical upwelling deduced from the ASUR N_2O observations is compared with the SLIMCAT simulations for September 2002 and February/March 2003. The dotted lines (on the left) stand for the altitude of the reference VMR in the fall (24 km for ASUR and 19 km for SLIMCAT) and the numbers represent altitude of the same reference VMR found in the winter. The plots on the right with the numbers illustrates the difference in the altitudes of the reference mixing ratio in the fall and the altitudes of the same mixing ratio values found in the winter/spring. The dotted lines (on the right plots) show a 2.5 km arbitrary reference to show the seasonal difference in the upwelling altitudes. See the text for a detailed discussion.

the same reference VMR in the winter profile) are calculated. This difference is a quantitative appreciation of the difference in the tropical upwelling. Since the reference altitude is an approximation and greatly depend on the resolution and accuracy of the profiles, the results should be compared on a qualitative basis only. In the ASUR measurements near-tropospheric values are extended up to 24 km against 19 km in SLIMCAT profiles. Thus, these altitudes are taken as the reference altitudes in the fall.

13.1.2 Results

The difference (winter-spring/fall) in the tropical upwelling is found to be the largest around 5°N, which is about ~3 km [see Figure 13.2 and Figure 13.3]. Since the thermal equator lies around 4°N, the largest uplift is expected at these latitudes. Hence, this study confirm that the tropical large scale airmass ascent is the highest in winter. In general, south of 10°N the upwelling is about ~ 2.5 km. Also, north of 10°N the upwelling is significantly lower and is about 0.5-1.0 km. Away from the equatorial bands (5°S-5°S) there is no significant mechanism to push the airmasses up. Thus, the relatively low ascent rates are anticipated at these latitude bands. There is a small interhemispheric difference in the upwelling as well. The ASUR N_2O shows that the southern hemispheric mixing ratio contours (winter/spring and fall mixing ratio values) are closer than the northern hemispheric isopleths at the equatorial latitudes (Figure 13.2). The SLIMCAT data also show the highest upwelling at 5°N-10°N. Furthermore, the simulated upwelling throughout the latitudes is also in the measured direction, which are in good agreement with the observations. The observed difference in the interhemispheric upwelling is also reproduced by the model.

13.1.3 Discussion on tropical upwelling

Planetary wave activities in the stratosphere have a prominent seasonal cycle (Scott and Haynes, 2002a). Additionally, the wave activities also alter with the hemispheres because of the asymmetries on the Earth surface between the northern and the southern hemisphere (Rosenlof, 1995). In the northern hemisphere planetary wave activity is weak in summer, moderate in fall and spring and very strong in winter (Randel, 1988; Hirota and Shiotani, 1983; Randel et al., 1993). Therefore, the momentum induced by these waves also changes in accord with the seasons. Since the wave activities are the main driving force for the transport, the tropical upwelling has also been featured with a similar seasonal cycle. Furthermore, the effect of planetary wave propagations is different in each hemisphere. Hence, in addition to the seasonal cycle, the hemispheric difference is also apparent in the measurements.

Trace gas transport in the tropical lower stratosphere is influenced by dynamical features such as semiannual oscillation (Gray and Pyle, 1986) and quasi-biennial oscillation (Trepte and Hitchman, 1992; Niwano et al., 2003). The quantitative estimation of the seasonal difference in tropical upwelling from observations is 'impossible' (Rosenlof, 1995, 1999) as well. Moreover, the analyses are highly influenced by the resolution and accuracy of the measurements/calculations as long as the study is carried out with a simple ascent rate calculation. Hence, as for the previous studies on the seasonal variations, this work should also be considered as a qualitative estimation on a quantitative basis.

13.2 Subtropical barrier

Subtropical barrier is a dynamical system in the lower stratosphere (21-26 km) where horizontal mixing is relatively slow as compared to the adjacent altitude and latitude regions (Murphy et al., 1993; Minschwaner et al., 1996; Mote et al., 1996; Volk et al., 1996; Keim et al., 1997; Andrews et al., 2001a). A sharp gradient is found around 20°N in Figure 13.1, where the subtropical barrier is expected. An abrupt shift in the mixing ratio values throughout the altitudes on the left and the right of the line at 20°N indicates the sluggishness of the horizontal mixing across the barrier. In Figure 13.2 the comparison between the position of the steep gradients in the fall and the winter is depicted for the measurements and the model calculations. The observed gradients are steeper in the winter due to higher stratospheric transport, which is well reproduced by the model as well.

13.3 Surfzone

In contrast to summer stratosphere, winter stratosphere is characterized by strong large scale amplitude waves. These waves intermittently break and stir the airmass isentropically across a region from the subtropical edge to the polar vortex edge. This latitude band is termed as 'the surfzone' coined by McIntyre and Palmer (1984). In Figure 13.1 a region in which the tracer gradients with the latitude is constant observed between 20 and 70°N, is the surfzone in the observed data. Since the data are not presented in an equivalent latitude plane, the exact boundary cannot be shown by the figure. Nevertheless, the location of the polar vortex boundary during the ASUR measurement days (around 70°N) coincides with the boundary

shown (70°N) in the figure. The subtropical barrier observed from the NO_y/O_3 ratio also coincides with the region where the steepest gradient found in the subtropical measurements. The model results are consistent with the measurements (Figure 13.2). The steep gradients are present more or less at the same latitude as found in the ASUR measurements.
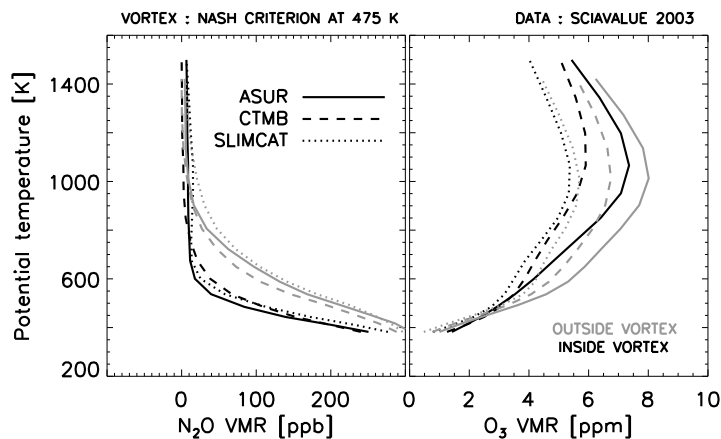

Figure 13.4: The N_2O and O_3 mixing ratios inside and outside the Arctic polar vortex observed by ASUR compared to the SLIMCAT and the CTMB calculations.

13.4 High latitude descent and polar vortex

The N_2O mixing ratios in Figure 13.1 with the flat contours right from 50°N illustrates the effect of airmass descent at the high latitudes. In the fall the contours are flat and nearly parallel (60°N ownwards). However, in the spring the contours have little slope and show lower VMRs than the fall values. It implies that the intensity of airmass descent is higher in winter and spring. The simulated mixing ratio in the spring is smaller than the fall values, which is consistent with the observed feature. However, north of 70°N, the descent in the ASUR measurements is rapid/greater than those in SLIMCAT in the spring. In addition, the descent in SLIMCAT has already been started from 60°N-65°N itself. In addition, the descent that ASUR measured between 50°N and 70°N is higher than the simulated descent between 50°N and 65°N.

   Figure 13.4 compares the N_2O mixing ratios inside and outside the vortex. The vortex edge is calculated using the Nash et al. (1996) criterion at 475 K with the ECMWF analysis. Apparently, the mixing ratios outside the vortex show higher values than those of inside. The diabatic descent inside the vortex produce low N_2O mixing ratios and the mixing with mid-latitude air produce relatively higher mixing ratios outside the vortex (Plumb, 2002). Thus, the diabatic descent is well represented in the ASUR measurements. Interestingly, the profiles outside the vortex also show signatures of the diabatic descent. These features in the tracer mixing ratios were noted in the SOLVE and EUPLEX data as well (Bremer et al., 2002; Kleinböhl et al., 2003). Downward propagation of planetary waves and gravity wave pumping at high latitudes could influence the airmasses outside the vortex to make such characteristic tracer profiles (Scott and Dritschel, 2004). The low O_3 values inside the vortex for all potential temperature levels as compared to the O_3 values outside the vortex show the impact of the

dynamical descent inside the vortex and its effect on the mixing ratios. The measured profiles inside and outside the vortex are reasonably reproduced by the model simulations as well.
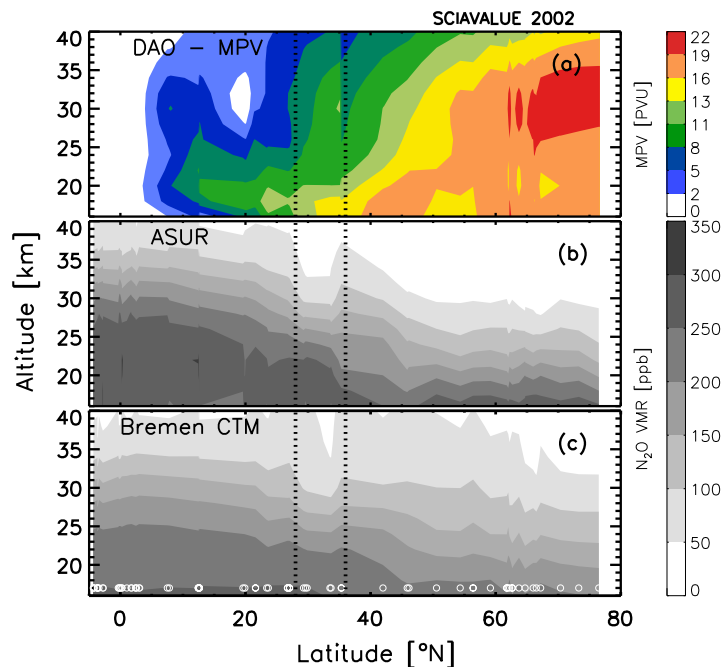
Figure 13.5: Contour plot of (a) the DAO modified potential vorticity (MPV), (b) the ASUR and (c) the smoothed CTMB N$_2$O vertical profiles as a function of latitude. The observations are carried out during the SCIAVALUE 2002. The circles on the bottom of the plot represent individual measurement points. The dash lines show the region of transported airmasses.

13.5 Case studies

13.5.1 Transport of the Arctic airmass into the northern mid-latitudes in September 2002

Rapid meridional transport in the stratosphere on isentropes are commonly associated with stratospheric dynamical systems like wave activities and concomitant warming events. In September 2002 the southern polar vortex split into two parts and experienced the extreme warming event ever observed over the southern pole (Sinnhuber et al., 2003). A sudden meridional transport of the Arctic stratospheric airmass into the mid-latitude upper stratosphere has occurred during the same period (there is no connection between these two events). The event is unveiled with ASUR N$_2$O measurements and trajectory calculations in this section.

Figure 13.5(a) shows low N$_2$O values in the middle stratosphere around 30°N (as a ridge in the contour plot marked with dashed lines). The model calculations also show the same feature. In addition, the modifies potential vorticity (MPV) profiles at the same location also show high values as compared to the nearby measurement points. The MPV (Lait, 1994) is featured with similar values in the lower stratosphere, indicate that the airmasses belong to the same latitude. Whereas the middle stratospheric MPV values are relatively higher as compared to the surrounding latitude regions, which are of the similar magnitude that found in the Arctic

as well. Apparently, the middle stratospheric airmasses must have been transported from the Arctic. In order to examine the airmass origin, trajectory analyses with the NOAA HYSPLIT READY model (Draxler and Rolph, 2003) have been performed. The ten-day back trajectory analysis results for selective measurements on 17, 26 and 28 of September 2002, in which the high values are observed, are plotted.
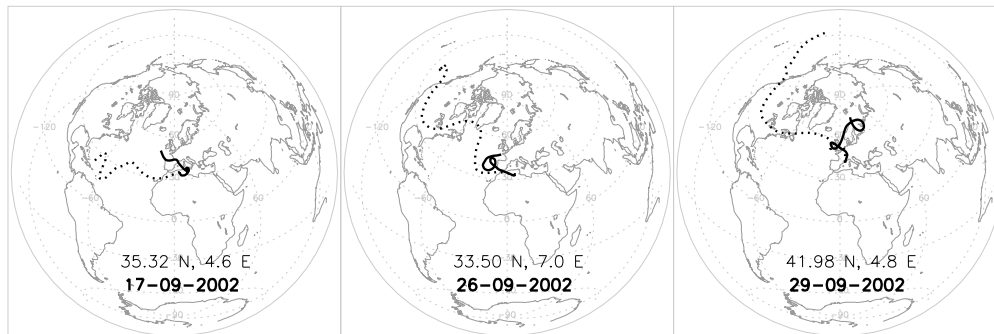

Figure 13.6: Airmass trajectories calculated using the NOAA HYSPLIT READY model for three days in September 2002 as noted on the figures. The solid line represent the trajectory at 15 km and the dotted line at 27 km. The back trajectories are calculated for 10 days.

Figure 13.6 illustrates the trajectory analyses for the days at specific measurement location as noted in the figure. The backward trajectory analyses for 10 days started from the measurement location and time. Only a couple of the airmass trajectories are shown here due to clarity reasons, at 15 and 27 km. As shown by the measurements, the airmass at the lower altitudes (solid lines) are of the same/nearby latitude origin and the airmasses at the higher altitudes (dotted lines) are of the high latitude origin. All the trajectory analyses show a similar pattern of airmass distribution. Thus, the airmass of the same/nearby latitude origin in the lower stratosphere exhibits the similar VMR values and the airmass of the high latitude origin in the middle and upper stratosphere possess the low mixing ratios. Hence, the trajectory analyses confirm the observed feature that the lower stratospheric airmasses are of the same/nearby latitude origin and the middle stratospheric airmasses are transported from the Arctic regions in a short period of time, in the order of 5-10 days.

13.5.2 Transport of the subtropical airmasses into the Arctic during the major warming event in January 2003

During the major stratospheric warming event associated with a wave-2 in January 2003 (EORCU, 2003), isentropic transport of the subtropical airmass into the Arctic latitudes is occurred. The ASUR measurements during the EUPLEX campaign are used to analyse the transport process.

Figure 13.7 shows unusually high values of N_2O around 60°N, which are similar to the ones found in the subtropical stratosphere, shown in Figure 13.5(a). The measured variabilities are well reproduced by the model as well. In addition, the MPVs show very low values as compared to the surrouding latitude sections. These values are similar to the ones found in the subtropics. Obviously, the airmass does not belong to this region, which must have been transported from the subtropical latitudes. There is an apparent increase in the MPV values at 54°N and at 51°N. In addition, the nitrous oxide profiles at these latitudes show very low VMR
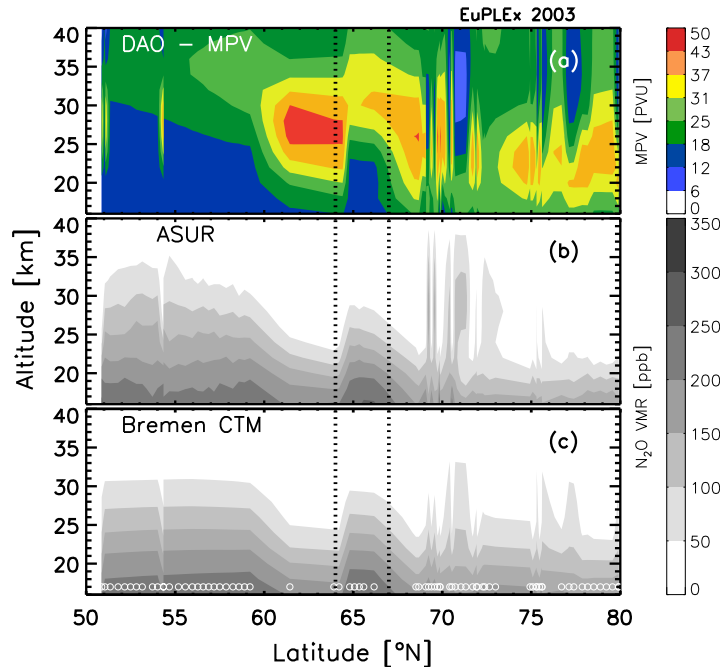
Figure 13.7: Same as Figure 13.5, but for EUPLEX measurements.

values above 24 km, where the MPV also show up with high values. Also, the magnitude of the MPV in the middle stratosphere is similar to the values found in the Arctic. Moreover, the simulated profiles clearly show the variations. Interestingly, the measurements were continuous and were observed during the crossing of a low pressure system. So the measured variabilities in the trace gas might be due to this particular meteorological and dynamical situation. This dynamical situation will be further explored in a separate paper.
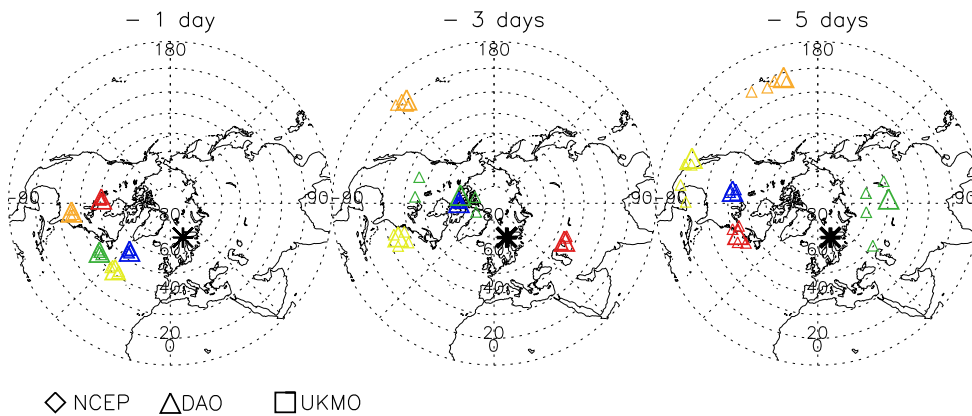
Figure 13.8: The co-ordinates of the origin points of a 5 day back trajectory calculated form DAO analyses at different potential temperature levels for 23 January 2003. The color codes stand for the potential temperatures 475 K-blue, 600 K-green, 800 K-yellow , 1000 K-orange, and 1200 K is for red. The black star represent the starting location of the trajectories (Figure courtesy: A. Kleinböl)

Figure 13.6 shows the origin points of 5 day back trajectory analyses for the day in which the high values are observed (23 January 2003) using three different meteorological data sets. In order to get a clear picture the airmass origin co-ordinates in DAO are shown only. The

color codes stand for different potential temperature levels, where blue is for 475 K, green is 600 K, yellow is 800 K, orange is 1000 K, and red is 1200 K. Apparently, the back trajectory analyses show that the airmasses are transported from northern subtropical and mid-latitude region around 15°N-20°N. This is particularly evident at 800K and 1000 K. All the three meteorological analyses agree with the fact the airmasses are transported from the northen subtropics within a short period of time, in the order $\sim$ 5 days. Hence, the trajectory analyses confirm the measured and the simulated rapid meridional transport of subtropical airmasses into the Arctic. A detailed study of the event in a different perspective is done by Kleinböhl et al. (2004b).

13.6 Conclusions

The ASUR N_2O measurements from SCIAVALUE and EUPLEX are used to identify and study the transport processes in the stratosphere. Dynamical features like tropical upwelling, subtropical barrier, mid-latitude surfzone, high latitude descent and polar vortex processes are analyzed using the tracer data. (a) A qualitative estimation on a quantitative terms of the difference in the tropical upwelling between the fall and the spring is performed. The calculation shows that the upwelling in the spring is about 2.5 km higher in the equatorial/tropical latitude belts (up to 10°N) as compared to the upwelling in the fall. (b) The signatures of the hemispheric difference in the tropical upwelling is also imprinted in the measurements. These estimations are consistent with the model calculations performed in this study and the estimations carried out in previous studies using various methods. Seasonal differences in the upwelling is due to the seasonal cycle of the wave activities. (c) Because of the higher stratospheric transport in the winter, the observed subtropical barrier is steeper than the measured gradient in the fall. (d) The Arctic airmass transport into the northern mid-latitude in September 2002 and the transport of the subtropical airmass in to the Arctic in January 2003 are studied with ASUR N_2O measurements. The model simulations, the MPV calculations and the trajectory analyses corroborate the observed transport processes.

14 Summary and Conclusions

This section summarises the important results of a three years graduate study. The work comprises measurements and modeling of stratospheric trace gases for which, the measurements were carried out by ASUR and the modeling studies were performed with CTMB. The ASUR trace gas measurements during the SOLVE, the SCIAVALUE, the EUPLEX and the PAVE campaigns are mostly used. In order to evaluate the simulations a tremendous amount of data observed from various platforms ranging from groundbased to spaceborne instruments, model calculations and climatologies are exploited.

For the first time in ASURs operational span, latitudinal cross-sections from the tropics to the Arctic have been made for a number of its operational products in two different seasons during SCIAVALUE. It is also for the first time that a dataset has simultaneously been explored to validate four different sensors (MIPAS, OSIRIS, SCIAMACHY, and SMR) onboard two different satellites (ENVISAT and Odin) for a number of species from 5°S to 80°N in three different seasons (fall, winter and spring). Since the retrievals are performed in a quasi operational basis, the molecules O_3, ClO, HCl, N_2O and HNO_3 are focused for the scientific analyses.

Retrievals south of 45°N is for the first time from the ASUR measurements. Comparisons with ozonesondes, radiometers and model calculations show that ASUR ozone retrievals are in good shape. Nevertheless, the ozone VMRs are about 12% higher than other independent measurements and model simulations. The ClO, HCl, N_2O and HNO_3 retrievals in comparisons with model simulations yield encouraging results. The vertical distributions, the altitude of maximum VMR, the latitudinal variations, and the seasonal signatures are well represented and are in good agreement with the simulations. Below 20 km, the ASUR N_2O measurements show slightly higher values. The comparisons between the mixing ratios (of O_3, ClO, HCl, N_2O and HNO_3) retrieved with two different radiative transfer models ('*the forward*' and ARTS), show negligible differences. So this study recommends the replacement of the old RTM with the new and fast ARTS for the ASUR trace gas retrievals.

The cross-comparisons show that deviation ASUR-SCIAMACHY OP 1.0 is -4 to 6%, ASUR-SCIAMACHY UB 1.6 is -12 to 15%, ASUR-MIPAS IPF 4.61 is up to 5%, ASUR-MIPAS IMK 1-O_3-1 is -3 to 6%, ASUR-OSIRIS 012 is about 3 to 15% and ASUR-SMR 222 is -4 to 15% at 20-40 km, depending on altitude. Hence, these good comparison results recommend the satellite ozone to be used in scientific analyses.

The intercomparisons with ASUR, MIPAS and SMR N_2O show that the differences are within 15%, in general. The agreement between ASUR and MIPAS HNO_3 profiles is excellent, where the deviation between the profiles is within 5%. The ClO intercomparisons with MIPAS show the potential of ASUR measurements to validate the molecule. Only a few instruments can measure these trace gases in the stratosphere and the measurements are sporadic as well. Hence, the intercomparison results are significant in the accuracy estimation of the spaceborne measurements.

A new stratospheric CTM is introduced as a part of this study. The model with parameter-

ized chemistry schemes provides simple but accurate simulations of O_3, N_2O and NO_y with negligibly small CPU usage. Hence, (the model with) the chemistry modules are suitable for incorporating into GCMs and CTMs for long term integration to perform trend analyses. Ozone takes 6 months and N_2O and NO_y need 3 years to reach equilibrium in the model. The main constraint of the simulations is the assumptions on climatological states of the trace gases, uncertainties in the reaction constants and inaccuracies in the meteorological analyses which are employed for the pre-calculated tables to simulate the chemical tendency of the molecules.

The evaluation of Linoz with the model shows that the ozone simulations have a negative bias of ~9% in the middle stratosphere. However, the lower and upper stratospheric calculations slightly overpredict the measurements by 10-20%, above 20 km, depending on altitude. Nevertheless, considering the uncertainties in the measurements and reasonably represented transport in the model, the Linoz bias of 9% (the lower and upper stratospheric high deviation is due to the fluctuations in the small absolute values as the VMRs are very small there) doesn't seem to give rise any problems in the scientific analyses of the model results to be used in any kind of studies related to stratospheric chemistry and dynamics. The comparisons also show that the polar ozone loss parameterization helps very much to simulate the high latitude ozone accurate and realistic.

The simulated N_2O is slightly smaller than that of the measurements and other model calculations. This could be due to uncertainties in the chemical reaction rates, inaccuracies in the model transport and possible bias/problems with the meteorological analyses used in the model. However, sensitivity tests with the increased heating rates in the model show that the tracer isopleths can be elevated (or the mixing ratios can be increased) and thus the simulations can be improved considerably with the additional heating in the model. An 80% increment in the total heating rate in the model improve the simulations. The simulated values are closer and the gradients are comparable to the measured ones. The experiment suggest that, with the current setup the model needs additional dynamic drive to simulate reasonable tracer isopleths and latitudinal gradients. Since there are still some slight discrepancies in the simulated results in comparison with observations, the tests indicate that the increased heating in the model is not a permanent solution. The NO_y simulations are in accord with the photochemical and transport processes in the atmosphere, which are in good agreement with the calculated results from the UCI GISS and the UCI models.

N_2O can be simulated with and without NO_y in the model. The simulations without NO_y slightly reduces the N_2O mixing ratios throughout the latitudes due to the omission of NO_y conversion back to N_2O (implies an additional source of stratospheric N_2O). Since the difference is very small, this study recommends the simulations N_2O without NO_y, provided the simulations are not needed for NO_y (since the simulations are already lower than the measured mixing ratios). The model derived correlation slopes are in very good agreement with the observed slopes. The correlation implies that the N_2O-NO_y coupled chemistry of the molecules is reasonably represented in the model. The subtropical and the polar vortex barriers are clearly depicted in the NO_y-O_3 ratio analyses. The representation of subtropical barrier is remarkable as most models fail to reproduce this dynamical system properly. The minute details like hemispheric difference and seasonal migration of these dynamic systems are even depicted in the calculations.

Drastic changes in the simulated trace gas mixing ratios are evident over the years from 1991 to 2003 for O_3, N_2O and NO_y. Also, a gradual and constant improvement in the calculations adjudged from the comparisons with measuremets are also noticed. Since the only

change in the input file is meteorological analyses, the inaccuracies in the forcing windfields are responsible for these characteristic simulations. In addition, the quality of UKMO analyses during the beginning period of the operational analyses is questionable, 1991 to 1995 in particular for which the simulations were not good. Hence, the study demonstrates the impact of inaccurate meteorological analyses on the simulations of stratospheric trace gases. This is particularly important for NO_y simulations since the vertical distribution and the altitude of the mixing ratio maxima are largely depend on the accuracy of meteorological analyses.

The latitudinal, longitudinal and seasonal variations in stratospheric O_3, ClO, HCl, HNO_3 and N_2O are clearly depicted in the ASUR observations and are in good accord with the SLIM-CAT and the CTMB calculations. As noted above, the CTMB calculates slightly lower O_3 values in the middle stratosphere and slightly smaller N_2O values in the lower stratosphere as compared to the ASUR measurements and the SLIMCAT calculations (the reasons for these discrepancies are discussed in the previous sections). Though the transport in the models is similar, SLIMCAT perform better than CTMB because of the good quality ECMWF wind fields. The ASUR measurements point out that the SLIMCAT calculations without the denitrification scheme fail to reproduce the observed winter stratospheric HCl and HNO_3 VMRs. Absence of seasonal variations of ozone in the Arctic SLIMCAT simulations and in the tropical ASUR measurements demand further comparisons to make strong conclusions on this regard.

The ASUR N_2O observations are clearly marked with features of tropical upwelling, mid-latitude surfzone, high latitude descent and polar vortex processes. The measurements show that the winter stratospheric tropical upwelling is stronger than that of the fall. The airmasses are lifted about 2.5 km higher in the winter as compared to the fall, which is in good agreement with the model calculations. The observed transport of the Arctic airmass in to mid-latitude in September 2002 and the transport of the subtropical airmass to the Arctic, which are occurred within 5 to 10 days, are well reproduced by CTMB. The MPV fields and trajectory analyses underpin the observed and simulated transport phenomena.

15 Prospectus

Retrievals of stratospheric Ozone, ClO, HCl, HNO$_3$ and N$_2$O from the ASUR measurements during the Polar Aura Validation Experiment (PAVE) are shown in Figure 15.1. The campaign was conducted aboard the NASA DC-8 research airplane to perform validation measurements for the NASA AURA satellite. Data analyses for the validation of various trace gases and the scientific studies with the data are the future plans. The validation of Microwave Limb Sounder (MLS) products with ASUR is particularly important in this context since both sensors operate in the same/similar frequency range. Investigation of interannual variabilities of the trace gases abundance (Ozone, ClO, HCl, HNO$_3$ and N$_2$O) in the Arctic stratosphere using the ASUR measurements and tracer correlations in the stratosphere are the other future studies.
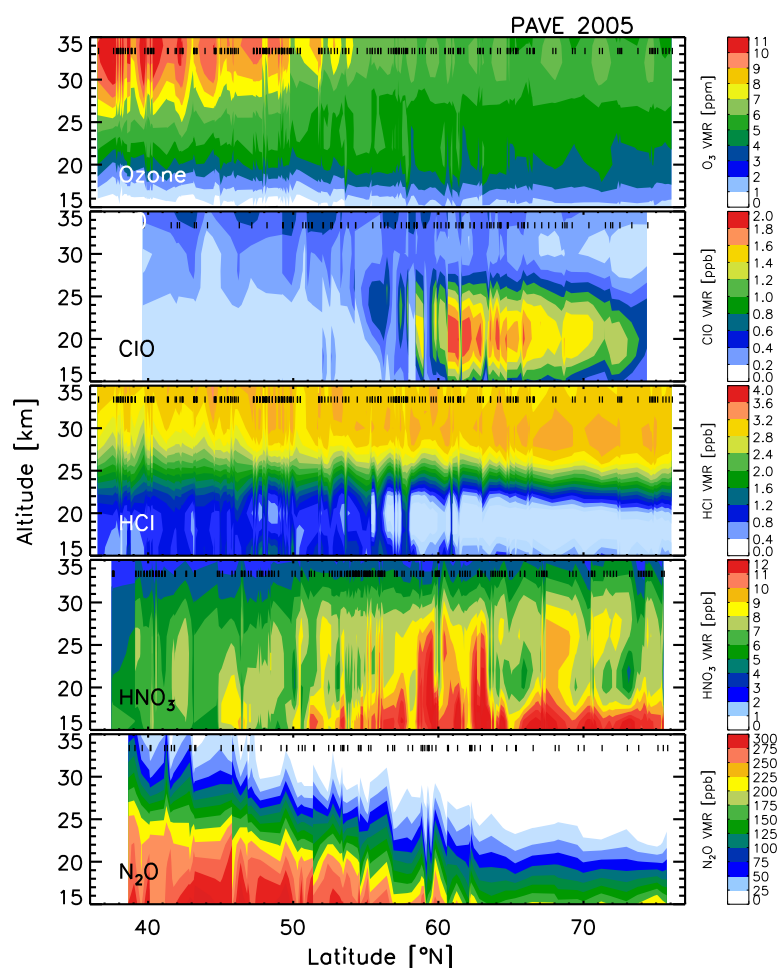

Figure 15.1: Ozone, ClO, HCl, HNO$_3$ and N$_2$O measurements by the ASUR sensor during the AURA validation campaign (PAVE 2005) in January-February 2005. The black sign on the top of the plots indicate the measurement locations.

Bibliography

Abrams, M. C., Chang, A. Y., Gunson, M. R., Abbas, M. M., Goldman, A., Irion, F. W., Michelsen, H. A., Newchurch, M. J., Rinsland, C. P., Stiller, G. P. and Zander, R., 1996: On the assessment and uncertainty of atmospheric trace gas burden measurements with high resolution infrared solar occultation spectra from space. *Geophys. Res. Lett.*, **23**, 2337–2340.

Andrews, A., Boering, K. A., Wofsy, S. C., Daube, B. C., Jones, D. B., Alex, S., Loewenstein, M., Podolske, J. R. and Strahan, S. E., 2001a: Empirical age spectra for the midlatitude lower stratosphere from in situ observations of CO_2: Quantitative evidence for a subtropical barrier to horizontal transport. *J. Geophys. Res.*, **106**, 10 257–10 274.

Andrews, G., 2000: *An introduction to atmospheric physics*. Cambridge University Press: London. 240 pp.

Appenzeller, C., Holton, J. R. and Rosenlof, K. H., 1996: Seasonal variation of mass transport across the tropopause. *J. Geophys. Res.*, **101**, 15 071–15 078.

Avallone, L. M. and Prather, M. J., 1997: Tracer-tracer correlations: three-dimensional model simulations and comparisons to observations. *J. Geophys. Res.*, **102**, 19 233–19 246.

Bovensmann, H., Burrows, J. P., Buchwitz, M., Frerick, J., Noel, S., Rozanov, V. V., Chance, K. V. and Goede, A. P. H., 1999: SCIAMACHY- Mission Objectives and Measurement Modes. *J. Atmos. Sci.*, **56**, C12, 127–150.

Bracher, A., Bramsted, K., Sinnhuber, M., Weber, M. and Burrows, J., 2004a: Validation of GOMOS (GOPR 6.0a) and SCIAMACHY (v5.1/2.1) O_3 and NO_2 products with GOME (v3.0), HALOE (v19) and SAGE II (6.2). *Proceedings of* ACVE-*2 workshop*, **56**, SP-562.

Bracher, A., Bramsted, K., Sinnhuber, M., Weber, M. and Burrows, J., 2004b: Validation of MIPAS O_3, NO_2, H_2O and CH4 profiles (v4.61) with collocated measurements of HALOE (v19) and SAGE II (6.2). *Proceedings of* ACVE-*2 workshop*, **56**, SP-562.

Brasseur, G., Orlando, J. and Tyndall, G. S., 1999: *Atmospheric chemistry and global change*. Oxford university press: Newyork. 654 pp.

Brasseur, G. and Solomon, S., 1984: *Aeronomy of the middle atmosphere*. Reidel publishing company: The Netherlands. 441 pp.

Bremer, H., 2001: *Measurements of dynamical tracers and ozone in the Arctic stratosphere: Analyses and interpretation of airborne submillimeter wave measurements*. PhD. thesis: Logos Verlag Berlin. 174 pp.

Bremer, H., von König, M., Kleinböhl, A., Küllmann, H., Künzi, K., Bramstedt, K., Burrows, J. P., Eichmann, K.-U., Weber, M. and Goede, A. P. H., 2002: Ozone depletion observed by ASUR during the Artic winter 1999/2000. *J. Geophys. Res.*, **107**, 10.1029/2001JD000 546.

Browell, E. V., Carter, A. F., Shipley, S. T., Allen, R. J., Butler, C. F., Mayo, M. N., Jr., J. H. S. and Hall, W. M., 1983: NASA multipurpose airborne DIAL system and measurements of ozone and aerosol profiles. *Appl. Optics.*, **22**, 522–534.

Bühler, S. and Eriksson, P., 2000: *Atmospheric millimeter and sub-millimeter wave radiative*

transfer modeling. Berichte aus der Physik: Shaker Verlag GmbH, Aachen. ISBN 3-8265-7486-9.

Bühler, S., Eriksson, P., Kuhn, T., von Engeln, A. and Verdes, C., 2004: ARTS, the Atmospheric Radiative Transfer Simulator. *J. Quant. Spectrosc. Radiat. Transfer*, **91**.

Camy-Peyret, C., Dufour, G., Payan, S., Oelhaf, H., Wetzel, G., Stiller, G., Blumenstock, T., Blom, C., Gulde, T., Glatthor, N., Engel, A., Pirre, M., Catoire, V., Moreau, G., Maziére, M. D., Vigouroux, C., Mahieu, E., Cortesi, U. and Mencaraglia, F., 2004: Validation of MIPAS N$_2$O profiles by stratospheric balloon, aircraft and ground based measurements. *Proceedings of* ACVE-*2 workshop*, **56**, SP-562.

Cariolle, D. and Déqué, M., 1986: Southern hemisphere medium-scale waves and total ozone disturbances in a spectral general circulation model. *J. Geophys. Res.*, **91**, 10825–10846.

Chipperfield, M., 1999: Multiannual simulations with a three dimensional chemical transport model. *J. Geophys. Res.*, **104**, 1781–1805.

von Clarmann, 2003: Retrieval of temperature and tangent altitude pointing from limb emission spectra recorded from space by the Michelson Interferometer for Passive Atmospheric Sounding (MIPAS). *J. Geophys. Res.*, **108**, doi:10.1029/2003JD003602.

Davies, S., Chipperfield, M. P., Carslaw, K. S., Sinnhuber, B. M., Anderson, J. G., Stimpfle, R. M., Wilmouth, D. M., Fahey, D. W., Popp, P. J., Richard, E. C., von der Gathen, P., Jost, H. and Webster, C. R., 2003: Modeling the effect of denitrification on Arctic ozone depletion during winter 1999/2000. *J. Geophys. Res.*, doi:10.1029/2001JD000445.

DeMore, W., Sander, S., Golden, D., Hampson, R., Kurylo, M., Howard, C., Ravishankara, A., Kolb, C. and Molina, M., 1997: *Chemical kinetics and photochemical data for use in stratospheric modeling*, vol. JPL Publication 97-4 of *Evaluation No. 12*. Pasadena, CA: Jet Propulsion Lab.

Douglas, A. R., Prather, M. J., Hall, T. M., Strahan, S. E., Rasch, P. J., Sparling, L. C., Coy, L. and Rodriguez, J. M., 1999: Choosing meteorological input for the global modeling initiative assessment of high-speed aircraft. *J. Geophys. Res.*, **104**, 27545–27564.

Draxler, R. and Rolph, G., 2003: HYSPLIT *(HYbrid Single-Particle Lagrangian Integrated Trajectory) Model access via* NOAA ARL READY, *website (http://www.arl.noaa.gov/ready/hysplit4.html)*. Silver Spring, MD.: NOAA Air Resources Laboratory.

Drayson, S., 1976: Rapid computation of the Voigt profile. *J. Quant. Spectrosc. Radiat. Transfer*, **16**, 611–614.

Dunkerton, T., 1989: Nonlinear Hadley circulation driven by asymmetric driven by asymmetric differential heating. *J. Atmos. Sci.*, **46**, 2325–2333.

Dunkerton, T., 1991: Nonlinear propagation of zonal winds in an atmosphere with Newtonian cooling and equatorial wave driving. *J. Atmos. Sci.*, **48**, 236–263.

Fahey, D., Donnelly, S., Keim, E., Gao, R., Wamsley, R., Negro, L. D., Woodbridge, E., Proffitt, M., Rosenlof, K., Ko, M., Weisenstein, D., Scott, C., Nevison, C., Solomon, S. and Chan, K., 1996: In situ observations of NO$_y$, O$_3$, and the NO$_y$/O$_3$ ratio in the lower stratosphere. *Geophys. Res. Lett.*, **23**, 1653–1656.

Fang, T. M., Wofsy, S. C. and Dalgarno, A., 1974: Opacity distribution functions and absorption in Schumann-Runge bands of molecular-oxygen. *Planet. Spa. Sci.*, **22**, 413–425.

Farman, J. C., Gardiner, B. G. and Shanklin, J. D., 1985: Large Losses of total ozone over Antarctica reveal seasonal ClO$_x$/NO$_x$ interactions. *Nature*, **315**, 207–210.

Fix, A., Ehret, G., Flentje, H., Poberaj, G., Gottwald, M., Finkenzeller, H., Bremer, H., Bruns,

M., Burrows, J. P., Kleinböhl, A., Küllmann, H., Kuttippurath, J., Richter, A., Wang, P., Heue, K.-P., Platt, U. and Wagner, T., 2004: SCIAMACHY validation by aircraft remote measurements: Design, execution, and first results of the SCIA-VALUE mission. *Atmos. Chem. Phys. Disscuss.*, **4**, 8381–8423.

Flittner, D. E., Bhartia, P. K. and Herman, B. M., 2000: O$_3$ profiles retrieved from Limb scatter measurements: Theory. *Geophys. Res. Lett.*, **27**, 2601–2604.

Fortuin, P. and Kelder, H., 1998: An ozone climatology based on ozonesonde and satellite measurements. *J. Geophys. Res.*, **103**, 31 709–31 734.

Frisk, U., Hagstrýom, M., Ala-Laurinaho, J., Andersson, S., Berges, J.-C., Chabaud, J.-P., Dahlgren, M., Emrich, A., Floren, H.-G., Florin, G., Fredrixon, M., Gaier, T., Haas, R., Hirvonen, T., Hjalmarsson, Jakobsson, B., Jukkala, P., Kildal, P., Kollberg, E., Lassing, J., Lecacheux, A., Lehikoinen, P., Lehto, A., Mallat, J., Marty, C., Michet, D., Narbonne, J., Nexon, M., Olberg, M., Olofsson, O., Olofsson, G., Origne, A., Petersson, M., Piiro-nen, P., Pons, R., Pouliquen, D., Ristocelli, I., Rosolen, C., Rouaix, G., anen, A. R., Serra, G., oberg, F. S., Stenmark, L., Torchinsky, S., Tuovinen, J., Ullberg, C., Vinterhav, E., Wade-falk, N., Zirath, H., Zimmermann, P. and Zimmermann, R., 2004: The Odin satellite: I. Radiometer design and test. *Astron. and Astrophys.*, **402 (3)**, 27–34.

Gray, L. J. and Pyle, J. A., 1986: The semiannual oscillation and equatorial tracer distributions. *Quart. J. Roy. Meteor. Soc.*, **112**, 387–407.

Greenblatt, J. B., Jost, H.-J., Loewenstein, M., Podolske, J. R., Hurst, D. F., Elkins, J. W., Schauffler, S. M., Atlas, E. L., Herman, R. L., Webster, C. R., Bui, T. P., Moore, F. L., Ray, E. A., Oltmans, S., Voemel, H., Blavier, J.-F., Sen, B., Stachnik, R. A., Toon, G. C., Engel, A., Mller, M., Schmidt, U., Bremer, H., Pierce, R. B., Chipperfield, B.-M. S. M. and Lefévre, F., 2002: Tracer-based Determination of Vortex Descent in the 1999/2000 Arctic winter. *J. Geophys. Res.*, **107**, D20, 10.1029/2001JD000 937.

Guthrie, P. D., Jackman, C. H., Herman, J. R. and C.J.McQuillan, 1984: A diabatic circulation experiment in a two-dimensional photochemical model. *J. Geophys. Res.*, **89**, 9589–9602.

Hall, T. and Plumb, A., 1994: Age as a diagnostic of stratospheric transport. *J. Geophys. Res.*, **99**, 1059–1070.

Hall, T., Waugh, D., Boering, K. and Plumb, A., 1999: Evaluation of transport in stratospheric models. *J. Geophys. Res.*, **104**, 18 815–18 839.

Haynes, P. H. and Shuckburgh, E. F., 2000a: Effective diffusivity as a diagnostic of atmospheric transport. Part I: stratosphere. *J. Geophys. Res.*, **105**, 22 777–22 794.

Hedin, A. E., 1991: Extension of the MSIS Thermospheric Model into the Middle and Lower Atmosphere. *J. Geophys. Res.*, **96**, 1159–1172.

Hirota, I. T. H. and Shiotani, M., 1983: Upper stratospheric circulations in the hemispheres observed by satellites. *Quart. J. Roy. Meteor. Soc.*, **109**, 443–454.

Holton, J., 1986: Meridional distribution of stratospheric trace constituents. *J. Atmos. Sci.*, **43**, 1238–1242.

Holton, J., 1992: *Introduction to Dynamic Meteorology*. Academic Press: London. 350 pp.

Holton, J., 1995: Stratosphere-troposphere exchange. *Rev. Geophys.*, **33**, 403–439.

Holton, J. and Choi, W.-K., 1988: Transport circulation deduced from SAMS trace species data. *J. Atmos. Sci.*, **45**, 1929–1939.

Kaiser, J. W., von Savigny, C., Noël, S., Eichmann, K.-U., Bovensmann, H., Frerick, J. and Burrows, J. P., 2004: Satellite-pointing retrieval from atmospheric limb-scattering of solar UV-B radiation. *Can. J. Phys.*, **82**, 1041–1052.

Kanzawa, H., Sugita, T., Nakajima, H., Bodeker, G. E., Oelhaf, H., Stowasser, M., Wetzel, G., Engel, A., Schmidt, U., Levin, I., Toon, G. C., Sen, B., Blavier, J.-F., Aoki, S., Nakazawa, T., Jucks, K. W., Johnson, D. G., Traub, W. A., Camy-Peyret, C., Payan, S., Jeseck, P., Murata, I., Fukunishi, H., von König, M., Bremer, H., Küllmann, H., Park, J. H., Pan, L. L., Yokota, T., Suzuki, M., Shiotani, M. and Sasano, Y., 2003: Validation and data characteristics of nitrous oxide and methane profiles observed by the Improved Limb Atmospheric Spectrometer (ILAS) and processed with the Version 5.20 algorithm. *J. Geophys. Res.*, **108**, doi:10.1029/2002JD002 458.

Keim, E., Loewenstein, M., Podolske, J., Fahey, D., Gao, R., Woodbridge, E., Wamsley, R., Donnelly, S., Negro, L. D., Nevison, C., Solomon, S., Rosenlof, K., Scott, C., Ko, M., Weisenstein, D. and Chen, K., 1997: Measurements of the NO_y-N_2O correlation in the lower stratosphere: Latitudinal and seasonal changes and model comparisons. *J. Geophys. Res.*, **102**, 13 193–13 212.

Kleinböhl, A., Bremer, H., von König, M., Küllmann, H., Künzi, K., Goede, A. P. H., Browell, E. V., Grant, W. B., Toon, G. C., Blumenstock, T., Galle, B., Sinnhuber, B.-M. and Davies, S., 2003: Vortexwide Denitrification of the Arctic Polar Stratosphere in Winter 1999/2000 determined by Remote Observations. *J. Geophys. Res.*, **108**, D5, 10.1029/2001JD001 042.

Kleinböhl, A., Kuttippurath, J., Sinnhuber, M., Sinnhuber, B.-M., Küllmann, H., Künzi, K. and Notholt, J., 2004b: Rapid meridional transport of tropical airmasses to the Arctic during the major stratospheric warming in January 2003. *Atmos. Chem. Phys. Disscuss.*, **4**, 7121–7138.

Ko, M., Sze, N.-D. and Weisenstein, D., 1989: The roles of dynamical and chemical processes in determining the stratospheric concentration of ozone in one-dimensional and two-dimensional models. *J. Geophys. Res.*, **94**, 9889–9896.

Kondo, Y., Koike, M., Engel, A., Schmidt, U., Mueller, M., Sugita, T., Kanzawa, H., Nakazawa, T., Aoki, S., Irie, H., Toriyama, N., Suzuki, T. and Sasano, Y., 1999: NO_y-N_2O correlation observed inside the Arctic vortex in February 1997: Dynamical and chemical effects. *J. Geophys. Res.*, **104**, 8215–8224.

von König, M., 2001: *Chlorine activation and PSC formation in the Arctic stratopshere: Analyses and interpretation of Submillimeter measurements*. PhD. thesis: Logos Verlag Berlin. 234 pp.

von König, M., Bremer, H., Kleinböhl, A., Küllmann, H., Künzi, K., Goede, A. P. H., Browell, E. V., Grant, W. B., Burris, J. F., McGee, T. J. and Twigg, L., 2002: Using gas-phase nitric acid as an indicator of PSC composition. *J. Geophys. Res.*, **107**, D20, 10.1029/2001JD001 041.

Kopp, G., Berg, H., Blumenstock, T., Fischer, H., Hase, F., Hochschild, G., Höfner, M., Kouker, W., Reddmann, T., Ruhnke, R., Raffalski, U. and Kondo, Y., 2003: Evolution of ozone and ozone related species over Kiruna during the THESEO-2000 SOLVE campaign retrieved from ground-based millimeter wave and infrared observations. *J. Geophys. Res.*, **108**, D5, 8308, doi:10.1029/2001JD001 064.

Kuhn, T., 2003: *Atmospheric absorption models for the millimeter wave range*. University of Bremen. 273 pp.

Lait, 1994: An alternative form for potential vorticity. *J. Atmos. Sci.*, **51**, 1754–1759.

Lamsal, L., Weber, M., Tellmann, S. and Burrows, J. P., 2004: Ozone column classified climatology of ozone and temperature profiles based on ozonesonde and satellite data. *J. Geophys. Res.*, **109**, D20, doi:10.1029/2004JD004 680.

Langer, J., 1999: *Measurements of Arctic stratospheric ozone: Comparison of ozone mea-*

surements at at Ny-Aalesund, Spitsbergen, in 1997 and 1998. PhD Thesis: University of Bremen.

Lautié, N., 2003: *Traitement des mesures satellitaires sub-millimétriques effectuées par Odin/*SMR*: étude non-linéaire de la vapeur déau. Étude stratosphérique de HCN au moyen de mesures micro-ondes.* PhD Thesis: Université Paris VI, Paris, France.

Liebe, H., Hufford, G. and Cotton, G., 1993: Propagation modeling of moist air and suspended water/ice particles at frequencies below 1000 GHz. *52nd Specialists Meeting of The Electromagnetic Wave Propagation Panel*, 663–665.

Llewellyn, E. J., Lloyd, N. D., Degenstein, D. A., Gattinger, R. L., Petelina, S. V., Bourassa, A. E., Wiensz, J. T., Ivanov, E. V., McDade, I. C., Solheim, B. H., McConnell, J. C., Haley, C. S., von Savigny, C., Sioris, C. E., McLinden, C. A., Griffioen, E., Kaminski, J., Evans, W. F. J., Puckrin, E., K.Strong, Wehrle, V., Hum, R. H., Kendall, D. J. W., Matsushita, J., Murtagh, D. P., Brohede, S., Stegman, J., Witt, G., Barnes, G., Payne, W. F., Piché, L., Smith, K., Warshaw, G., Deslauniers, D.-L., Marchand, P., Richardson, E. H., King, R. A., Wevers, I., McCreath, W., Kyrälä, E., Oikarinen, L., Leppelmeier, G. W., Auvinen, H., Mégie, G., Hauchecorne, A., F.Lefévre, de La Nöe, J., Ricaud, P., Frisk, U., Sjoberg, F., von Schéele, F. and L.Nordh, 2004: The OSIRIS instrument on the Odin spacecraft. *Can. J. Phys.*, **82**, 411–422.

Loewenstein, M., Podolske, J. R., Fahey, D. W., Woodbridge, E. L., Tin, P., Weaver, A., Newman, P. A., Strahan, S. E., Kawa, S. R., Schoeberl, M. R. and Lait, L. R., 1993: New observations of NO$_y$/N$_2$O correlation in the lower stratosphere. *Geophys. Res. Lett.*, **20**, 2531–2534.

Logan, J., 1999: An analysis of ozonesonde data for the lower stratosphere: Recommendations for testing models. *J. Geophys. Res.*, **104**, 16,151–16,170.

London, J., 1980: *Proceedings of the* NATO *Advanced Institute on Atmospheric Ozone (Portugal).* Tech. Rep., U. S. Dept. of Transportation.

Mahlman, J. D., Levy, H. and Moxim, W. J., 1986: Three-dimensional simulations of stratospheric N$_2$O: Predictions of other trace constituents. *J. Geophys. Res.*, **91**, 2687–2707.

McCormack, J. P., Eckermann, S. D., Coy, L., Allen, D. R., Kim, Y.-J., Hogan, T., Lawrence, B., Stephens, A., Browell, E. V., Burris, J., McGee, T. and Trepte, C. R., 2004: NOGAPS-ALPHA model simulations of stratospheric ozone during the SOLVE2 campaign. *Atmos. Chem. Phys.*, **4**, 2401–2423.

McGee, T. J., Ferrare, R. A., Whitman, D. N., Butler, J. J., Burris, J. F. and Owens, M. A., 1995: LIDAR Measurements of Stratospheric Ozone during the STOIC Campaign. *J. Geophys. Res.*, **100**, 9255–9262.

McIntyre, M. and Palmer, T., 1984: The 'surf zone' in the stratosphere. *J. Atmos. Sci.*, **46**, 825–849.

McLinden, C., Olsen, S., Hannegan, B., Wild, O., Prather, M., and Sundet, J., 2000: Stratospheric Ozone in 3-D Models: A simple chemistry and the cross-tropopause flux. *J. Geophys. Res.*, **105**, 6671–6681.

McLinden, C., Olsen, S., Prather, M. and Liley, J., 2001: Understanding trends in stratospheric NO$_y$ and NO$_2$. *J. Geophys. Res.*, **106**, 27 787–27 793.

McPeters, 1993: *Ozone Profile Comparisons in The Atmospheric Effects of Stratospheric Aircraft*, vol. 1292 of *edited by M.J. Prather and E.E. Remsberg*. Report of the 1992 Models and Measurements Workshop: NASA Ref. Publ. D1-D37 pp.

McPeters, 2000: The retrieval of O$_3$ profiles from Limb scatter measurements: Results from

the Shuttle Ozone Limb Sounding Experiment. *Geophys. Res. Lett.*, **27**, 2597–2600.

Melsheimer, C., Verdes, C., Buehler, S. A., Emde, C., Eriksson, P., Feist, D. G., Ichizawa, S., John, V. O., Kasai, Y., Kopp, G., Koulev, N., Kuhn, T., Lemke, O., Ochiai, S., Schreier, F., Sreerekha, T. R., Suzuki, M., Takahashi, C., Tsujimaru, S. and Urban, J., 2004: Intercomparison of General Purpose Clear Sky Atmospheric Radiative Transfer Models for the Millimeter/Submillimeter Spectral Range. *Radio Sci.*, submitted.

Minschwaner, K., Dessler, A., Elkins, J., Volk, C., Fahey, D., Loewenstein, M., Podolske, J., Roche, A. and Chan, K., 1996: The bulk properties of isentropic mixing into the tropics in the lower stratosphere. *J. Geophys. Res.*, **101**, 9433–9439.

Mote, P., Rosenlof, K., McIntyre, M., Carr, E., Gille, J., Holton, J., Kinnersley, J., Pumphrey, H., Russell, J. and Waters, J., 1996: An atmospheric tape recorder: The imprint of tropical tropopause temperatures on stratospheric water vapor. *J. Geophys. Res.*, **101**, 3989–4006.

Murphy, D., Fahey, D., Proffitt, M., Liu, S., Chan, K., Eubank, C., Kawa, S. and Kelly, K., 1993: Reactive nitrogen and its correlation with ozone in the lower stratosphere and upper troposphere. *J. Geophys. Res.*, **98**, 8751–8773.

Nagatani, R. and Rosenfield, J., 1993: *Temperature, Net Heating and Circulation, in The Atmospheric Effects of Stratospheric Aircraft*, vol. 1292 of *edited by M.J. Prather and E.E. Remsberg*. Report of the 1992 Models and Measurements Workshop: NASA Ref. Publ. A1-A47 pp.

Nakamura, N. and Ma, J., 1997: Modified Langrangian-mean diagnostics of the stratospheric polar vortices, 2., Nitrous oxide and seasonal barrier migration in the Cryogenic Limb Array Etalon Spectrometer and SKYHI general circulation model. *J. Geophys. Res.*, **102**, 25 721–25 735.

Nash, E. R., Newman, P. A., Rosenfield, J. E. and Schoeberl, M. R., 1996: An objective determination of the polar vortex using Ertel's potential vorticity. *J. Geophys. Res.*, **101**, 9471–9478.

Newman, P. A., Harris, N. R. P., Adriani, A., Amanatidis, G. T., Anderson, J. G., Braathen, G. O., Brune, W. H., Carslaw, K. S., Craig, M. S., DeCola, P. L., Guirlet, M., Hipskind, R. S., Kurylo, M. J., Kuellmann, H., Larsen, N., Megie, G. J., Pommereau, J.-P., Poole, L. R., Schoeberl, M. R., Stroh, F., Toon, O. B., Trepte, C. R. and van Roozendael, M., 2002: An Overview of the SOLVE-THESEO 2000 Campaign. *J. Geophys. Res.*, **107**, D20, 10.1029/2001JD001 303.

Niwano, M., Yamazaki, K. and Shiotani, M., 2003: Seasonal and QBO variations of ascent rate in the tropical lower stratosphere as inferred from UARS HALOE trace gas data,. *J. Geophys. Res.*, **108**, 4794, 10.1029/2003JD003 871.

van Noije, T. P. C., Eskes, H. J., van Weele, M. and van Velthoven, P. F. J., 2004: Implications of the enhanced Brewer-Dobson circulation in European Centre for Medium-Range Weather Forecasts reanalysis ERA-40 for the stratosphere-troposphere exchange of ozone in global chemistry transport models. *J. Geophys. Res.*, **109**, D 19308, doi:10.1029/2004JD004 586.

Olsen, S., McLinden, C. and Prather, M., 2001: The stratospheric N_2O-NO_y system: Testing uncertainties in a 3-D framework. *J. Geophys. Res.*, **106**, 28 771–28 784.

Park, J. H., Ko, M., Jackman, C., Plumb, A., Kaye, J. and Sage, K., 1999: *Models and measurements: Intercomparison - II*. NASA, Langely Research Center: Virginia.

Petelina, S. V., Llewellyn, E. J., Degenstein, D. A., Lloyd, N. D., Gattinger, R. L., Haley, C. S., von Savigny, C., Griffioen, E., McDade, I. C., Evans, W. F. J., Murtagh, D. P. and

de La Noë, J., 2004: Comparison of the Odin/OSIRIS stratospheric ozone profiles with coincident POAM III and ozonesonde measurements. *Geophys. Res. Lett.*, **31**, L07 104, doi:10.1029/2003GL019 299.

Plumb, R. A., 2002: Stratospheric transport. *J. Meteor. Soc. Japan.*, **80**, 793–809.

Plumb, R. A. and Eluszkiewicz, J., 1999: The Brewer-Dobson Circulation: Dynamics of the tropical upwelling. *J. Atmos. Sci.*, **56**, 868–890.

Plumb, R. A. and Ko, M. K. W., 1992: Interrelationships between mixing ratios of long-lived stratospheric constituents. *J. Geophys. Res.*, **97**, 10 145 – 10 156.

Prather, M., 1986: Numerical advection by conservation of second-order moments. *J. Geophys. Res.*, **91**, 6671–6681.

Prather, M. J., Garcia, M. M., Suozzo, R. and Rind, D., 1990: Global impact of the Antartic ozone hole: Dynamical dilution with a three-dimensional chemical transport model. *J. Geophys. Res.*, **95**, 3449–3471.

Press, W. H., Teukolsky, S. A., Vetterling, W. T. and Flannery, B. P., 1992: *Numerical recipes in C*. Cmbridge University Press: Cambridge.

Proffitt, M., Kelly, K., Powell, J., Gary, B., Loewenstein, M., Podolske, J., Strahan, S. and Chan, K., 1989: Evidence for diabatic cooling and poleward transport within and around the 1987 Antarctic ozone hole. *J. Geophys. Res.*, **94**, 16 797.

Randall, C. E., Rusch, D., Bevilacqua, R., Hoppel, K. W. and Lumpe, J. D., 2003: Validation of POAM-3 O_3: Comparison to ozonesonde and satellite data. *J. Geophys. Res.*, **108**, 4367, doi:10.1029/2002JD002 944.

Randel, W. J., 1988: The seasonal evolution of planetary waves in the southern hemisphere stratosphere and troposphere. *Quart. J. Roy. Meteor. Soc.*, **114**, 1385–1409.

Randel, W. J., Gille, J. C., Roche, A. E., Kumer, J. B., Mergenthaler, J. L., Waters, J. W., Fishbein, E. F. and Lahoz, W. A., 1993: Stratospheric transport from tropics to middle latitudes by planetary-wave mixing. *Nature*, **365**, 533–535.

Rasch, P. J., Boville, B. A. and Brasseur, G. P., 1995: A three-dimensional general circulation model with coupled chemistry for the middle atmosphere. *J. Geophys. Res.*, **100**, 9041–971.

Riese, M., Manney, G., Oberheide, J., Tie, X., Spang, R., Kuell, V. and Offermann, D., 2002: Stratospheric transport by planetary wave mixing as observed during CRISTA-2. *J. Geophys. Res.*, **107**, 10.1029/2001JD000 629.

Riese, M., Preusse, P., Spang, R., M.Ern, Jarisch, M., Grossmann, K. and Offermann, D., 1997: Measurements of Trace Gases by the CRyogenic Infrared Spectrometers and Telescopes for the Atmosphere (CRISTA) Experiment. *Adv. Space Reas.*, **19**, 563–566.

Roche, A. E., Kumer, J. B., Nightingale, R. W., Mergenthaler, J. L., Ely, G. A., Bailey, P. L., Massie, S. T., Gille, J. C., Edwards, D. P., Gunson, M. R., Abrams, M. C., Toon, G. C., Webster, C. R., Traub, W. A., Jucks, K. W., Johnson, D. G., Murcray, D. G., Murcray, F. H., Goldman, A. and Zipf, E. C., 1996: Validation of CH_4 and N_2O measurements by the CLAES instrument on the Upper Atmosphere Research Satellite. *J. Geophys. Res.*, **101**, 9679–9710.

Rodgers, C., 1976: Retrieval of atmospheric temperature and composition from remote measurements of thermal radiation. *Rev. Geophys.*, **14**, 609–624.

Rodgers, C., 1990: Characterization and error analysis of profiles retrieved from remote sounding measurements. *J. Geophys. Res.*, **95**, 5587–5595.

Rosenfield, J. and Schoeberl, M., 1986: A computation of stratospheric heating rates and the diabatic circulation for the Antarctic spring. *Geophys. Res. Lett.*, **13**, 1339–1342.

Rosenkranz, P. W., 1998: Water vapor microwave continuum absorption: A comparison of measurements and models. *Radio Sci.*, **33**, 4, 919–928.

Rosenlof, K., 1995: Seasonal cycle of the residual mean meridional circulation in the stratosphere. *J. Geophys. Res.*, **100**, 5173–5191.

Rosenlof, K., 1999: Estimates of the seasonal cycle of mass and ozone transport at high northern latitudes. *J. Geophys. Res.*, **104**, 26 511–26 523.

Rosenlof, K. and Holton, J., 1993: Estimates of the stratospheric residual circulation using the downward control principle. *J. Geophys. Res.*, **98**, 10 465–10 473.

Rothman, L., Gamache, R., Tipping, R., Rinsland, C., Smith, M., Benner, D., Devi, V., Flaud, J., Camy-Peyret, C., Perrin, A., Goldman, A., Massie, S., Brown, L. and Toth, R., 1992: The HITRAN molecular database: editions of 1991 and 1992. *J. Quant. Spectrosc. Radiat. Transfer*, **48**, 469–507.

Russell, J. I., Gordley, L., Deaver, L., Thompson, R. and Park, J., 1996: An Overview of the Halogen Occultation Experiment (HALOE) and Preliminary Results. *Adv. Space Reas.*, **9**, 13–20.

Sander, 2000: *Chemical kinetics and photochemical data for use in stratospheric modeling.* JPL Publ. 00-3, California: Jet Propul. Lab.

Sander, 2003: *Chemical kinetics and photochemical data for use in stratospheric modeling.* JPL Publ. 033, California: Jet Propul. Lab.

Sankey and Shepherd, 2003: Correlations of long-lived chemical species in a middle atmosphere general circulation model. *J. Geophys. Res.*, **108**, 10.1029/2002JD002 799.

Santee, M. L., Manney, G. L., Livesey, N. J. and Read, W. G., 2004: Three-dimensional Structure and Evolution of Stratospheric HNO_3 based on UARS Microwave Limb Sounder Measurements. *J. Geophys. Res.*, **109**, D15, D15 306,10.1029/2004JD00 457.

von Savigny, C., Haley, C. S., Sioris, C. E., McDade, I. C., Llewellyn, E. J., Degenstein, D., Evans, W. F. J., Gattinger, R. L., Griffioen, E., Kyrölä, E., Lloyd, N. D., McConnell, J. C., McLinden, C. A., Mégie, G., Murtagh, D. P., Solheim, B. and Strong, K., 2003: Stratospheric O3 profiles retrieved from limb scattered sunlight radiance spectra measured by the OSIRIS instrument on the Odin satellite. *Geophys. Res. Lett.*, **30(14)**, 1755, doi:10,1029/2002GL016 401.

von Savigny, C., Rozanov, A., Bovensmann, H., Eichmann, K.-U., Noël, S., Rozanov, V. V., Sinnhuber, B.-M., Weber, M. and Burrows, J. P., 2004: The ozone hole break-up event in September 2002 as seen by SCIAMACHY on ENVISAT. *J. Atmos. Sci.*, in press.

Scott, R. K., 2002b: Wave-driven mean tropical upwelling in the lower stratosphere. *J. Atmos. Sci.*, **59**, 2745–2759.

Scott, R. K. and Dritschel, D. D., 2004: Downward wave propagation on the polar vortex. *J. Atmos. Sci.*, submitted.

Scott, R. K. and Haynes, P. H., 2002a: The seasonal cycle of planetary waves in the winter stratosphere. *J. Atmos. Sci.*, **59**, 803–822.

Shia, R.-L., Ko, M., Weisesnetein, D., Scott, C. and Rodriguez, J., 1998: Transport between the tropical and mid-latitude lower stratosphere: Implication for ozone response to HSCT emissions. *J. Geophys. Res.*, **103**, 25 435–25 446.

Shine, K. P., 1987: The middle atmosphere in the absence of dynamical heat fluxes. *Quart. J. Roy. Meteor. Soc.*, **113**, 603–633.

Sinnhuber, B.-M., Langer, J., Klein, U., Raffalski, U., Künzi, K. and Schrems, S., 1998: Ground based millimeter-wave observations of Arctic ozone depletion during winter and

spring of 1996/97. *Geophys. Res. Lett.*, **17**, 3227–3330.

Sinnhuber, B.-M., Müller, R., Bovensmann, H., Eyring, V., Klein, U., Langer, J., Trentmann, J., Burrows, J. and Künzi, K., 1999: Interpretation of mid-stratospheric Arctic ozone measurements using a photochemical box-model. *J. Atmos. Sci.*, **34**, 281–290.

Sinnhuber, B.-M., Weber, M., Amankwah, A. and Burrows, J., 2003: Total ozone during the unusual Antarctic winter of 2002. *Geophys. Res. Lett.*, **30**, 1580, doi: 10.1029/2002GL016 798.

Solomon, S., 1999: Observations of Ozone Trends. *Rev. Geophys.*, **37**, 275–316.

Solomon, S., Kiehl, J. T., Garcia, R. R. and Grose, W., 1986: Tracer transport by the diabatic circulation deduced from satellite observations. *J. Atmos. Sci.*, **43**, 1603–1617.

Staehelin, J., Harris, N., Appenzeller, C., Eberhard, J. and Piechowski, M., 2001: Observations of Ozone Trends. *Rev. Geophys.*, **39**, 231–290.

Sugita, T., Kondo, Y., Nakajima, H., Schmidt, U., Engel, A., Oelhaf, H., Wetzel, G., Koike, M. and Newman, P. A., 1998: Denitrification observed inside the Arctic vortex in February 1995. *J. Geophys. Res.*, **103 (D13)**, 16 221–16 234.

Sugita, T., Yokota, T., Nakajima, H., Kanzawa, H., Nakane, H., Gernandt, H., Yushkov, V., Shibasaki, K., Deshler, T., Kondo, Y., Godin, S., Goutail, F., Pommereau, J.-P., Camy-Peyret, C., Payan, S., Jeseck, P., Renard, J.-B., Bösch, H., Fitzenberger, R., Pfeilsticker, K., von König, M., Bremer, H., Küllmann, H., Schlager, H., Margitan, J. J., Stachnik, B., Toon, G. C., Jucks, K., Traub, W., Johnson, D. G., Murata, I., Fukunishi, H. and Sasano, Y., 2002: Validation of ozone measurements from the Improved Limb Atmospheric Spectrometer (ILAS). *J. Geophys. Res.*, **107 (D24)**, 10.1029/2001JD000 602.

Swinbank, R. and O'Neill, A., 1994: A stratosphere-troposphere data assimilation system. *Mon. Wea. Rev.*, **122**, 686–702.

EORCU, 2003: *The northen hemisphere stratosphere in the 2002-03 winter*. European Ozone Research Coordinating Unit Report, Cambridge.

WMO, 2002: *Scientific Assessment of Ozone Depletion: 2002, Global Ozone Research and Monitoring Project*. 47, Geneva: World Meteorological Organization. 498 pp.

Thompson, A., J.Witte, R.McPeters, Oltmans, S., Schmidlin, F., Logan, J., Fujiwara, M., Kirchhoff, V., Posny, F., Coetzee, G., Hoegger, B., Kawakami, S., Ogawa, T., Johnson, B., Vömel, H. and Labow, G., 2003a: Southern Hemisphere Additional Ozonesondes (SHADOZ) 1998-2000 tropical ozone climatology 1. Comparison with Total Ozone Mapping Spectrometer (TOMS) and ground-based measurements. *J. Geophys. Res.*, **108**, 8238, doi: 10.1029/2001JD000 967.

Thompson, A., Witte, J., Oltmans, S., Schmidlin, F., , Logan, J., Fujiwara, M., Kirchhoff, V., Posny, F., Coetzee, G., Hoegger, B., Kawakami, S., Ogawa, T., Fortuin, J. and Kelder, H., 2003b: Southern Hemisphere Additional Ozonesondes (SHADOZ) 1998-2000 tropical ozone climatology 2. Tropospheric variability and the zonal wave-one. *J. Geophys. Res.*, **108**, 8241, doi: 10.1029/2002JD002 241.

Tian, W. and Chipperfield, M., 2004: A New Coupled Chemistry-Climate Model for the Stratosphere: The Importance of Coupling for Future O_3-Climate Predictions. *Quart. J. Roy. Meteor. Soc.*, submitted.

Trepte, C. R. and Hitchman, M. H., 1992: The stratospheric tropical circulation deduced from aerosol satellite data. *Nature*, **355**, 626.

Urban, 2005: 'manuscript submitted'. *J. Geophys. Res.*

Urban, J., 1998: *Measurements of stratospheric trace gases ClO, HCl, O_3, N_2O, H_2O and OH*

using airborne submillimeter radiometer at 650 and 2500 GHz., vol. 264. ISSN 0176-5027, Reports on Polar Reseach, PhD thesis, University of Bremen. 182 pp.

Urban, J., Lautié, N., Flochmoën, E. L., Eriksson, P., de La Noë, J., Dupuy, E., Amraoui, L. E., Frisk, U., Jégou, F., Murtagh, D., Olberg, M., Ricaud, P., Camy-Peyret, C., Dufour, G., Payan, S., Huret, N., Pirre, M., Robinson, A. D., Harris, N. R. P., Bremer, H., Kleinböhl, A., Küllmann, K., Künzi, K., Kuttippurath, J., Ejiri, M., Nakajima, H., Sasano, Y., Sugita, T., Yokota, T., Piccolo, C., Raspollini, P. and Ridolfi, M., 2004: Odin/SMR limb observations of stratospheric gases: Validation of N$_2$O. *J. Geophys. Res.*, in press.

Volk, C. M., Elkins, J. W., Fahey, D. W., Salawitch, R. J., G. S. Dutton, J. M. G., Proffitt, M. H., Loewenstein, M., Podolske, J. R., Minschwaner, K., Margitan, J. J. and Chan, K. R., 1996: Quantifying transport between the tropical and mid-latitude lower stratosphere. *Science*, **272**, 1763–1768.

Waugh, D. W., 1996: Seasonal variation of transport out of the tropical stratosphere. *J. Geophys. Res.*, **101**, 4007–4023.

Waugh, D. W. and Hall, T. M., 2002: Age of stratospheric air: Theory, observations, and models. *Rev. Geophys.*, **40(4)**, 10.1029/2000RG000 101.

Wayne, R. P., 1991: *Chemistry of Atmospheres*. Oxford Press: New York. 404 pp.

Wirth, M. and Renger, W., 1996: Evidence of large scale ozone depletion within the Arctic polar vortex 94/95 based on airborne LIDAR. *Geophys. Res. Lett.*, **13**, 813–816.